energies

Review

Harmonic Mitigation Using Meta-Heuristic Optimization for Shunt Adaptive Power Filters: A Review

Minh Ly Duc [1,2,*], Lukas Hlavaty [2], Petr Bilik [2] and Radek Martinek [2]

[1] Faculty of Commerce, Van Lang University, 69/68 Dang Thuy Tram, Ward 13, Binh Thanh District, Ho Chi Minh City 70000, Vietnam

[2] Department of Cybernetics and Biomedical Engineering, Faculty of Electrical Engineering and Computer Science, VSB–Technical University of Ostrava, 17. Listopadu 2172/15, 708 00 Ostrava, Czech Republic; lukas.hlavaty@vsb.cz (L.H.); petr.bilik@vsb.cz (P.B.); radek.martinek@vsb.cz (R.M.)

* Correspondence: minh.ld@vlu.edu.vn

Abstract: Shunt Adaptive Power Filter (SAPF) is widely used in the performance of power quality improvement activities in the power supply industry for processing industries or civil power sources in the world today based on its simplicity, transparency, high reliability, efficiency, and reliability, and their powerful compensating current-providing nature. The PI controller integrated into the SAPF operation mechanism works with extra high efficiency in selecting the current to compensate for the lost current generated in the power supply due to harmonics generated by the K_p, K_i parameter values. The system operates by the PWM method for bridge rectifier circuits that perform the function of selecting the appropriate compensating current, providing correct compensation for the amount of current loss in the power supply. Adjusting the K_p, K_i parameter to reach the optimal value by different methods is a promising and popular research direction at present. The K_p, K_i parameter serves the right purpose for the PI controller to generate enough PWM pulses to excite the bridge rectifiers to generate just the right amount of compensating current and enough current to be compensated on the power supply. The commonly used K_p, K_i parameter adjustment methods include the Ziegler Nichols closed-loop vibration method, the P-Q theoretical method, and several other methods. This study conducts a comprehensive review of the literature on modern strategies for adjusting the K_p, K_i parameters in the PI controller in the SAPF suite by using the meta-heuristic optimization method. This study performs classification according to the operation mode of meta-heuristic optimization methods to adjust the K_p, K_i parameter to control the PI to select the correct PWM frequency to activate bridge rectifiers to select the most optimal compensation current to compensate for the loss of current on the power supply to meet the goal of improving power quality in accordance with IEEE 519-2022 standard, leading to the total harmonic distortion (THD) value is below 5%. The study presents in detail some meta-heuristic optimization algorithms, including applications, mathematical equations, and implementation of flow charts for SAPF and provides some open problems for future research. The main objective of this study is to provide an overview of applying meta-heuristic optimization algorithms to the K_p, K_i parameter tuning of PI controllers.

Keywords: shunt adaptive power filter; SAPF; harmonic mitigation; IEEE 519-2022; meta-heuristics; swarm optimization

check for updates

Citation: Duc, M.L.; Hlavaty, L.; Bilik, P.; Martinek, R. Harmonic Mitigation Using Meta-Heuristic Optimization for Shunt Adaptive Power Filters: A Review. *Energies* **2023**, *16*, 3998. https://doi.org/10.3390/en16103998

Academic Editors: Mojtaba Ahmadieh Khanesar and Abu-Siada Ahmed

Received: 16 March 2023
Revised: 25 April 2023
Accepted: 4 May 2023
Published: 9 May 2023

1. Introduction

Power quality and, in particular, reducing power loss during transmission or distribution caused by harmonic components and methods need to be taken urgently [1,2]. There are many methods, as well as models, for reducing and eliminating harmonics and improving power quality in the transmission and distribution process [3,4] (Figure 1).

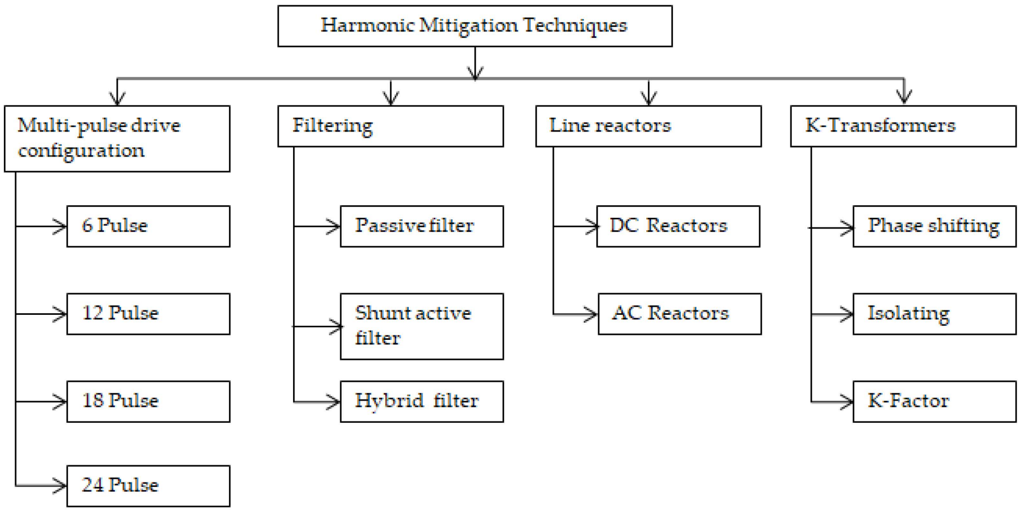

Figure 1. Methods to reduce and eliminate harmonics.

The power system has the problem of generating harmonics, causing a loss of productivity, and techniques to control and minimize harmonics are proposed [5]. To understand these techniques, it is necessary to analyze the advantages and disadvantages of each technique and analyze the technical conclusions and their performance. To so harmonic-related problems, there are different techniques like Line reactor [6], Isolation transformer [7], K-factor transformer [8], tuned harmonic filter [9], IGBT-based fast switched harmonic filter [10], Low pass harmonic filter [11], 12 and 18 pulse rectifier [12], Phase-shifting transformer [13], and active harmonic filters [5]. The current reactor implements a series connection with an individual nonlinear current and is the simplest means of harmonic reduction [3,4]. The isolation transformer is known as an electrostatic shield between the primary and secondary coil; they couple capacitance between each coil and shield together, then a low impedance is created to reduce noise, transient current, and zero sequences current [14]. The shielding helps to reduce harmonic interference in normal mode for the initial side of the transformers [15]. The K-factor transformer is designed as a constant that determines the transformer's ability to handle transformer warming caused by generated harmonics [16]. Usually made by coupling multiple insulated and interchanged conductors to reduce phase effect, magnetic errors are designed with lower flux density [8]. Factor K has two variables with harmonic current magnitude and harmonic order [15].

The turn harmonic filter is a device that is connected in a series of inductive and capacitive reactance forming a tuned LC circuit, shaped like a shunt device, which is a frequency-modulated resonant circuit that provides impedance short helps to reduce harmonic distortion [17,18]. Insulated Gate Bipolar Transistor (IGBT) has a very fast circuit switching function, about 60 times per second, meeting the requirements of reactive power and ensuring harmonic distortion within the specified standard. A low-pass harmonic filter is to connect multiple string elements into a set of tuning elements, increases input impedance, effectively controls harmonics, and attenuates all harmonic frequencies in the circuit [19]. A pulse rectifier is a device made up of many rectifiers and connected to a special type of transformer and guarantees a displacement of each secondary phase of 360 divided by the number of rectifier pulses [20]. The Phase Shifting Transformer is made up of two nonlinear loads fed by the two-phase shifting of the transformer windings and acts as 12 pulses, canceling the fifth and seventh harmonics on the primary side of the transformer [21,22]. Active filters are considered independent harmonic filters or combined with technological techniques in the rectification stage of other power electronic devices. It can analyze the frequency content and the magnitude of the current or filter out the fundamental frequency of the current. It provides suitable inverting currents to eliminate individual harmonics through Insulated Gate Bipolar Transistors (IGBTs) [3–5]. Considering the approximate cost (USD) and performance of the above harmonic reduction techniques for 3-phase harmonics, the following table gives the comparison results (Table 1).

Table 1. Considering the approximate cost (USD) and performance of the above harmonic reduction techniques for three-phase harmonics.

Harmonic Mitigation Techniques	15 kW (Price)	75 kW (Price)	300 kW (Price)	THD-I (%) (Non-Linear Loads)	THD-I (%) (Mixed (50–50) Loads)
Reactor (5%)	520	1100	3800	35	17.5
Isolation Transformer	2650	6340	18,000	35	17.5
K-factor (13) Transformer	5300	11,000	48,000	35	17.5
Tuned Filter	2800	3900	7000	12–20	3–12
Low Pass Filter	2400	5600	13,000	8–15	N/A
Active Filter	N/A	27,000	65,000	5	5

In this study, the focus is on understanding meta-heuristic algorithm methods and AI engineering models, combining the above models to improve power loss compensation through a shunt adaptive power filter (Figure 2).

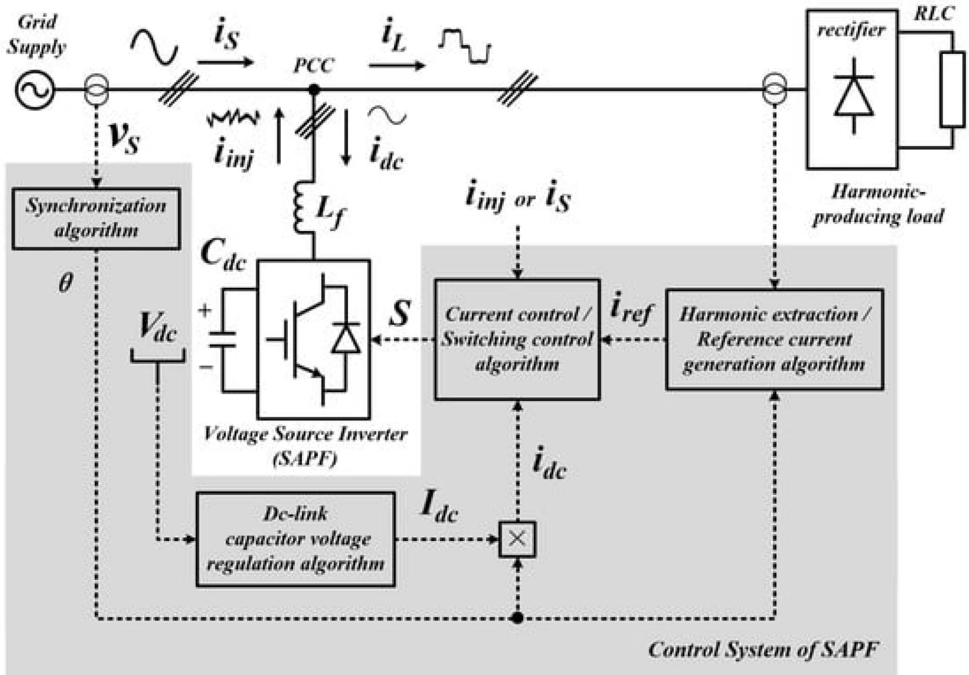

Figure 2. Block diagram of the system for compensation of higher harmonic components using Shunt Active Power Filter (SAPF).

Combining AI engineering modeling with meta-heuristic algorithm models improves the model's prediction accuracy and improves the model's convergence speed [23]. Along with today's trend, the amount of electricity is increasing, specifically in addition to the fact that countries around the world want to gradually reduce their dependence on energy and gas sources, improve the use of renewable energy sources and save electric energy, reduce power loss caused by harmonics by applying [1] meta-heuristic algorithm techniques and technical models. AI techniques to control active filter circuits, such as shunt adaptive power filters [23,24]. This study has several implications as follows:

1. AI engineering models and meta-heuristic algorithm models are applied to SAPF to perform the extraction of the harmonic component from the measurement signals of the sensors and, at the same time, perform the selection of the optimal compensating current value providing compensation to the power supply;

2. Models that combine meta-heuristic algorithm techniques with AI engineering models in shunt adaptive power filter to increase convergence speed into selecting current compensation and improve the quality of the sine wave shape of the power signal.
3. The equation relationship between the meta-heuristic algorithm models is also compared via the pseudo-code algorithm;
4. Overview of applying shunt adaptive power filter to compensate for power loss for power sources that have been connected to the national power grid such as PV Solar, wind power, and combined AI techniques models with meta-heuristic algorithm models into the above power system;
5. Overview of current control circuits that compensate for power loss caused by harmonics and harmonic analysis circuits generated in power systems are also described in general.

Power quality problems are phenomena that arise in the power supply [1]. The causes that give rise to the above problems are harmonic distortion [5] and the consequences for the power system and electrical equipment when there is a voltage variation problem as above [3,4]. The waveform of the voltage source or the current source of the power source is distorted, and harmonics are measured as integer multiples of the fundamental supply frequency or the waveform of the voltage or the waveform of the current source, which has a non-sine shape [4,5]. Sources of classical equipment causing harmonics such as arc furnaces, fluorescent lamps), welding machines, rectifiers (Microprocessors, motor drives, any electronic loads), and DC brush motors. Modern sources of equipment cause harmonics such as all non-linear loads such as power electronics equipment, including ASDs, switched-mode power supplies, data processing equipment, and highly efficient lighting [6].

Devices such as rectifiers, ASDs, soft starters, electronic ballasts for discharge lamps, switched-mode power suppliers, and HVAC using ASDs use power and generate harmonics. Harmonic is a form of noise signal that has a direct negative impact on power quality. Harmonics are noticed when the sum of harmonic currents is above the allowable limit. The frequency of the harmonic current is a set of times higher than the fundamental signal frequency. Characteristic oscillations of complete harmonics are in the frequency spectrum. The harmonic component in an AC source is the sine component of a wave period whose frequency is integer times the fundamental frequency of the system [25]. Harmonics is the main cause of power quality loss and affects other electrical equipment such as transformers, motors, cables, interrupters, capacitors, and protective switching devices [3]. Bad switching will affect the performance of electrical appliances or electronic control devices, and neutral current is also generated when the electronic devices perform switching modes, devices such as PCs, printers, photocopies, and any triplets generators. The temperature generated in the conductor is caused by the neutral current acting and generated. In addition, the neutral current also adversely affects the performance of the transformer continuously.

Harmonics are generated from static frequency converters, cycle converters, induction motors, and arcing devices [5]. Power quality issues affect devices differently, just as electrical equipment responds to the impact of power quality problems differently, the presence of power electronics is also a factor related to power quality issues, and harmonics management standards are regulated based on the IEEE 519-2022 standard [26] (Tables 2 and 3).

Since 1980, harmonics have been considered an essential element that needs to be controlled in electrical systems and electrical equipment [1]. Harmonics are the cause of voltage source waveforms being distorted; they are causing wires to overheat, which is a serious problem in power transmission and distribution systems [6]. Harmonics cause transformers to generate heat and heat up transformers and are the cause of failures in electrical equipment [26]. Harmonic control, eliminating or limiting the generation of harmonics in the power supply, is an urgent issue; currently, solving problems related to harmonics is done by shunt adaptive power filters (SAPF) [27,28].

Table 2. Current distortion limits for systems rated 120 V–69 Kv (IEEE 519-2022, pg. 19).

$\frac{I_{sc}}{I_L}$	Harmonic Limits a,b					TDD Required
	$2\leq h<11$	$11\leq h<17$	$17\leq h<23$	$23\leq h<35$	$35\leq h\leq 50$	
<20	4.0	2.0	1.5	0.6	0.3	5.0
20 < 50	7.0	3.5	2.5	1.0	0.5	8.0
50 < 100	10.0	4.5	4.0	1.5	0.7	12.0
100 < 1000	12.0	5.5	5.0	2.0	1.0	15.0
>1000	15.0	7.0	6.0	2.5	1.4	20.0

a: For $h \leq 6$, even harmonics are below 50% of the harmonic limit; b: Current distortion has resulted in a dc offset; Where I_{sc}: Maximum short circuit current is current that flows through a conductor with very low resistance, almost zero at the point of common coupling (PCC). I_L: Maximum demand load current at PCC under normal operating conditions, a function of many factors over time P(t), so they do not obey a certain law. Therefore, it is very difficult to identify them. The electrical load is an important parameter in selecting the equipment for the power system at PCC.PCC (Point of Common Coupling): In many cases, when there is enough source reactance calculated at the point we consider to reduce harmonics, a filter placed at this point can absorb harmonics from many different harmonic sources flowing to them. Even harmonics are limited to 25% of the odd harmonic limits above. Current distortions that result in a dc offset. I_{sc}/I_L: All power generation equipment is limited to these values of current distortion.

Table 3. Voltage distortion limits (IEEE 519-2022, pp. 17).

Bus Voltage (V) at PCC	Total Voltage Distortion THD (%)	Individual Voltage Distortion (%)
$V \leq 1.0$ kV	≤8.0%	≤5.0%
1.0 kV $\leq V \leq$ 69 kV	≤5.0%	≤3.0%
69 kV $< V \leq$ 161 kV	≤2.5%	≤1.5%
69 kV $< V$	≤1.5%	≤1.0%

Previous studies presented algorithms applied to SAPF to perform the harmonic compensation task in the power source. However, many limitations still arise when applying algorithms (Table 4).

Table 4. Brief summary of harmonic mitigation methods in SAPF.

Ref.	Years	Methodology	Feature	Result and Advantage	Disadvantage
[29]	2019	p-q theory	Power 3 phase	THD_i = 8.2%, Generate reference currents for modern power systems based on the steady-state variation of current and voltage vectors.	Unsatisfactory harmonic compensation efficiency less than 5% according to IEEE 519-2022 standard.
[29]	2019	DCAP method		THD_i = 3.5%, Divide the sinusoidal current into n parts and balance the source side.	Satisfactory harmonic compensation efficiency is less than 5% according to IEEE 519-2022 standard.
[30]	2019	Predictive Direct Power Control (P-DPC)		THD_i = 1.2%, Maintain the DC bus offset voltage to a specified value and the anti-reverse compensated PI controller to regulate the DC bus voltage.	Effect of the sampling period and parameter error on power quality of distribution system.
[31]	2020	LCL Filter		THD_i = 4.56%, The design is higher than the harmonic frequency compensation that the SAPF has to compensate for the higher order harmonics of the grid.	The control algorithm is complex. Resonance generation. The parameters of the LCL Filter are very complicated.

Table 4. *Cont.*

Ref.	Years	Methodology	Feature	Result and Advantage	Disadvantage
[32]	2020	SiC-MOSFET		THD_i = 4.15%. Using the L-locator to suppress the switch sub-harmonics to a smaller level simplifies circuit design and control algorithms. The switching frequency is increased to 50 kHz.	Increases the second harmonic.
[33,34]	2020	An ADALINE-based Neural Network (ANN)		THD_i = 2.39%, The current is measured using the Least Mean Square (LMS) algorithm; the weights are obtained with the help of online calculations.	Analysis under severe abnormal conditions is the direction of future research.
[35]	2021	Space Vector Pulse Width Modulation (SVPWM)		THD_i = 3.73%, Trace and identify the reference voltage in a static coordinate system through coordinate transformation and determine the reference voltage.	The reference structure has only 4 transformation modes and no vector 0. This reduces the freedom of the composite vector and is difficult to control.
[36]	2021	Triangle Orthogonal Principle (TOP)		THD_i = 4.98%, Using the phase signal from the phase-locked loop is synchronized with the grid signal based on the principle of triangle orthogonality.	Lack of selective harmonic compensation.
[37]	2021	Computation Fluid Dynamics (CFD)		THD_i = 4.25%, Simulation of a heat transfer coupling under forced cooling conditions.	Designing power electronic components requires high precision.
[38]	2022	Least Mean Square (LMS)		THD_i = 3.7%, Separation of the elementary active, reactive, and harmonic components of the distorted current.	Performance is low when using the same speed for components when estimating the feedback operation.
[39]	2022	Modified Symmetrical Sinusoidal Integrator (MSSI)		THD_i = 3.94%, Extract the basic components of the corresponding forward sequence and use instantaneous reactive power theory to process the reference flow.	Look up the parameters of the transfer function.
[40]	2020	Adaptive Backstepping Fuzzy Neural Controller based on Fuzzy Sliding Mode (FNN-based FSM)		THD_i = 4.48%, Establish a subsystem and use virtual controls to simplify controller design.	Satisfactory harmonic compensation efficiency is less than 5% according to IEEE 519-2022 standard.
[41]	2021	Long and Short Term Memory Fuzzy Neural Network (LSTMFNN)	Power 1 phase	THD_i = 4.67%, Combine fuzzy neural network and long and short-term memory mechanism to enhance self-learning ability and high performance.	Improve control effect, new neural network learning strategies, finite time control and reduction of system chattering are future research directions.
[42]	2022	Modified Multiport Interleaved Flyback Convertor (MMPIFC)	Photovoltaic (PV) three-phase power	THD_i = 2.61%, Multi-port interlaced flyback conversion to connect n number of input sources to DC bus to overcome partial shadow problem.	Replacing fuzzy controls with advanced artificial intelligence algorithms like bio-inspired optimization is the direction of future research.

The parts of the research paper are organized as follows: Section 2 shows the details of random models and optimization models. Section 3 provides an overview of harmonic mitigation using meta-heuristic algorithms and artificial intelligence. Section 4 presents a discussion and future research problems, and Section 5 presents conclusions.

2. Random Models and Optimization Models

The input parameters of the optimal models are usually partially known, or they are not defined to be known; these parameters can also be called uncertain parameters. They are implemented through probabilistic statistical models or experimental design [6]. The model used to implement the above parameters is called the stochastic programming model and is expressed through Formula (1) as follows:

$$\min_{x \in X}\{g(x) = f(x) + E[Q(x,\varepsilon)]\} \tag{1}$$

With: X is a nonempty closed subset of R^n, ε is a random vector whose probability distribution P is supported on a set $[I] \subset R^d$ and $Q : X \times [I] \to R$. In the framework of two-stage stochastic programming, $Q(x,\varepsilon)$ is given by the optimal value of the corresponding second-stage problem. $g(x)$ is well-defined and finite valued for all $x \in X$. This implies that for every $x \in X$ the value $Q(x,\varepsilon)$ is almost surely finite.

The key to making the model change is the input parameters, and in particular, the objective functions that are set up containing random parameters whose values are unknown or known. However, the input variables of the objective function obey the distribution law of a given probability previously [6]. There are many related studies applying models using unknown, unspecified random input parameters and following probability distributions, such as the meta-heuristic algorithm (Figure 3).

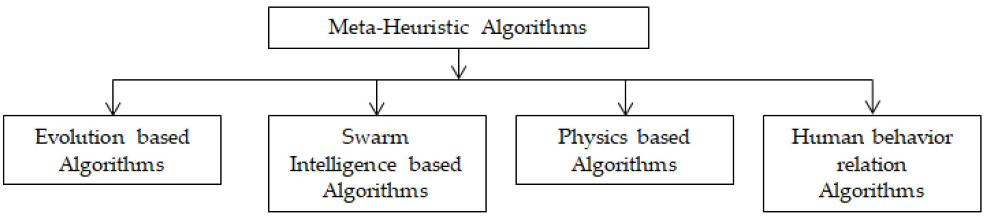

Figure 3. Classification of meta-heuristic algorithms.

Evolution-based algorithms are models that form algorithms inspired by natural evolution to generate populations for algorithmic solutions [43,44]. Individuals are created from the best solution of the mathematical model, mutation, or crossover, or select the best solution in the mathematical model to create new individuals [45]. The genetic Algorithm (GA) is a figure point. This mathematical modeling technique is based on Darwin's evolutionary technique. In addition, there are other techniques that have been developed, such as evolution strategy, genetic programming, Backtracking Search Algorithm (BSA), and Differential Evolution (DE).

Swarm Intelligence based Algorithms are social behavior from insects, animals such as fish, birds, and so on while they are foraging or hunting, specifically their behavior of moving to find the best location and space best for the process of social behavior. Mathematical models are built from those social behaviors [46,47]. The most popular is particle swarm optimization (PSO),developed by Kennedy and Eberhart. There are also many other algorithm models, such as Ant Colony Optimization, Honeybee colony optimization algorithm, and Cat Swarm Optimization (CSO).

Physics-based algorithms are based on the laws of physics in the universe around us, re-modeled [48] into algorithms like Simulated Annealing (SA) and Gravitational Search Algorithm (GSA).

Human behavior relation algorithms are based on human behavior modeled into mathematical models. The performance of a mathematical model is directly related to human behavior [49,50]. The algorithms were conceived as a teaching-learning-based optimization (TLBO) and a League Championship algorithm.

The above plans meet the requirements of high equivalence search criteria and have fast convergence when using stochastic methods with unknown input parameter variables or undefined according to the distribution law of probability statement. However, because the input factor is a random variable, the meta-heuristic optimization methods can loop around to find the approximate value of the criterion function over a long time or possibly indefinitely [6]. This is a limitation of the above optimization models; the variables can be used to optimize the randomness of the input parameter variables of the optimal model, to reduce the randomness, reduce the size of the random data or eliminate the finite difference, as well as remove the confounding factors, to bring the optimal results for the model [44,46]. Each meta-heuristic optimization model has its own characteristics, its own mainstream, and at the same time, its own limitations [48,49]. Meta-heuristics-based optimization is considered for use on the following grounds:

1. Meta-heuristic optimization is applied by many researchers to research many aspects of optimization and is widely used, which means that there are many recent research publications in many prestigious journals around the world catalog ISI/SCOPUS and is used in almost every field from engineering to economics and other sciences;
2. Artificial intelligence uses meta-heuristic optimization models in training activities and as well as improves the ability to predict results of artificial intelligence (AI) technical models such as artificial neural network (ANN), fuzzy logic, and adaptive neural fuzzy system (ANFIS);
3. Meta-heuristic optimization is done very simply with not too complicated mathematical models, with no need for additional training data or initial implementation solutions, just building suitable mathematical models and precise distribution functions' respective performance to improve the optimization level for the operations;
4. Researchers only need to use the population size and number of iterations to build an optimal research model using meta-heuristic optimization without the need to delve into the knowledge of complex mathematical models;
5. Researchers only need to build fitness functions and constraints to freely choose meta-heuristic models and modify them to perform optimal problem-solving;
6. Meta-heuristic research models are integrated into the test models and validated based on simulation models with various tools available;
7. Meta-heuristic optimization gives good processing results for multi-objective processing models and, with many decision variables and constraints, does not restrict solutions and is not dominated;
8. Meta-heuristic optimization is used to solve multi-disciplinary problems, and along with many publications in prestigious journals in the world at the present time, it is useful for analysis, comparison, and analysis activities to compare the research results of the proposed work of the authors;
9. Compared with the training and learning requirements with complex mathematical models of artificial intelligence (AI) techniques, meta-heuristic optimization shows that the computation process is much simpler with the use of algorithms. Math models are much simpler than those applied in AI techniques;
10. Nowadays, the development of computer technology needs to use optimization models more and more to optimize the processing time of real-time problems.

3. Harmonic Mitigation Using Meta-Heuristic Algorithms and Artificial Intelligence

Models of harmonic control and reduction are often related to (1) analyzing and detecting harmonic components. (2) Control and generate a suitable compensating current into the power supply to compensate for the electrical loss caused by the harmonic component (Figure 2). In some cases, researchers create analyzers that identify harmonics used in single-phase [51] or three-phase power networks [52]. In many cases, the problem to be optimized is necessary; the reason is that the problems are very complex. Nowadays, modern optimization methods implemented into SAPF filters are a promising research direction. Meta-heuristic optimization and artificial intelligence techniques have been applied by many researchers to SAPF control to generate a compensating current that provides compensation to the power supply [46]. Finding the optimal power supply parameter to compensate for the harmonic component is a very complex problem. Applying a mathematical model or more to solve a problem is necessary. Choose one or more available information about the problem, or interactions between them, to apply to the optimization algorithm, which produces an optimal result better than the individual algorithms [3,6]. Meta-heuristic optimization models using combined with shunt adaptive power filters to control harmonics is a research direction that is interesting in scientists and managers at the current time, as well as a development orientation for the application of advanced signal processing control by computer in power quality improvement activities [26–28].

3.1. Analyze and Detect Harmonic Components

Detecting and extracting harmonic components of voltage and current sources is essential for power quality improvement [3]. The purpose of this work is to find a suitable method to select the compensating current to compensate for the current, or power voltage, loss caused by harmonic components. Components such as amplitude and phase of harmonics require a reasonable technique for extraction, detection, and classification at the input source. Harmonics cause distortion of the voltage waveform or input voltage current, and a suitable compensating current is required to compensate for the loss caused by harmonic distortion to correct the waveform distortion of the voltage source or current source [3]. To do this, a suitable method is needed (Figure 4). The methods for extracting, detecting, and classifying harmonics are divided into two groups. Group 1 is a type of frequency harmonic component analysis technique, and group 2 is a time domain harmonic component analysis technique.

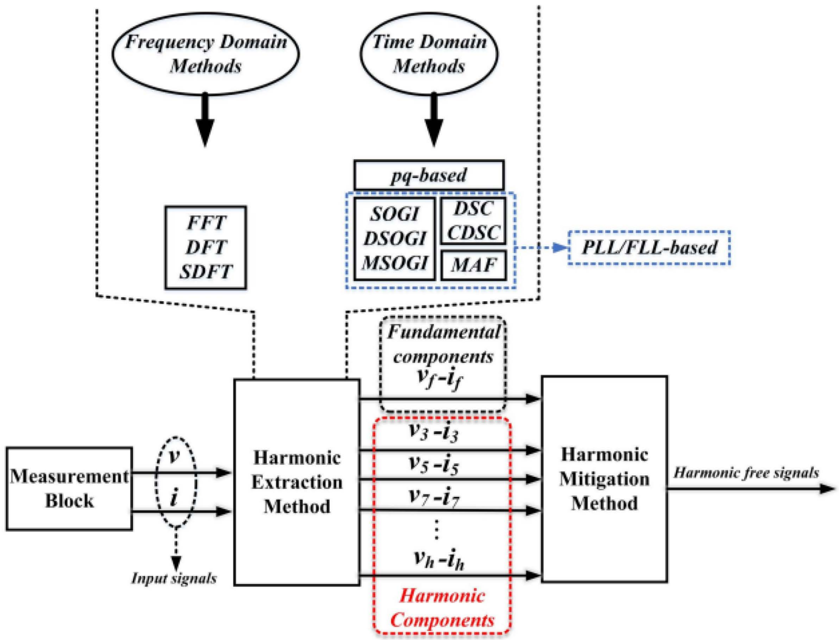

Figure 4. Harmonic detection methods.

Group 1 is a group of frequency harmonic component analysis techniques performed by Fourier series analysis to extract the harmonic components of the input source. The methods of analyzing and extracting harmonic components in the power source include Discrete Fourier Transform (DFT) [53], Fast Fourier Transform (FFT) [54], and Sliding Discrete Fourier Transform (SDFT) [55].The disadvantages to note when using the above methods are that it takes a certain period of time to solve the problem, requires a large memory, the fundamental frequency must be synchronized with the frequency number of samples, and sometimes generates an unnecessary reactive power under a transient condition. However, the remarkable strength of the above methods is that the harmonic components generated in the power supply are closely measured and monitored, and the calculation formulas require very few mathematical equations, which leads to fast processing speed during current compensation for voltage distortions caused by harmonics faster. The p-q instantaneous power theory is a widely used method and has been applied by many researchers to operations that exploit harmonic components and eliminate fundamental harmonics [56]. However, the harmonic component in the power supply circuit is also analyzed and detected by applying a high pass filter (HPF) [57]. There is a disadvantage of this method that if the system is unbalanced, the function will be damaged. Their performance and computation are significantly affected. Currently, there are many techniques for analyzing and extracting harmonics, which are SOGI [58], DCS [59,60], MAF [60], DSOGI [61], MSOGI [62], DCS [63], and CDSC [64].

Group 2 includes time-domain-based harmonic analysis methods such as using a phase- or frequency-locked loop (PLL/FLL) to analyze and monitor fundamental frequencies of voltage waves in the source even if the voltage source is unbalanced [65,66]. The advantages of the above method are that it can work well even when using single-phase or three-phase power, and even when the source state is unbalanced, the above techniques still work normally without the use of digital filters, the positive and negative wave sequences are also extracted and detected clearly. However, the above techniques also have disadvantages when using such as frequency is prone to oscillation when using the SOGI technique [58]. MSOGI has a lot of complicated calculation equations, which affect processing speed and slow signal response [62]. SOGI and DSOGI techniques give rise to an unstable state for the input source. The DSC technique has many complex computational equations and the potential for errors in digital implementation [61,62]. Based on the results of a brief analysis of the advantages and disadvantages of the above harmonic analysis and extraction techniques, when using the above techniques, it is necessary to consider and use the appropriate methods above for maximum performance. Optimizing the selection of parameters in the operation of extracting harmonic components in the signal source using meta-heuristic optimization methods is a promising research direction for the future. This study does not focus on analyzing the overall harmonics extraction methods.

3.2. Harmonic Mitigation Using Meta-Heuristic Algorithms

This study conducts a literature review on the application of the optimization algorithm to SAPF to find the optimal compensation power source that provides compensation for the loss of current in the power supply to meet the THD value of less than 5% according to the IEEE 519-2022 standard (Figure 5).

3.2.1. Evolution-Based Algorithms

Calculated in the period from 1966 to 2021, there are 16 methods to the advantage of Evolution based Algorithms. However, the study authors have applied two methods to harmonics mitigation in shunt adaptive power filters, which are Evolution based Algorithms and Genetic Algorithms (GAs).

Difference Evolution Algorithms (DE) for SAPF

The DE method used to improve multi-object control integral scaling is applied to the control currently used in the shunt adaptive power filter [67]. The performance of this method is limited due to the use of the Maslin polynomial. The act of using the DE method to optimally minimize the fitness function and generate the control current to reduce the total harmonic distortion (THD) of the power supply, eliminating the error of the control loop compensating current and the saturation of the controlled loop within limits [68,69]. The PI-MR controller is based on the frequency domain to analyze the harmonic component generated in the power supply [70].

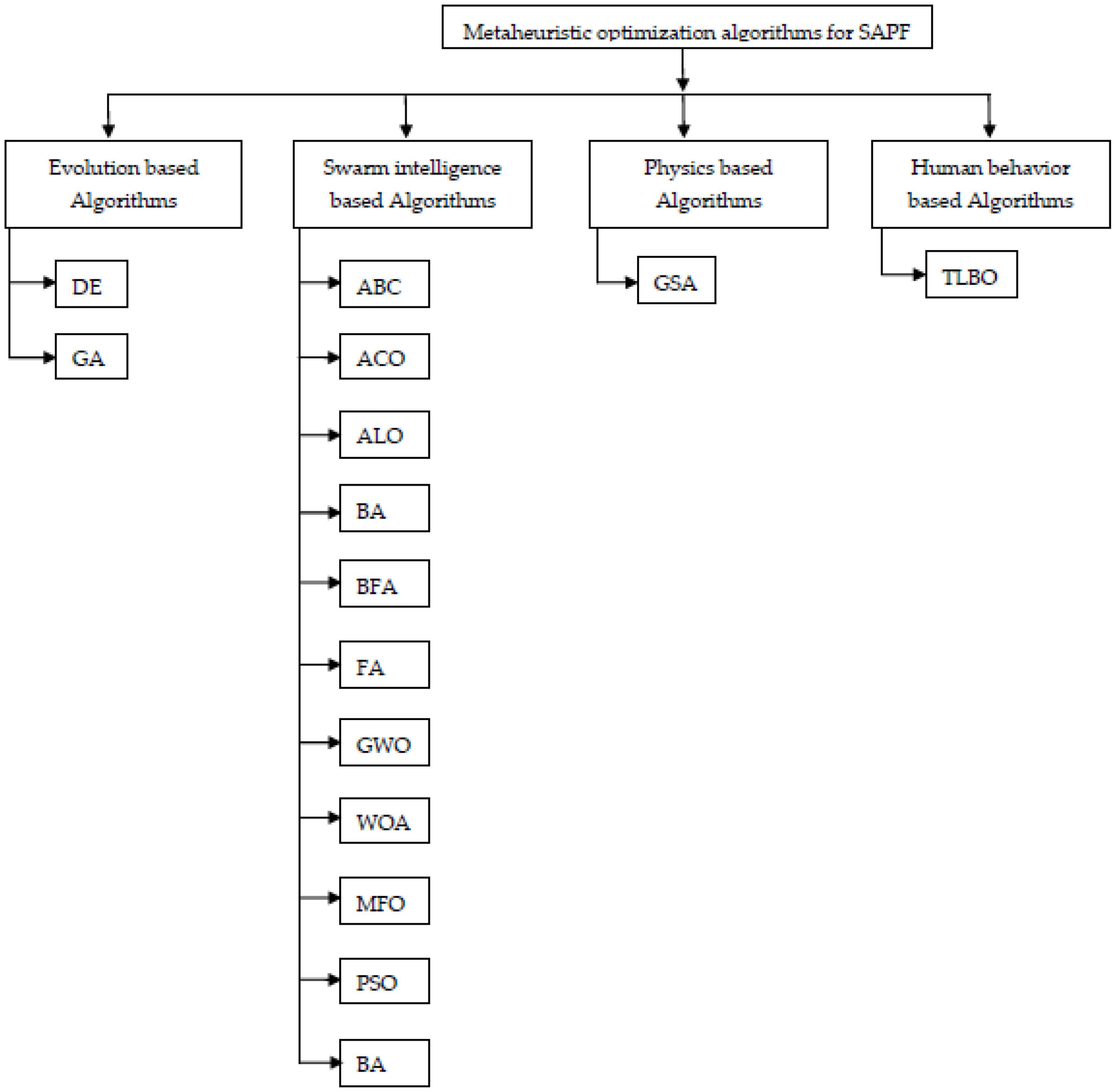

Figure 5. Meta-heuristic optimization algorithms for SAPF.

GAINS controller is controlled through parameter adjustment by PI parameter adjustment. The extent to which the search for reliable parameters is performed in the optimization process and the system performs well is due to the responsiveness of the operating cost function. The global search region is not clearly defined. The model will be stuck in the local minimum, and the optimal solution result will not be as expected. The following requirements must be met for the model to respond well. (1) Determine the exact benefit level of the PI control parameters (Equation (2)); (2) Apply the PI parameter to the NP adjustment levels, aiming to improve the gain of PI-MR (Equation (3)); and (3) search scope partitioning during DE optimization (Equation (4)).

$$G_{PI}(S) = K_{Pi} + \frac{K_{Ii}}{s} \tag{2}$$

$$G_C(s) = G_{PI+4R}(s) = K_P + \frac{K_I}{s} + \sum_{n=1}^{7} \frac{K_{rn}(s)}{s^2 + (n\omega_1)^2} \tag{3}$$

$$G_{rn}(s) = \frac{b_{rn}\left(1 - z^{-2}\right)}{d_1 z^{-1} + d_2\left(1 + z^{-2}\right)} \tag{4}$$

The total harmonic distortion in the SAPF controller compared with IEEE 519-2022 is 5% and reaches the lowest level of 3.42%, and the third, fifth, and seventh harmonic components are reduced compared to previous studies. The Levy flight method combined with the DE method improves local area search, this is considered a promising research direction to improve model accuracy, and another promising direction is combining with the neural network at the output of the DE model to choose the best estimator for the model.

Genetic Algorithms (GAs) Algorithms for SAPF

The Genetic Algorithms (GAs) technique incorporates fuzzy logic into the power supply current compensation time control via the SAPF controller, with the overall sinusoidal current control strategy (SCC) and total harmonics distortion control (THD) of current and voltage sources [71]. However, the results are limited compared to the method using CIPC; the result for SCC is THD_i is 0.41% and THD_v is 0.34%, and response time is 0.0032 s compared to for constant when applying GA-Fuzzy is THD_i is 0.41% and THD_v is 0.62%, and the response time is 0.0040 s [72]. The optimal value of the inductors in the SAPF filter is searched and determined by Gas [73,74]. The fuzzy logic control technique controls the voltage loop in the SAPF filter, and the Artificial Neural Network (ANN) technique controls and controls the operation of the SAPF to create a bias current that multiplies reactive power compensation, controls components harmonics generated in the current source while controlling the unbalance point in the source current, the GA-FL-ANN Combined Controller gives a THD_i of 0.99%, and a THD_v of 1.4% and a response time of 0.0058 s [75]. The compensating current-controlled GAs in the SAPF filter circuit improve the performance of reactive power compensation, control total harmonic distortion (THD) and speed up the frequency response [76].

The GAs technique applied to SAPF control in a three-phase PI factor control circuit seeks the optimal value of the dc-link capacitor and the optimal value of the inductor coupling (Figure 6). The processing system depends on the SAPF controller values, which are the dc link capacitor parameter values, the coupled inductor parameter values, the current controller parameter values, and the voltage source of the power circuit [71,72]. Taking a lot of time to process parameter adjustment in SAPF, GAs also has some benefits such as ease of understanding, ease of design and ease of implementation. Several parameters of SAPF optimized the minimum value of the total harmonic distortion (THD) to select the fitness value from the objective function (Equation (5)).

$$THD = f\left(L_f, C_{dc}, V_{dc}^*, K_{pC}, K_{iC}, K_p, K_i\right) \tag{5}$$

With: Inductor L_f, DC link voltage C_{dc}, DC link voltage V_{dc}^*, K_{pC}, K_{iC} of the PI DC link voltage, K_p, K_i of the PI current controller.

The GA code for optimizing objective function step-by-step is shown in Table 5; the population is the collection of individual parameters into a solution to the problem. Initially, a population is generated naturally from basic GA parameters, including chromosome length and population size.

Table 5. GAs code for optimizing.

Step	Step-By-Step Explanation of the GA Method
Step 1:	Determining the ranges of the parameters; the upper and lower bound
Step 2:	Set the value
Step 3:	Set population size
Step 4:	Set the initial population by random within the space of parameters
Step 5:	Set maximum numbers of generations
Step 6:	Set the selection process following the tournament method, mutation, and crossover

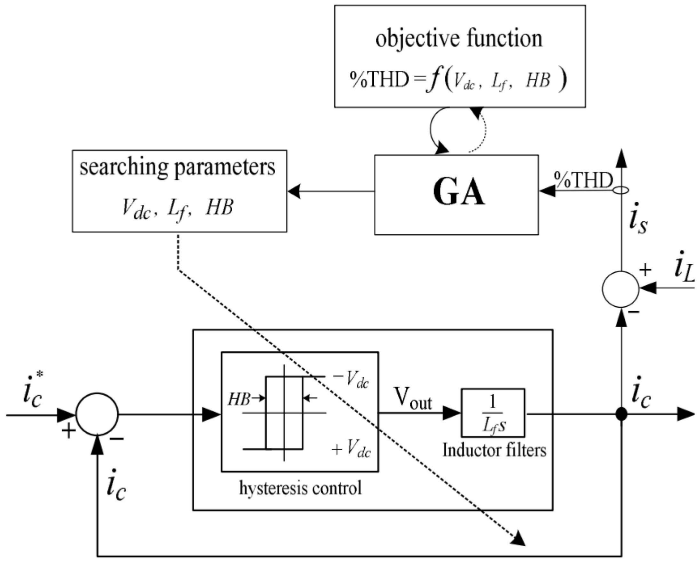

Figure 6. The GA approach for SAPF.

The GA working principle for optimizing the parameters of SAPF is illustrated via the flowchart shown in Figure 7.

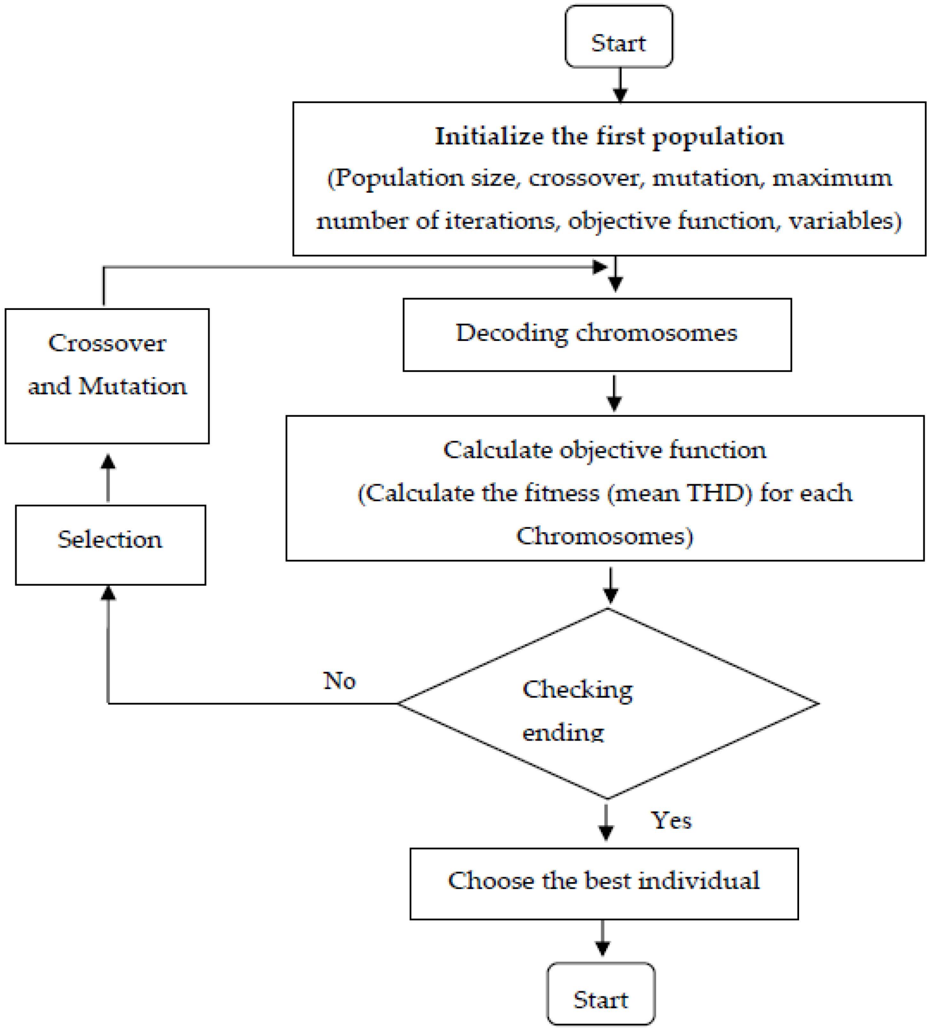

Figure 7. The flowchart of the GAs Algorithm.

The GA algorithm is based on natural selection and genetics. Chromosomes convert decision variables into coding alphabetic sequences of finite length and the fitness function GAs (Equation (6)). ISE = integrate square error between actual capacitor voltage and reference dc voltage.

$$ISE = \int_0^T \left(V_{ref} - V_{dc}\right)^2 \tag{6}$$

The strength of GA is that it is possible to fine-tune the PI controller to achieve the optimal gain value for SAPF conversion. GA performs global optimization and fitness functions because of SAPF's corresponding transition state selection. The switching state is coded and selected by the fitness function linking the cost function to the output current fault input reactive power system making the SAPF easy to handle.GA combined with SAPF achieves noise-free performance with a balance condition. GA demonstrates the ability to localize regions of high efficiency in complex domains without the difficulties associated with signal highs.

The SAPF controller generates many uncertain and time-varying parameters. For the GAs technique to give good results, the ANN technique combined with GAs is a good direction to improve the performance of the model [76]. GA techniques can also be combined with other algorithms in meta-heuristics, such as the Bee familiarization method (QBGAs), to improve model performance [77].

3.2.2. Swarm Intelligence-Based Algorithms

Between 1992 and 2021, Swarm Intelligence-based Algorithms has a total of 38 algorithms developed. Up to now, 11 algorithms have been deployed to harmonic mitigation for shunt adaptive power filters. Specifically, Artificial Bee Colony (ABC) Algorithm, Ant Colony Optimization (ACO), Ant Lion Optimizer (ALO), Bat Algorithm (BA), Bacterial Foraging Algorithm (BFA), Firefly Algorithm (FA), Gray Wolf Optimization (GWO), Whale Optimization Algorithm (WOA), Moth Flame Optimization (MFO), Particle Swarm Algorithm (PSO), and Bees Algorithm (BA).

Artificial Bee Colony (ABC) Algorithm for SAPF

Implement the Artificial Bee Colony (ABC) algorithm to remove harmonics in power circuits by solving nonlinear equations and turning seven power supplies to perform direct isolation of unequal power sources [78]. In 2005, Dervis Karaboga was inspired by the foraging behavior of honeybee swarms, based on a multi-dimensional, multi-modal hyper-simulation and optimization process, and applying a mathematical model of neighborhood search combined with random search. There are three main groups of bees that perform foraging behavior: hired bees, observation bees and scout bees. The work is specified as follows, the global foraging work is performed by observation bees and scout bees, and the purpose is to find random food sources and find out which areas have the most nectar [79,80]. The procedure for applying the ABC algorithm to the shunt adapter power filter is specified in the flowchart of the ABC algorithm (Figure 8). The ABC algorithm performs SHE optimization of the cascaded seven-level inverter. The DC voltage sources are assumed to be unequal and determine the magnitude value of the parameter Ki and the ABC algorithm code step-by-step (Table 6).

ABC algorithm is applied to current control in photovoltaic (PV) system to improve frequency, improve fast response and estimate input amperage of phase-locked loop (PLL) model and adjust the parameters K_p, K_i, K_v, and K_o. Another application of the ABC algorithm is to control the predictive current to control the future value and select the best switching state for the power converter. An application of the ABC algorithm is to modify the three-phase PLL to prevent DC error of the three-phase bridge input signal. The loop adjusts this quantity to zero and converts the φ value to the θ value. Values in DC power, such as $(d_a,\ d_b,\ d_c)^T$, will overlap the value of V_d and if an imbalance occurs when the DC compensation will generate the same frequency error. An ABC algorithm applied to the shunt adaptive power filter circuit to perform the reactive power compensation operation in the power supply mistakenly reduces the harmonics generated by the DC electric motor as the main cause. The ABC algorithm performs the search for the controller parameters. The performance of the ABC-SAPF filter gives better results than the ANN-SAPF filter or the Fuzzy Logic-SAPF filter [76,81].

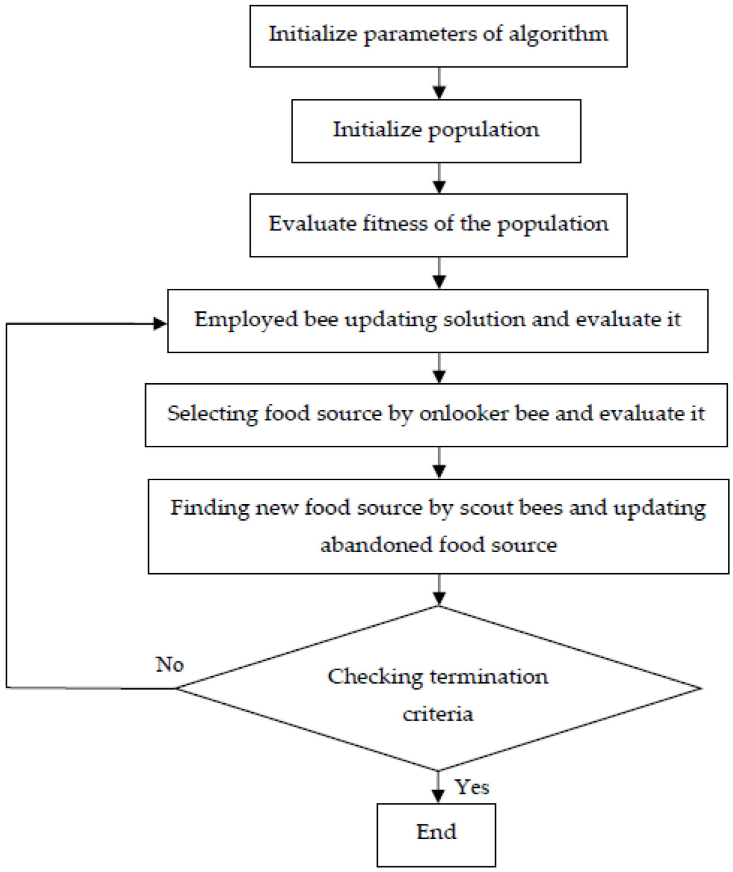

Figure 8. Flowchart of Artificial Bee Colony (ABC) algorithm.

Table 6. The ABC algorithm code step-by-step.

Step	Step-By-Step Explanation of the ABC Algorithm Method
Step 1:	Parameters are set like colony number, size, the value of limits, restrictions and maximum number of cycles for foraging
Step 2:	Initial conditions of level 2 of the algorithm like $(\theta = [\theta_1 \theta_2 \theta_3])$, with constraints set up for each bee at random (Equation (7)). $$0 < \theta_i < \frac{\pi}{2};\ \theta_1 < \theta_2 < \theta_3 \quad (7)$$
Step 3:	The function value is established (Equations (8) and (9)) $$f(i) = \left(100\frac{V_1^* - V_1}{V_1^*}\right)^4 + \frac{1}{5}\left(50\frac{V_5}{V_1}\right)^2 + \frac{1}{7}\left(50\frac{V_7}{V_1}\right)^2 \quad (8)$$ $$Fitness(i) = \frac{1}{f(i)+1} \quad (9)$$ where V^*: The desired value of the input voltage source and $f(i)$: The i-th root obtained in the cost function.
Step 4:	Establish a foraging process for hired bees, observers and scout bees. There, the role of the hired bees is to search and evaluate the quality of the found food source; if the food source is unsatisfactory, they store it in memory and start looking for a new and better food source, and they divide this information to the observer bees in the hive.

Table 6. *Cont.*

Step	Step-By-Step Explanation of the ABC Algorithm Method
Step 5:	bees observe, receive information, evaluate the information received and choose a quality food source. They then pass the information back to the swarm, and together they rate the quality of the nectar and compare it to the quality of the previous nectar. Where the quality of the nectar is better than the quality of the previous nectar, they switch to a source with better quality nectar. At the same time, they also change the memory of the old nectar information (Equation (10)). $$P(i) = \frac{\alpha \times Fitness(i)}{max(Fitness) + b} \quad (10)$$ With, *i*: is the *i*-th food source. *P*(*i*): Probability that the observed bee chooses a food source.
Step 6:	The old food source is also removed and improved with a new food source after each establishment, and this work is performed by scout bees.
Step 7:	Loop when reaching the maximum value, the algorithm terminates. Otherwise, the loop is updated next with the formula iter = iter + 1 and goes back to step 4 to continue executing the program.

The ABC method solves the nonlinear equation of the Harmonic and Selective rejection sample considering unequal DC current sources. The ABC method classifies the fundamental components that respond to the rejection of low-order harmonics. ABC method is one of the powerful and new evolutionary optimization patterns, finding optimized transformation angles with higher accuracy and higher convergence than others. The ABC algorithm determines the optimal switching angles and finds the optimal switching angles to generate the desired voltage. The ABC algorithm outperformed algorithms such as GA, PSO and BA in 30 runs with the same initial values according to the criteria of convergence and accuracy. ABC algorithm finds the optimal gain value of controller PI for SAPF for different errors as functional fitness variables. The ABC algorithm gives good results for monitoring the reference voltage and adjusting the PI for THD minimization. Stable dc-link voltage is in less than 1 cycle during transient load. ITSE is a performance indicator that shows better dynamic response harmonic compensation in a current source. ABC algorithm is a good tool to find the optimized gain of PI controller with ITSE as a fitness function.

Ant Colony Optimization (ACO) for SAPF

Ant Colony Optimization (ACO) is applied to Shunt Adaptive Power Filter (SAPF) with the goal of optimizing the gain K_p, K_i of the PI controller [82,83], and optimize the indicators of Integral Square Error (ISE), Integral Time Square Error (ITSE), Integral Absolute Error (IAE) and Integral Time Absolute Error (IATE) [84]. Dorigo (1992) introduced the ACO method based on the foraging behavior of ants used when foraging, such as (1) positive feedback, (2) distributed computation, and (3) constructive greedy heuristics. The goal of the ant colony's foraging behavior is to find the best solutions to discover the fastest food source, evaluate and select the best food source for the ant colony, prevent mistakes in choosing food sources, and choose the best method for the ants to find the best food source [84,85].

Artificial ants mimic the behavior of biological ants and find the best way to find food sources. The leader ant emits hormones; the ant follows the shortest distance, with many hormones remembering positive feedback. All the ants in the ant colony move at the same speed and send the same proportions of hormones [78]. The ACO modulating the K_p, K_i gain in the PI controller is depicted in the block diagram (Figure 9).

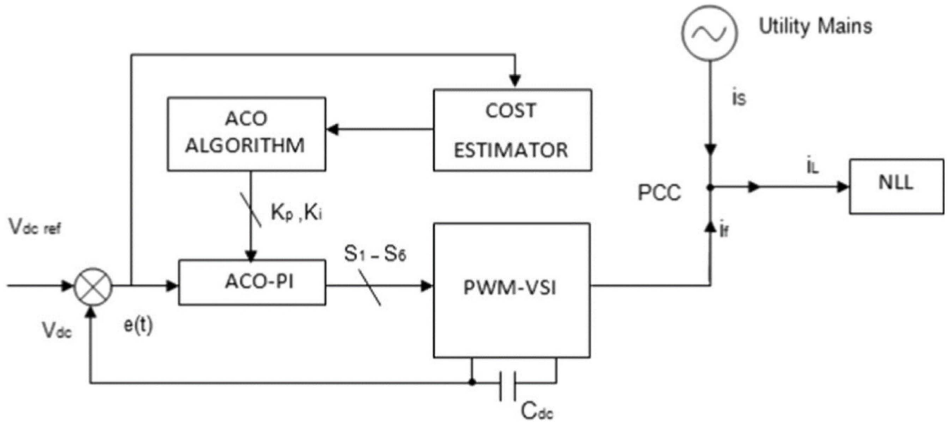

Figure 9. ACO tuning approach for SAPF PI controller.

The cost function $e(t)$ provides a mathematical model for ACO's optimal search. Each ant moves through the $K_p,\ K_i$ nodes, and the K_i search space for 100 nodes. Each node K_p in the range (0.1~1.0) and K_i in the range of 1–300 and is condensed in two different vectors. The goal of ACO is to find the path with the smallest cost function, that is, to find the most suitable $K_p,\ K_i$ parameters. Each ant is made to move according to the probability function. When the Kth ant moves to the *i*th position and builds each part S^p, according to the distribution law of the *K*th ant selected according to the *j* nut from the *i* nut. The distribution function is:

$$\rho_{ij}^{k} = \left\{ \frac{\left[\tau_{ij}^{\alpha}(n)\right]\left[\mu_{ij}^{\beta}(n)\right]}{\sum N(s^p)\left[\tau_{il}^{\alpha}(n)\right]\left[\mu_{il}^{\beta}(n)\right]} if C_{ij} \epsilon N(S^p) \right\} \tag{11}$$

where τ_{ij} *and* μ_{ij}: pheromone and metaheuristic intensity value index information between nodes *i and j*. Indexes $N(S^p)$ and l are the set values of nodes and paths that may not have been visited by ant k.

The ant deposit updates hormone value (Local hormone) according to Formula (12).

$$\tau_{ij}^{k}(n) = \tau_{ij}^{k}(n-1) + \left(\frac{0.2 * \alpha}{C}\right) \tag{12}$$

The global hormone is updated according to Formula (13).

$$\tau_{ij}(n)^{best} = \tau_{ij}(n)^{best} + \left(\frac{\alpha}{C_{best}}\right) \tag{13}$$

The negative hormone is updated according to Formula (14).

$$\tau_{ij}(n)^{worst} = \tau_{ij}(n)^{worst} - \left(\frac{0.3 * a}{C_{worst}}\right) \tag{14}$$

Global hormones are updated after each hour according to Formula (15).

$$\tau_{ij}(n) = \tau_{ij}(n)^{\partial} + \Delta \tag{15}$$

where $\tau_{ij}(n)^{best}$ and $\tau_{ij}(n)^{worst}$ is the hormone of the paths for the ant to follow in its search for a food source with the lowest cost (C_{best}) and maximum cost (C_{worst}) values. λ is the evaporation constant, and Δ is the sum of Formulas (13) and (14). The ACO algorithm for PI tuning is shown in Table 7.

Table 7. The ACO algorithm code.

Step 1:	*(Parameter Initiation)* SettherangeforK_p, K_i, tour = 0, m = 20, maximumtour = 100, $\alpha = 0.06$, $l = 0.95$
	For every combination (i, j)
	Set an initial value $\tau_{ij}(0) = 1$, $\Delta\tau_{ijlocal}(0) = 0$ *and* $\Delta\tau_{ijglobal}(0) = 0$
	End
Step 2:	*(Local Update Rules)*
	For $k = 1$ to m and choose K_p, K_i with a transition probability given in Equation (12).
	Calculate cost k
	End
	For $\forall(i, j)$
	For k = 1 to m
	For $\forall(i, j)$
	For k = 1 to m
	Update the pheromone using Equation (11)
	End
	End
Step 3:	*(Global update rules)* Update pheromone for best and worst tours of ant using Equations (11) and (12).
	Globally update pheromone using Equation (16)
	Tour = tour + 1
	If (tour < maximum tour)
	Go to step 2
	Else
	Print the best node values for the minimum cost function
	End

Details of the steps to implement the ACO algorithm in SAPF are described in Figure 10 in the flow chart of ACO for SAPF.

The ACO method performs optimal tuning of the membership functions and normalized gain in SAPF. The ACO method is a choice for an effective DC link voltage to compensate for harmonic currents in the power supply [86]. The ACO algorithm is the best for the controller, and satisfactory performance is an effective solution for the growing energy demands now and in the future. Ant colony optimization (ACO) is a technique that optimizes the gain values of the PI controller used in the Shunt Active Power Filter (SAPF), improving its dynamic performance [87]. The minimization of Integral Square Error (ISE), Integral Time Squared Error (ITSE), Integral Absolute Error (IAE), and Integrated Time Absolute Error (ITAE) are considered functional costs of the ACO-SAPF system and the ACO method improve the resolution time (Ts) with ISE as the cost function.

Ant Lion Optimizer (ALO) for SAPF

ALO is implemented in SAPF to adjust the control parameters and K_P K_I in the PI controller to adjust the compensatory current for the power supply in order to reduce harmonic according to IEEE 519-2022 standards for both power and current on the load [88]. ALO implements the gain and loss adjustment method of the PI controller to adjust the required DC current at the output and meet the required voltage compensation on the power supply [89]. The synchronous and theoretical P-Q reference method is implemented in the circuit to generate a suitable compensating current [90,91].

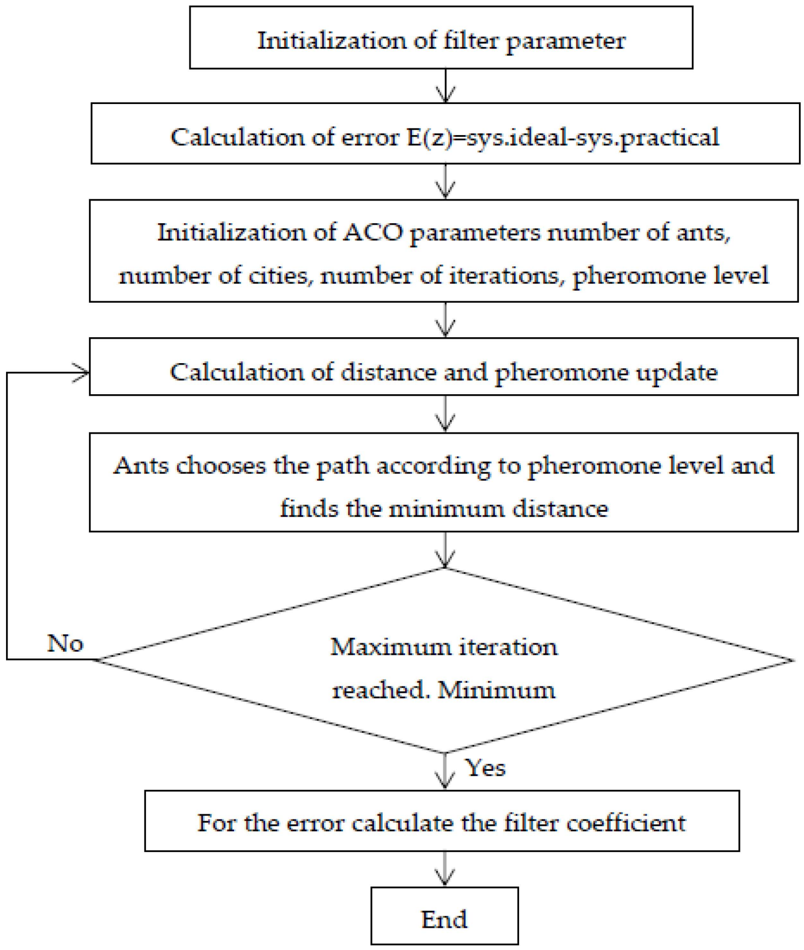

Figure 10. Flow chart of ACO for SAPF.

ALO uses two search agents, including ant lions and ants, in a swarm. Ant lions are always looking for the best food element, and their location is always known to be fixed. Ants in the swarm are always free to move in space foraging and are likely to be caught when trapped in a wormhole [90]. The position of Ants in the swarm is done according to Formula (16).

$$Ant_j^k = \frac{P_A^K - P_E^K}{2} \quad (16)$$

where P_A^K represents the nearest random path of the Ant lion. P_E^K represents the position of the *i*th ant closest to the ant lion in the E group of the ant.

The distance between ant j and ant lion g after ant j moves in loop K is determined by Formula (17).

$$M_g^K = \frac{(w_j - r_j) * (d_j - C_j)}{\left(b_j^K - r_j\right)} \quad (17)$$

where r_j, b_j determines the largest and smallest steps of ants in the foraging zone of size *K*. *C*, *d* the random walk region of ant j and the maximum and minimum limits of the threshold are in the range [0.5].

In the natural environment, ants roam randomly around in search of food sources. This behavior is expressed by Formula (18).

$$X(it) = [0, cusu(2r(it_1)),\ cus(2r(it_2)), \ldots, cusu(2r(it_n) - 1)] \quad (18)$$

where *cusu*: cumulative sum spending time $r(it)$ and is valued according to Formula (19)

$$r(it) = \begin{cases} 1, & if\ rand > 0.5 \\ 0, & if\ rand\ \leq 0.5 \end{cases} \tag{19}$$

The antlion senses that prey has entered the hole. The antlion throws sand to reassemble the prey and captures the prey into the hole. This action is described by Formulas (20) and (21).

$$C^{it} = \frac{C^{it}}{10^{w} \cdot \frac{it}{it_{max}}} \tag{20}$$

$$d^{it} = \frac{d^{it}}{10^{w} \cdot \frac{it}{it_{max}}} \tag{21}$$

where C^{it}, d^{it}: the low and high variables are converged. W: the constant is fixed at the current loop and is determined by Formula (22).

$$w = \begin{cases} 2,\ if it > 10\%.\ it_{max} \\ 3,\ if it > 50\%.\ it_{max} \\ 4,\ if it > 75\%.\ it_{max} \\ 5,\ if it > 90\%.\ it_{max} \\ 6,\ if it > 95\%.\ it_{max} \end{cases} \tag{22}$$

The final stage is ALO traps the prey and stops the trap, and this action is built according to Formula (23)

$$Antlion_j^{it} = Ant_i^{it}; iff\left(Ant_i^{it}\right) > f\left(Antlion_j^{it}\right) \tag{23}$$

where $Antlion_j^{it}$: the jth chosen location of the antlion at ith. Ant_i^{it}:the ant's i-th position.

The pseudo-code (Algorithm 1) and flow chart of ALO for SAPF are shown in Figure 11.

Algorithm 1: The pseudo-code of the ALO Algorithm

Input (Set input data of SAPF. Set parameters of ALO)
K = 1
Create 3 initial sizes of ant and ant lion are $K_p,\ K_i,\ G_\alpha$
Run SAPF with $K_p,\ K_i,\ G_\alpha$ and evaluate the fitness function value of ants and ant lions
Identify the best ant lion
While $K \leq K_{max}$ do
    For i = 1 to the number of agents, do:
        Choose the antlion based on the movement circle
        Update the position of ants according to Formulas (18) and (19)
        Update the location of the antlion (update the $K_p,\ K_i,\ G_\alpha$ value) according to Formula (17).
        Run SAPF updates the $K_p,\ K_i,\ G_\alpha$ value and evaluates the fitness function value of the ant lion
        Substitute the antlion with ants according to Formula (24)
        Update elite position
        K = K + 1
    End for
End while
Return optimization elite
Output: Print optimization gains $K_p,\ K_i,\ G_\alpha$ of the PI controller in SAPF according to the optimal elite value

The objective function $f(g)$ performs error minimization of the two gains, K_P and K_I, of the PI controller according to Formula (24).

$$f(g) = ITSE = f(q,t) = \int_0^\infty e^2(q,t)tdt \tag{24}$$

where *ITSE* = Integral Time Square Error. ITSE extracts and provides data for ALO to optimize the parameters of gain, K_P and K_I, of the PI controller. The *error*(e) of the index showing the agreement between the reference voltage $V_{dc,ref}$ and the voltage of the capacitor V_{dc} is shown by Formula (25).

$$Error(e) = V_{dc,ref} - V_{dc} \tag{25}$$

The gain controller K_P, K_I is determined according to Formula (26). Gain Control (GC) is a closed-loop feedback regulating circuit in an amplifier or chain of amplifiers to maintain a suitable signal amplitude. The average or peak output signal level is used to dynamically adjust the gain of the amplifiers, allowing the circuit to work satisfactorily with a greater range of input signal levels.

$$q = \left(K_p, K_i\right)^T \in M \tag{26}$$

where M is a positive real value index.

The foraging space is expressed by Formula (27).

$$S = \{q \in M,\ q_{min} \le x \le q_{max}\} \tag{27}$$

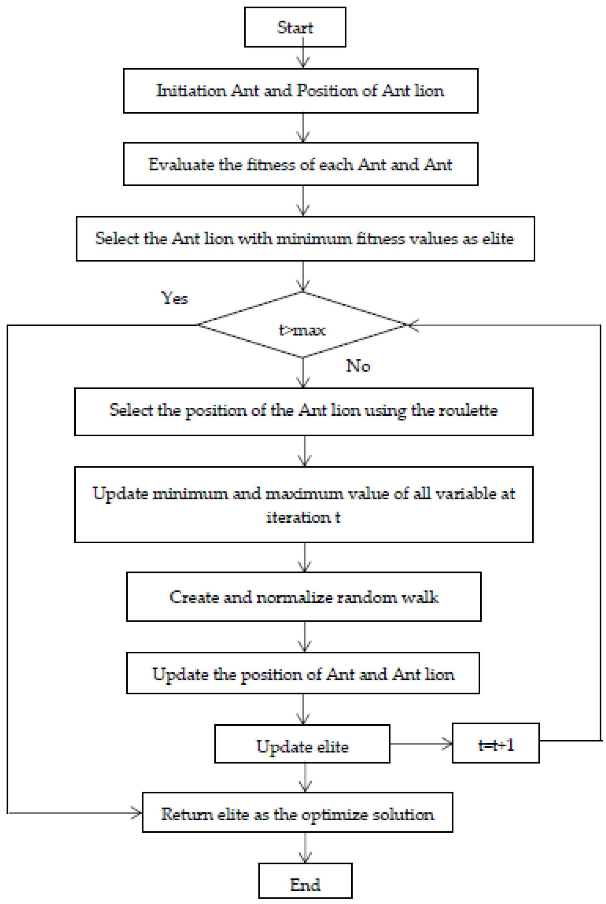

Figure 11. Flow chart of ALO for SAPF.

The ALO method searches for the parameter values of K_p and K_i that achieve the minimum value of the fit function, then is provided as the optimal parameter at the output of ALO-SAPF. The goal is to reduce the maximum overshoot and lower the DC-link voltage with reduced power ripple and as low THD as possible. The ALO method properly adjusts the circuit to reduce harmonics in the source current and load voltage, adjusting the gain of the controller to adjust the required DC output voltage. The ALO method is used to extract the optimal values of frequency and increase the PI voltage of the PI controller in SAPF. The reception ALO algorithm maintains sinusoidal patterns for the source current waveform with a good terminal voltage and frequency within a limited range under unbalanced and variable load conditions. THD is less than 5%. The reception control algorithm with ALO integrated into SAPF is very efficient in terms of power quality.

Bat Algorithm (BA) for SAPF

BA is implemented into SAPF, which performs DC voltage rectifier controller optimization and reactive power theory and P-Q theory used to extract the reference current of the power supply [92].

BA builds on the bat's perceptual behavior by using echolocation to recognize and classify food sources and barriers. Bat's velocity speed (V_i) and Bat's position (X_i), Bat's broadcast frequency (F_{min}), the wavelength of echo (∂) and reverberation (A_0) during the search for food sources. The magnitude of A_0 is calculated according to the A_{min} constant. BA adjusts the DC index value to optimize the PI controller. However, BA is limited by the foraging region (in this case, the tuning parameters K_P and K_i in the PI controller) [93].

BA follows two main activities, including exploration and exploitation. Exploration to find new solutions is given by Formula (28), and exploitation to search for food sources in the vicinity is given by Formula (29).

$$X_i(t+1) = X_i(t) + V_i(t) \tag{28}$$

$$X_{new} = X_{old} + \epsilon \times A_0(t) \tag{29}$$

BA pseudo codes are done in the following steps (Table 8).

Table 8. BA Algorithm code.

Step	**Step-By-Step Explanation of the ABC Algorithm Method**
Step 1:	Establish the function of the bat according to the formula F.
Step 2:	Initialize functional variables, including upper bound information and lower bound information of each bat, number of bats, maximum number of repetitions, and number of variables looking for food sources. Each bat has different upper and lower bound parameters in the foraging zone.
Step 3:	Call and Find the initial value of the objective function
Step 4:	The maximum number of repetitions is to be performed from the start of the main loop, and the frequency is randomly chosen according to Formula (30). $F(i) = F_{min} + (F_{max} - F_{min}) \times rand$ (30)
Step 5:	Update the speed and position of the bat. After each update of the upper and lower bound values, the new position of the bat is updated according to Formula (31). $X_{new} = \left(X_{old} + \left(X^+ - X^-\right)\right) + ub \times X^+ + lb \times X^-$ (31)
Step 6:	Check the pulse rate of each bat. The random step size limiting factor is 0.001.
Step 7:	Recalculate the fitness value after optimization according to Formula (32). Plot the convergence curve for the best fit and repeat. The best position is also called the optimized value. $F_{min} = fitness_{new}$ (32)

The results of applying BA to SAPF (Figure 6) and THD coefficient = 0.7% meet the requirements of IEEE 519-2022 standard. The objective function is for the optimization controller parameter, according to Formula (33).

$$F = min\left(min(ITAE) + min(T_r) + min(T_s) + min\left(M_p\right) + min(e_{ss})\right) \tag{33}$$

where $ITAE$: Integral Time Absolute Error, T_r : rise time, T_s: setting time, M_p : peak overshoot, and e_{ss} : steady state error.The flow chart of BA for SAPF is shown in Figure 12.

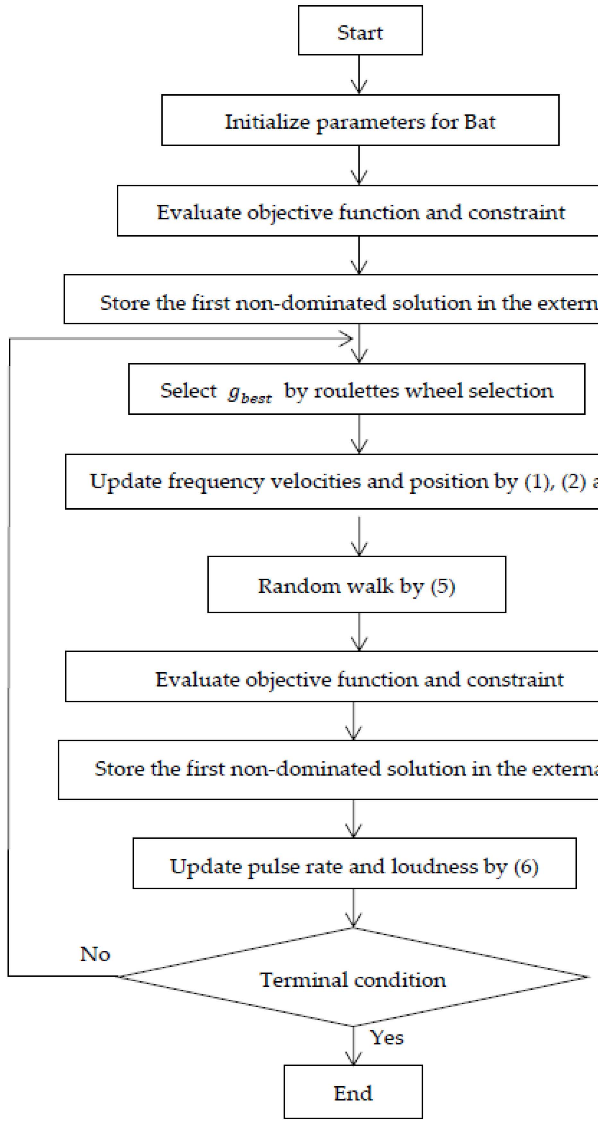

Figure 12. Flow chart of BA for SAPF.

The BA method performs dc-link voltage regulator optimization. The stability of the current controller with the SAPF system is a mathematical model evaluated in terms of time and frequency area. The BA method implements a PI controller to adjust the harmonic current in SAPF theoretically analyzed for stability and suitability; dc-link optimization performs well harmonic harmonization and reactive power consumption of the load. The harmonics in the current are effectively suppressed by the SAPF, the reactive power required by the load is compensated by the SAPF, and the power supply operates the power required by the load and the inverter losses. A faster SAPF dynamic response is achieved to sudden load changes of nonlinear loads.

Bacterial Foraging Algorithm (BFA) for SAPF

BFO deployed in SAPF adjusts the control coefficients KP and KI of the PI controller (Figure 13) to provide compensatory power for the power system to improve the quality of power supply for balanced loads and unbalanced [94,95]. The results show that the THD = 1.37% value is within the IEEE 519-2022 standard.

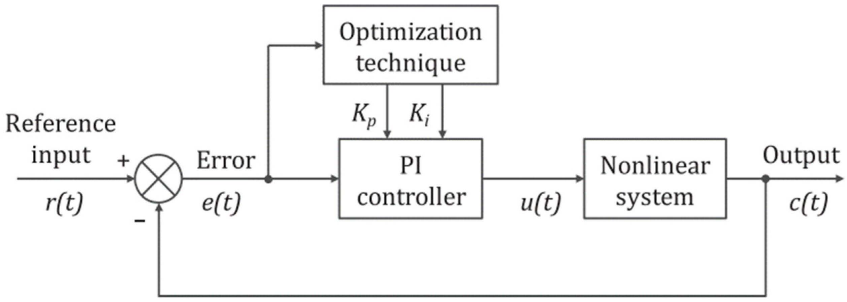

Figure 13. Block diagram of BFO for PI controller.

BFO was built inspired by microbial foraging with the goal of optimizing bacterial energy consumption per unit of time (T). BFO works by four observed mechanisms of micro-emergent, including chemotaxis, swarming, reproduction, and elimination or dispersal [96,97]. The four mechanisms of action of BFO are explained as follows (Table 9).

Table 9. BFO Algorithm code.

Step	Step-By-Step Explanation of the BFO Algorithm Method
Step 1:	(Chemotaxis): bacteria move to find a source of more nutrients in the intestines thanks to the mechanism of bladder action in directions such as swimming or somersaults. Assume $\theta^i(j,k,l)$ is the ith bacterium in the jth trophic zone, the kth spawning zone, and the lth elimination dispersal step. The bacteria in motion were calculated according to Formula (34). $$\theta^i(j+1,k.l) = \theta^i(j,k,l) + C(i)\frac{\Delta(i)}{\sqrt{\Delta^T(i)\times\Delta(i)}} \quad (34)$$ where $C(i)$ is the size of a single step and movement in a random direction, and $\Delta(i)$ is the vector in an arbitrary direction of the elements in the range [−1, 1].
Step 2:	(Swarming): bacteria move in swarms with high density in the activity of sourcing nutrients through mechanisms of attracting and repelling substances given by Formula (35). $$J_{cc}(\theta(i,j,k,l)) = \sum_{i=1}^{S} J_{cc}\left(\theta,\theta^i(j,k,l)\right) = = \sum_{i=1}^{S}\left[-d_{attractant}exp\left(-w_{attractant}\sum_{m=1}^{p}\left(\theta_m-\theta_m^i\right)^2\right)\right] + + \sum_{i=1}^{S}\left[h_{repellant}exp\left(-w_{repellant}\sum_{m=1}^{p}\left(\theta_m-\theta_m^i\right)^2\right)\right] \quad (35)$$ where $J_{cc}(\theta(i,j,k,l))$ is the objective function used to optimize goals over time. $S:$ Totalnumber of bacteria in the population. p is the optimization variable and $\theta = \left[\theta_1,\ \theta_2,\ldots,\theta_p\right]^T$ is a point in the $p-$ dimension in the search for nutrients. $d_{attractant},\ w_{attractant},\ h_{repellant},\ w_{repellant}$ are measures of the number, rate of diffusion, and strength of the forward and backward effects of bacteria, respectively.
Step 3:	(Reproduction): the acclimatization value of bacteria i in NC migration and calculated according to Formula (36). $$J_{health}^i = \sum_{j=1}^{N_c+1} J^i(j.k.l) \quad (36)$$ where J_{health}^i is the health of the representative ith bacterium. The healthy bacteria eventually eliminate other healthy bacteria, and the population stays the same in the end.

Table 9. *Cont.*

Step	Step-By-Step Explanation of the BFO Algorithm Method
Step 4:	(Elimination or Dispersal) : the bacteria are removed and dispersed with probability p_{ed} after the N_{re} spawning event with the goal that the bacteria are not trapped and ensure that the local optimum replaces the global optimal. The objective function is optimized following Formula (37). $$J = \int_0^t (\Delta V_{dc})^2 dt = \beta * \Delta V_{dcmax} + (1-\beta)(t_s - t_0) + \alpha * \lvert E_{ss} \rvert \quad (37)$$ where α: steady − state voltage error correction index $E_{ss.}$ β is the decisive index of the value of voltage (ΔV_{dcmax}). t_s is the maximum value of β without overshoot, and t_0 is the start time, t_s is the steady-state time of the transition period.

The BFO method gives optimal results that outperform traditional methods by ensuring excellent SAPF functionality and rapidly overpowering harmonics in the current source, even when the power supply is unbalanced [98]. The BFO method is implemented to adjust the coefficients of the PI controller in SAPF to improve the performance of the power system under balanced and unbalanced supply voltage conditions. The dc link voltage is stable for about one cycle, and also the voltage variation is less than that of conventional PI controllers. The BFO-SAPF method performs harmonic rejection and function superior to the PSO-SAPF method and has excellent functional confirmation of its superior and powerful harmonic compensation.

Firefly Algorithm (FA) for SAPF

Predator-Prey-based firefly optimization (PPFO) is implemented into SAPF to select the appropriate compensation current to provide compensation for the loss of mains current to improve power quality [99,100]. Shape the sine wave shape of the power supply for balanced and unbalanced loads. The results for the THD = 1.909% index belong to the IEEE 519-2022 standard [99].

PPFO is inspired by the flickering light of fireflies to explore and exploit food sources in the search for food sources [101]. The proposed problem variables form fitness functions, and these variables formed in SAPF include C_{dc}, $V_{dc,ref}$, L_f, R_f, K_p, and K_i and randomly generate a swarm of fireflies from initialization. Each firefly represents an optimal solution in the foraging zone and has as many dimensions as the number of designed variables. Each firefly is parameterized according to Formula (38).

$$f = \left[C_{dc}, V_{dc,ref}, L_f, R_f, K_p, K_i\right] \quad (38)$$

The final search area space is limited according to Formula (39)

$$f^K(min) \le f^K \le f^K(max),\ K = 1, 2, \ldots, n \quad (39)$$

A mathematical model is established from bioluminescence communication to change into the motion of fireflies in the foraging space. Every firefly is mesmerized by other fireflies'brightness, and they try to fly toward where the light is. Firefly's brightness has an impact on the efficiency of the designed problem point [99,101]. In repeating theprocess, the algorithm model is evaluated by each firefly's brightness and attractiveness, and the position value of the firefly is updated based on these values. The brightness function (BFun) is made to reduce total harmonic distortion (THD) and is calculated by Formula (40).

$$MaximizeBFun = \frac{1}{1 + THD} \quad (40)$$

Attractiveness of the i^{th} and j^{th} fireflies are shown by Formula (41).

$$\beta_{ij} = \beta_0 \exp\left(-\gamma {r_{ij}}^2\right) \quad (41)$$

where r_{ij} is the distance between the i^{th} and j^{th} fireflies calculated by Formula (42).

$$r_{ij} = ||f_i, -, f_j|| = \sqrt{\sum_{k=1}^{n} (f_i^k - f_i^k)^2} \quad (42)$$

The flow chart of BFO for SAPF is shown in Figure 14.

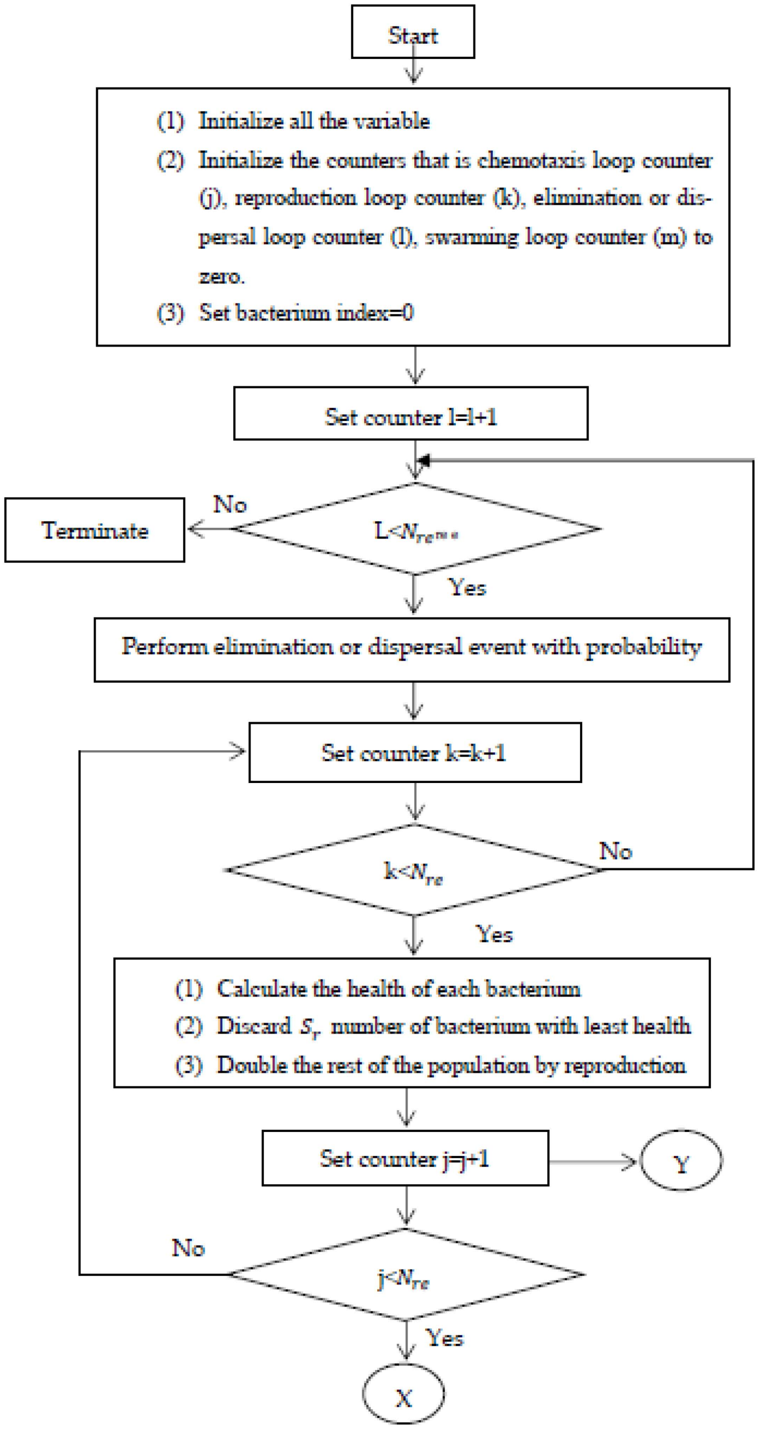

Figure 14. *Cont.*

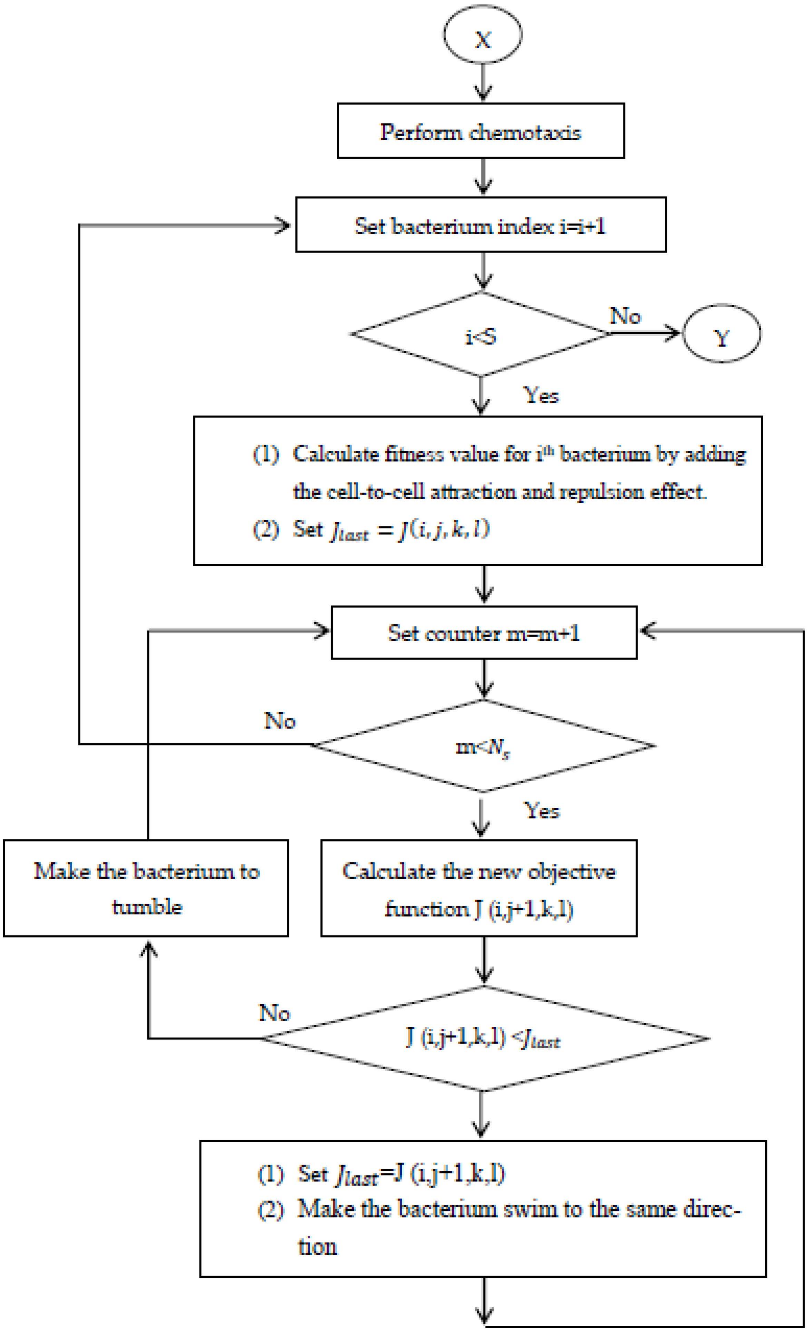

Figure 14. Flow chart of BFO for SAPF.

In the swarm, the i^{th} firefly flies to the j^{th} firefly and updates the position change in case the $BFun_j$ value is greater than the $BFun_i$ value at time t and is calculated by Formula (43).

$$f_i(t) = f_i(t-1) + \beta_{ij}\big(f_j(t-1) - f_i(t-1)\big) + \alpha(rand - 0.5) \tag{43}$$

The common fireflies (prey) are attacked by predators, and they often find places where there are no enemies and see this as a better position.

Enemies help fireflies explore the search area more efficiently, and enemy hunting is done probabilistically (μ). This enemy is modeled by Formula (44).

$$f_{predator}(t) = f_{worst}(t) + \rho\left(1 - \frac{1}{T_{max}}\right) \tag{44}$$

Firefly is always looking for a way to stay away from its enemies and is modeled by Formula (45).

$$f_{(t+1)} = f_{(t)} + \rho.e^{-|d|}, \text{ if} d > 0$$
$$f_{(t+1)} = f_{(t)} + \rho.e^{-|d|}, \text{ if} d < 0 \quad (45)$$

PPFO does not converge in the search area but improves detection and population enhancement to enhance the best possible global solution. The solution starts with generating random values within the corresponding limit for each firefly in the population. Based on the BFun value, the firefly moving to the side with the best light represents the better solution [102,103]. The enemy chases the fireflies based on the probability of the fireflies escaping and getting out of the suboptimal trap. This process is repeated until convergence. The pseudo-code of PPFO is shown in Table 10.

Table 10. PPFO algorithm code.

Step	Step-By-Step Explanation of PPFO Algorithms
Step 1:	Read the problem data
Step 2:	Choose parameter ϱ, nf, β_0, α, ...
Step 3:	Generate the initial population of fireflies as represented by Equations (38) and (39)
Step 4:	Set the iteration counter $t = 0$
	While termination requirements are not met, do
	For $i = 1 : nf$
	Assign the value of the i^{th} firefly as a design parameter in the Simulink model of SAPF.
	Run the Simulink model and compute THD
	Evaluate $BFun_i$ using Equation (40)
	For $j = 1 : nf$
	Assign the value of the j^{th} firefly as a design parameter in the Simulink model of SAPF.
	Run the Simulink model and compute THD
	Evaluate $BFun_j$ using Equation (40).
	If $BFun_i > BFun_j$
	Compute r_{ij} using Equation (42).
	Evaluate β_{ij} using Equation (41).
	Move j^{th} firefly toward i^{th} firefly through Equation (43).
	End if
	If rand < n?.
	Hunt j^{th} firefly using Equations (44) and (45).
	End
	End-(i)
	End-(j)
	Rank the fireflies and find the current best and worst fireflies.
	End-(while)
	The firefly possessing the largest brightness is the optimal solution.

Predator-prey-based firefly optimization (PPFO) adjusts the gain parameters of the PI controller in SAPF to provide high efficiency in current selection operation to compensate for distorted current in power supply due to wave comedy caused [104]. PPFO guarantees global value optimization and does not depend on optimization traps. PPFO is designed with the FO function to avoid optimization traps during problem optimization in SAPF. Parameters such as C_{dc}, $V_{dc;ref}$, L_f, R_f, k_p, and k_i are designed as variables in SAPF and are necessary problems for PPFO to perform their optimization. The results of optimal implementation of the above parameters in SAPF show that PPFO selects and provides an appropriate compensating current to compensate for the disturbed current in the power system that the harmonics generate and shapes the sine wave shape of the power source to improve the power quality.

3.2.3. Spider Net Search (ASNS) for SAPF

Spider Net Search is used to optimize the controller used in shunt adaptive power filters (SAPF) in balanced and unbalanced conditions [105]. Source current is controlled by standard sinusoidal control and givesthe load; the results of THD_I and THD_v are 1.21%, 1.42%, 1.11%, 2.93%, 3.44%, and 3.48%, respectively. All of them meet the IEEE 519-2022 standard.

The three-phase power system supplies balanced, unbalanced, and distorted loads with a 50 Hz frequency and voltage source. The SAPF circuit performs the function of compensating the current for the power source when the source current is lost. The adaptive Spider Net Search (ASNS) algorithm solves complicated math problems. ASNS performs a discretization of the search space and performs a reverse search of them in that space. The search performance of the ASNS method is correspondingly enhanced within the radius of search space. ASNS is proposed to search for the optimal K_p and K_I values in the PI controller [106,107].

First, the surrounding values of K_p , K_I are the highest and lowest levels. Next, the radius value, ASNS rollback condition.The objective function and stopping criterion are defined at specific lines.A random value of K_p , K_I is placed in the hexagon to set the initial value. The optimal value will be updated, replacing the original value after each iteration. This process stops when the stopping criterion meets the most optimal value level.

The evaluation function of research is the THD power index. The aim is to find the lowest THD value and the shortest computation time algorithm. Algorithm's reliability is evaluated the less computation time. Standard equation of the K_p , K_I is set according to the setting time ($T_{setting}$), rise time (T_{rise}), and percentage overshoot ($P.O$) is used for the objective function, Formula (46).

$$O.F(T_{rise}, T_{setting},\ P.O) = R(T_{rise}) + S(T_{setting}) + P(P.O) \tag{46}$$

with: $R + S + P = 1$, where R, S, and P are the priority factors of T_{rise}, $T_{setting}$, and $P.O$. The ASNS algorithm is explained in Table 11, and the flow chart of ASNS for SAPF is shown in Figure 15.

Table 11. ASNS algorithm's code.

Step	Step-By-Step Explanation of ASNS Algorithms
Step 1:	The first value of K_p , K_I is set to 0, and the value of K_p , K_I is updated after each iteration
Step 2:	The value of the objective function is calculated according to the first value of K_p , K_I
Step 3:	The objective function value of ASNS is compared to step 2 and updated at the first corner starting from the left of the hexagon
Step 4:	If the value does not meet the optimal level, the value automatically updates to the value of K_p , K_I and replaces the objective function. Then, turn back to step 3
Step 5:	If the value meets the optimal level, ASNS is selected as the optimal solution and saved in the best solutions list
Step 6:	If the loop runs to the end, the value will be updated for K_p , K_I. Then, update the objective function and reperform step 3

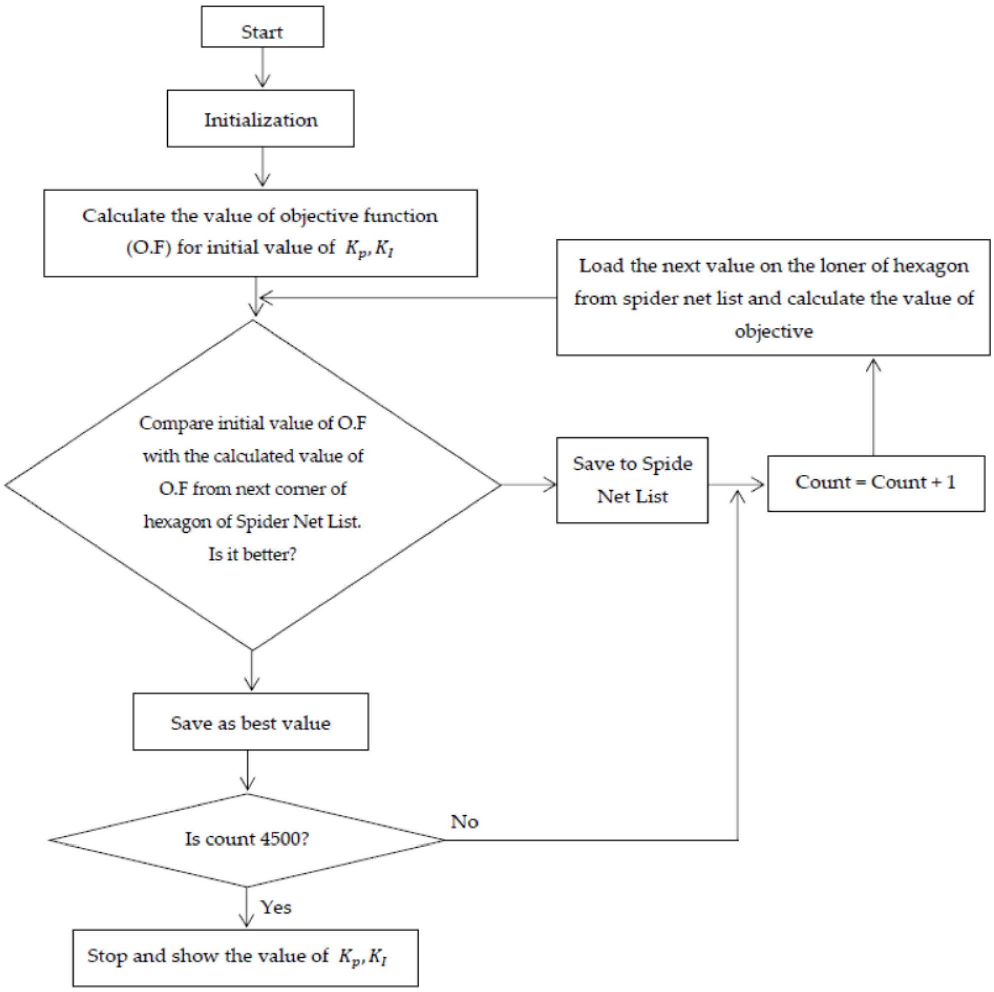

Figure 15. Flow chart of ASNS for SAPF.

The ASNS algorithm adjusts the value of the gain factor in the PI controller designed in the SAPF block and provides a compensating current that matches the current generated by the harmonic measurement noise to improve the quality. Electrical Power and enhance the sine wave shape of the power supply. The ASNS algorithm does a good job of power supply disturbance current compensation under balanced, unbalanced, and distorted current supply conditions. The noise current compensation time is fast in just a few seconds, and compared with the GA algorithm in SAPF, the ASNS algorithm applied to SAPF has more advantages.

Adaptive Tabu Search (ATS) for SAPF

Artificial intelligence engineering Tabu Search into shunt control adaptive power filter (SAPF) to find compensating power for source to improve the quality of power [108,109].

Active ATS includes a reverse tracking mechanism and search area radius adaptation mechanism [110]. The ATS algorithm's code is explained in Table 12.

Reverse tracking activity helps the system turnback the previous solutions in TL.Flow chart of ATS algorithm for SAPF (Figure 16). The Tabu search algorithm is considered an artificial intelligence algorithm applied to SAPF, which performs well the function of adjusting gain parameters in the PI controller in SAPF to choose a suitable compensating current power supply to eliminate harmonics and improve power quality [111,112]. The Tabu search algorithm applied in SAPF brings high efficiency in SAPF's compensating current supply operation for power supply.

Table 12. ATS algorithm's code.

Step	Step-By-Step Explanation of ATS Algorithms
Step 1:	Initialize Tabu TL and count values to 0
Step 2:	Randomly select the initial solution S_o in the search space. S_o is set as the local minimum, and S_o is the best neighbor
Step 3:	Update the count value and choose N new solutions randomly at the R radius, which is in the search space. Call $S_1(r)$ is the set of N solutions
Step 4:	Calculate the $\cos$t value of each member $S_1(r)$, then choose the optimal value and assign it to the best neighbor 1
Step 5:	If best neighbor 1 $<$ best neighbor, save the best neighbor in TL. Set the best neighbor as thebest neighbor 1 and set S_o as thebest neighbor. In addition, set the best neighbor 1 in TL
Step 6:	Evaluate the last criteria (TC) and the aspiration criteria (AC). If count max = count (the maximum number allowed in the search area), stop the search process. The current best solution is the best overall solution. If not, go back to step 2 and continue the process

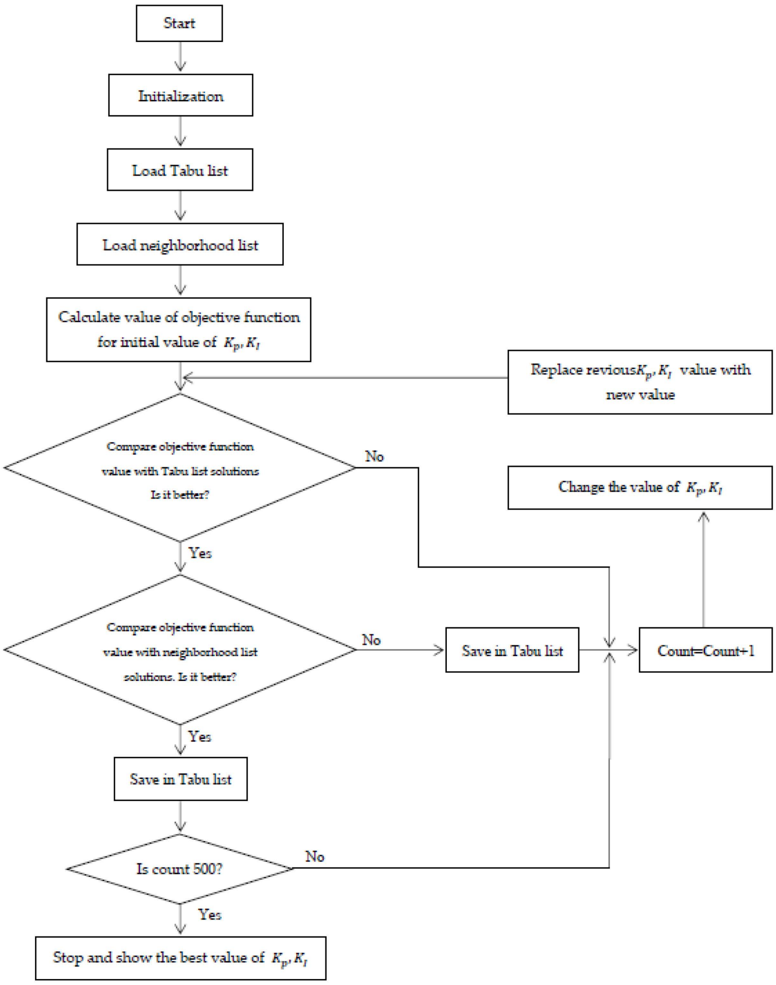

Figure 16. Flow chart of ATS for SAPF.

Whale Optimization Algorithm (WOA) for SAPF

WOA is inspired by the foraging activity of whales using the bubble-net method. The process of whales diving into and out of the water creates swirling bubbles that surround their prey [113,114]. The WOA code is explained step-by-step in Table 13, and the flow chart of WOA for SAPF is shown in Figure 17.

Table 13. WOA code.

Step	Step-By-Step Explanation of ATS Algorithms
Step 1:	At first, the whale acquaints itself with the prey, then surrounds the prey. The whale predicts the best solution and calls it objective prey and is substituted when there is another better solution. Variables are updated according to the Formulas (47) and (48). $$\vec{D} = \left\lvert \vec{C} \,.\, \vec{X}^{*}_{(t)} - \vec{X}_{(t)} \right\rvert \quad (47)$$ $$\vec{X}(t+1) = \vec{X}^{*}_{(t)} - \vec{A}.\vec{D} \quad (48)$$ Vector of coefficients $\vec{A}$ and $\vec{C}$ are updated by Formulas (49) and (50) $$\vec{A} = 2\vec{a}.\vec{r} - \vec{a} \quad (49)$$ $$\vec{C} = 2.\ \vec{r} \quad (50)$$ wheret $=$ indicates the current iteration. $\vec{X}^{*} =$ position vector of the current best solution obtained. $\vec{X} =$ position vector should be updated whenever there is a better solution. $\vec{A} =$ coefficient vector. $\vec{C} =$ coefficient vector. $\vec{a} =$ linearly decreased vector from 2 to 0. $\vec{r}$ = random vector between [0, 1].
Step 2:	Exploitation phase, whales will attack their prey with a bubble net strategy and do so with twomethods, including shrinking, encircling, and spiral updating. Shrinking encircling performs a new search defined between the current best range and the updated $\vec{a}$ value search range with Formula (11) and the$\vec{a}$ value is assigned from 1 to -1. Sprial updating performs a calculation of the distance between whale X and Y from the prey X^{*} and Y^{*}. Spiral is shown according to Formulas (51) and (52). $$\vec{X}(t+1) = \vec{D'}\,.e^{b_1}.\cos(2\pi L) + \vec{X}^{*}(t) \quad (51)$$ $$\vec{D'} = \left\lvert \vec{X}^{*}(t) - \vec{X}(t) \right\rvert \quad (52)$$ Formula (13) calculates the distance from the i^{th} whale compared to the best updated solution. L = random number in [−1,1], b = fixed number for the spiral algorithm. The algorithm model is built as Formula (53). $$\vec{X}(t+1) = \begin{cases} \vec{X}(t) - \vec{A}.\vec{D} if p \leq 0.5 \\ \vec{D'}.tt + \vec{X}^{*}(t) if p\ \geq 0.5 \end{cases} \quad (53)$$ where the random value of p is selected in [0, 1] and H $=$ $e^{b_1}.\cos(2\pi L)$.
Step 3:	The search for prey or the exploration phase and the$\vec{a}$ vector number is selected randomly to update the search location and perform according to Formulas (54) and (55). $$\vec{D} = \left\lvert \vec{C}.\vec{X}_{rand} - \vec{X} \right\rvert \quad (54)$$ $$\vec{X}(t+1) = \vec{X}_{rand} - \vec{A}.\,\vec{D} \quad (55)$$ where $\vec{X}_{rand}$ = random vector chosen from whales' location from the current population. After applying WOA and SAPF, the THD = 1.49%, within the IEEE 519-2022 standard, where the objective function is according to Formula (56). $$P_{Loss} = K_p.Error + K_i \int_0^t (Error)dt \quad (56)$$ With : $Error = V_{dc\ ref} - V_{dc\ actual}$

The WOA algorithm implemented in SAPF performs optimization of gain parameters in the PI controller to select the current to compensate for the disturbance current in the power supply and compare the results of optimal performance parameters with other parameters. For other algorithms, the WOA algorithm gives the best results [115,116]. The WOA algorithm used in SAPF shows that the signal processing by Width Modulation (PWM) is very simple and uses the Technical Width Modulation (PWM) parameter to tune the controller in SAPF [117]. The WOA method addresses power quality problems caused by interruptions caused by electrical equipment using electricity, such as nonlinear loads or renewable energy sources. The WOA method performs direct tuning of the relevant parameters to facilitate power quality improvement.

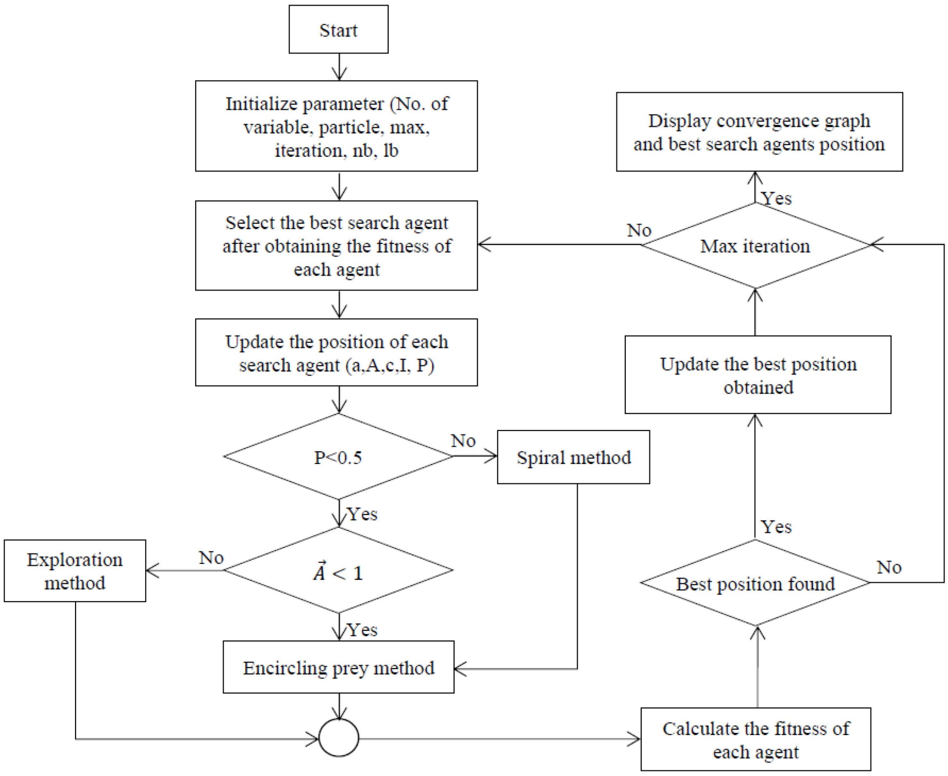

Figure 17. Flow chart of WOA for SAPF.

Swarm Particle Swarm Optimization (PSO) for SAPF

PSO is applied in compensating current control for the shunt adaptive power filter (SAPF). The goal is to ensure the quality of the power supply to the load [118–120].

PSO is inspired by the swarm, and PSO's mechanism generates particles randomly and is assigned an arbitrary parameter. The velocities of particles in space group together to form a global convergence value [98,121–129]. The flight movements of the particles in the respective search area of each individual and their particles in the swarm population, the position of the i^{th} particle in the swarm $x_{id}(t)$ moving with speed $V_{id}(t)$, the positions and the velocities of the particles repeated successive times, $x_{id}(t+1)$ and $V_{id}(t+1)$, respectively, are updated as Formulas (57) and (58):

$$V_{id}(t+1) = n.V_{id}(t) + C_1.r_1[P_{id}(t) - x_{id}(t)] + C_2.r_2[g_{id}(t) - x_{id}(t)] \quad (57)$$

$$x_{id}(t+1) = x_{id}(t).V_{id}(t+1) \quad (58)$$

where w isthe inertia constant which maintains the balance between the neighborhood and global search regions. C_1, C_2 = accelerator constant. r_1, r_2 = two random constants are generated independently and evenly distributed in the interval $[-1, 1]$. $P_{id}(t)$ = coordinatesof the best position detected at the i^{th} particle. $g_{id}(t)$ = coordinates of the best-detected location for the entire swarm or global optimal.

The value of the inertia constant w specifies the search space operation and is performed according to Formula (59).

$$w = w_{max} - (w_{max} - w_{min})\frac{g}{G} \quad (59)$$

where g = the current number of evolutionary generations. W_{max}, W_{min} = maximum and minimum weight. The initial value w = 0.9 allows the fastest global optimal value search. W = 0.4 isoptimal for search switching from exploratory mode to exploitative mode. The search process ends when the global optimal value is defined to be the best. PSO algorithms are explained step-by-step in Table 14.

Table 14. PSO algorithm's code.

Step	Step-By-Step Explanation of PSO Algorithms
Step 1:	Initialization particle size, search space size, maximum number of iterations and constant values of the PSO included w, C_1, C_2 and determine the random number r_1, r_2, find the current fitness of each particle in the population.
Step 2:	Assign the particles a random initial position (x) and velocity (v). Set initial counter value $= 0$. Initial population value, current best Fitness value of each county with its own matching value and global best position P_{id} of each county at their respective current position according to Formula (60). $$P_{id} = \text{current position of } i^{th} \text{ particle} \quad (60)$$
Step 3:	The global best fitness value is calculated according to Formula (61) $$\text{Global best fitness} = \min(\text{local best fitness}) \quad (61)$$ The position that meets global best fitness is the position that meets global best g_{id}.
Step 4:	Update the position and velocity of the particles according to Formulas (62) and (63).
Step 5:	Increase the number of iterations of $K = K + 1$ and find the current fitness of each particle. If current fitness < local best fitness, set. $$\text{Local best fitness} = \text{current fitness}, \quad (62)$$ $$P_{id} = \text{current fitness} \quad (63)$$
Step 6:	After calculating the local best fitness of each particle, the current global best fitness of the each k^{th} loop is calculated as follows: $$\text{Current global best fitness} = \min(\text{local best fitness}) \quad (64)$$ If current global best fitness < global best fitness, then. $$\text{Global best fitness} = \text{current global best fitness} \quad (65)$$ Position that meets global best fitness value, assigned for g_{id}.
Step 7:	Repeat steps 5 and 6 until k is equal to the maximum value of the loop defined in step 1 or there is no global best fitness improved.
Step 8:	End the algorithm loop or until no more loops are executed

The flow chart of the PSO algorithmis shown in Figure 18. The PSO algorithm is applied in SAPF to adjust the gain parameter of the PI controller in order to improve the performance of SAPF in the process of selecting suitable and accurate compensating current to provide current compensation. The interference in the distribution system is generated by harmonics and reactive power compensation to improve the power factor of the power supply. The PSO method implements DC link voltage regulation to adjust the offset current. The PSO method adjusts the gain of the PI controller and calculates the parameters according to IEEE 519-2022 conventions. The PSO algorithm applied in SAPF helps the system operate with little overshoot, providing the correct amount of compensation current to compensate for the noise current, helping to minimize the sine wave of the power supply and the compensation implementation time to the power supply with the least amount of time compared to other algorithms.

PSO + ANN

PSO and ANN hybrid method control parameter K_p, K_i of PI controller of SAPF filter to reduce THD value in power supply meeting IEEE 519-2022 standard. The PSO performs the optimization of the supply voltage and DC voltage of the SAPF filter operating under different load conditions. Optimal data set to improve the optimization prediction with the lowest error of SAPF [130,131].

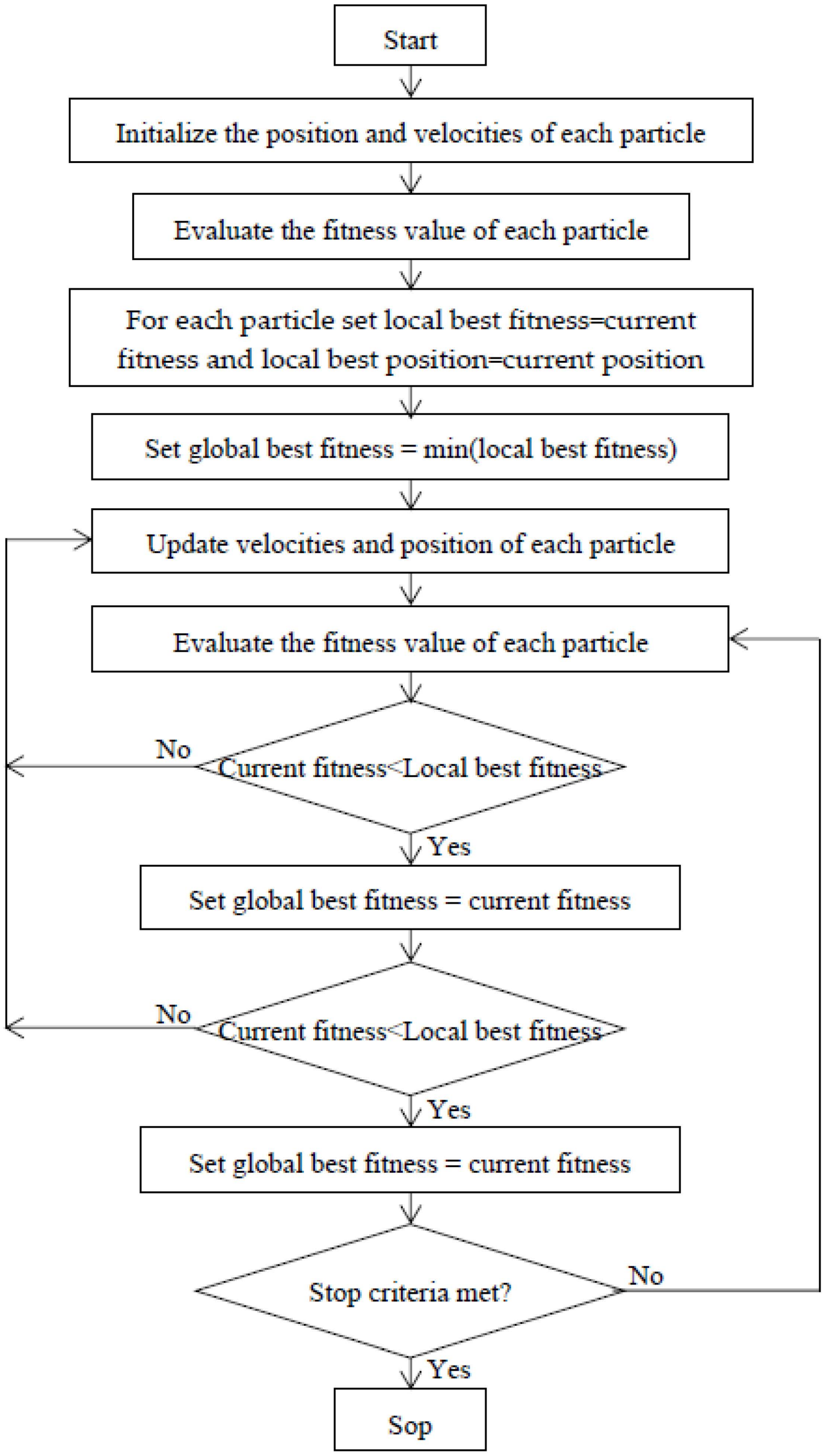

Figure 18. Flow chart of PSO algorithm.

PI amplification parameters are optimized by PSO and ANN (Figure 19), in which the optimal solutions are performed by the PSO algorithm after many iterations. The output of the PSO optimization serves as the input of the ANN for accurate PWM around prediction for increased minimal error tolerance. The result of this combined method is that the THD value reaches 2.22 to meet the IEEE 519-2022 standard [132].

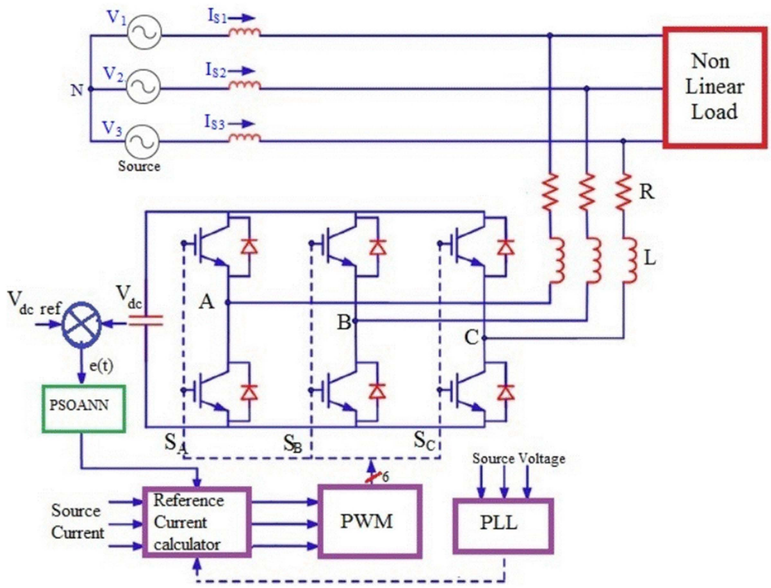

Figure 19. Schematic diagram of PSO ANN.

PSO is used for dataset generation. PSO starts with a group of random variables, then finds optimal solutions according to Formula (66).

$$\begin{matrix} I_{s1} \\ I_{s2} \\ I_{s3} \end{matrix} = \begin{bmatrix} \sin(w_s t) & \cos(w_s t) \\ \sin\left(w_s t - \frac{2\pi}{3}\right) & \cos\left(w_s t - \frac{2\pi}{3}\right) \\ \sin\left(w_s t + \frac{2\pi}{3}\right) & \cos\left(w_s t + \frac{2\pi}{3}\right) \end{bmatrix} \begin{bmatrix} I_d * \\ I_q * \end{bmatrix} \tag{66}$$

PSO updates the twobest values after each iteration; the first best solution is P_{best}, and the second best value solution is called the global best value G_{best}. The optimization process is done as follows:

$$P_{best} = P_{bestk1}, \ P_{bestk2}, \ \ldots \ P_{bestkd} \tag{67}$$

The best global particle G_{best} is defined, and the velocity of the k^{th} particle is calculated by Formula (68).

$$V_k = V_{k1}, \ V_{k2}, \ \ldots \ V_{kd} \tag{68}$$

The current velocity is recalculated according to the newly calculated position and velocity. Then the distance is calculated from $P_{best\ kd}$ to $G_{best\ kd}$ using Formulas (69) and (70).

$$x_{k_1 m}^{t+1} = wV_{k_1 m}^{(t)} + C_1 rand()\left(P_{bestk1m} - x_{k_1 m}^t\right) + C_2 rand()\left(P_{bestk1m} - x_{k_1 m}^t\right) \tag{69}$$

$$x_{k_1 m}^{t+1} = x_{k_1 m}^t + V_{k_1 m}^{(t+1)} \tag{70}$$

The optimal solution is calculated so that the PSO reaches the minimum error value, and the system calculates those parameters by Formula (71).

$$x_i = \begin{bmatrix} K_p^{11} K_i^{11} & K_p^{12} K_i^{12} & \ldots & K_p^{1n} K_i^{1n} \\ K_p^{21} K_i^{21} & K_p^{22} K_i^{22} & \ldots & K_p^{2n} K_i^{2n} \\ K_p^{m1} K_i^{m1} & K_p^{m2} K_i^{m2} & \ldots & K_p^{mn} K_i^{mn} \end{bmatrix} \tag{71}$$

In the control scheme of ANN, the proposed parameters are implemented by PSO. ANN is implemented as a three-layer network, including threenodes in the input layer, 20 nodes in the hidden layer, and one node in the output layer. The optimized performance of core functions and training time is done by the hidden layers. Selected hidden layers are validated by cross-validation. Sigmoid functions are used as the hidden layers and show all effects obtained from a random mapping of standard sigmoidal functional variables in the range [0, 1]. The weights of the neural network are updated by the Levenberg–Marquardt back-propagation algorithm (LMBP) [133].The output of the ANN is used for a three-phase reference current. The LMBP algorithm is a combination of Gauss–Newton and Gradient using good responses for local or global transport. The 2D recursive neural network used restricts overtraining of the whole process. The ANN network is performed according to the following steps (Table 15).

Table 15. The ANN network's code.

Step	Step-By-Step Explanation of ANN Network Algorithms
Step 1:	The training network generates a control pulse (z) with a time interval (t) input
Step 2:	The error target of $x_{(1)}, x_{(2)}, \ldots,\ x_{(n)}$ is made using Formula (72) $$LMBP^1_{error} = Z_{(1)}{}^{NN(target)} - Z_{(1)}{}^{NN(out)} \quad LMBP^2_{error} = Z_{(2)}{}^{NN(target)} - Z_{(2)}{}^{NN(out)} \quad LMBP^n_{error} = Z_{(n)}{}^{NN(target)} - Z_{(n)}{}^{NN(out)} \tag{72}$$
Step 3:	The above equation is the output of the network. $$Z_{(1)}{}^{NN(out)} = a_1 + \sum_{n=1}^{N} w_{1n}.z_{(1)}{}^{NN(k)} \quad Z_{(2)}{}^{NN(out)} = a_2 + \sum_{n=1}^{N} w_{1n}.z_{(2)}{}^{NN(k)} \quad Z_{(n)}{}^{NN(out)} = a_n + \sum_{n=1}^{N} w_{1n}.z_{(1n)}{}^{NN(k)} \tag{73}$$ where a is a function node deviation of one or two and n
Step 4:	The weight of each neuron is calculated using Formula (74). $$z_{(1)}{}^{NN(k)} = \frac{1}{1+\exp(-h_{1n}.z(1)-h_{2n}.z(2))} \quad z_{(2)}{}^{NN(k)} = \frac{1}{1+\exp(-h_{2n}.z(2)-h_{nn}.z(n))} \quad z_{(n)}{}^{NN(k)} = \frac{1}{1+\exp(-h_{nn}.z(n)-h_{1n}.z(1))} \tag{74}$$
Step 5:	Weight adjustment is calculated as follows: $$\Delta h_1 = L_r.z(1).LMBP^1_{error} \quad \Delta h_2 = L_r.z(2).LMBP^1_{error} \quad \Delta h_n = L_r.z(n).LMBP^1_{error} \tag{75}$$
Step 6:	All above steps repeat until LMBP min (LMBP < 1)

The desired control signal is generated from the SAPF after the ANN is successfully trained. ANN training performance was assessed using Root Mean Square Error (RMSE), coefficient of determination (R^2) and Mean Absolute Error (MAE). The Artificial Neural Adaptive Linear Neural Network (ADALINE) (ANN) acts as the reference flow selector of the PSO and ANN application system in the SAPF. Meanwhile, the PSO performs the role of the gain parameter adjustment controller in the SAPF PI controller and controls the DC voltage to select the correct compensating current for the system with a noisy power source. The PSO algorithm has strengths in accurate estimation in terms of adjusting the gain parameters of the PI controller and is superior in performance compared to traditional methods. The application system that combines the ANN algorithm and the PSO algorithm into the SAPF shows high efficiency in providing compensating current for the power supply and improving the quality of the power supply.

Flower Pollination Algorithm (FPA)

FPA is used to maintain a constant DC voltage by controlling the PI ratio integrator of the SAPF unit between voltage reference V^*_{dc} and the actual DC voltage value V_{dc} in order to reduce harmonics in the power system.FPA is used to select the best value of K_p, K_I in the PI controller system [134–138].

FPA works based on flower pollination or the process of transferring pollen from one species to another, including two main activities: self-pollination/biological and cross-pollination/abiotic. The self-pollination process is the movement of pollen of the same species by wind. The cross-pollination process is the movement of pollen by honey bees, birds or bats. In fact, 90% is cross-pollination, and the remaining 10% is self-pollination. FPA performs self-pollination of flowers according to the following rules (Table 16) step-by-step to implement the FPA algorithm (Table 17).

Table 16. FPA algorithm's rule.

Rule	Explanation of the FPA Algorithm's Rules
Rule 1:	Pollen and the best global solutions are defined by Formula (76) $$x_i^{k+1} = x_i^k + L\left(G_{best} - x_i^{-k}\right) \quad (76)$$ where G_{best} is the most recent best pollen with oneset of pollen. L = represents theLevy factor that is responsible for the movement of the pollen group, and this factor follows the Levy distribution and is calculated using Formula (77) $$L = \frac{\lambda\Gamma(\lambda)\sin\left(\frac{\pi\lambda}{2}\right)}{\pi}\frac{1}{s^{1+\lambda}}\left(S \gg S^0 > 0\right) \quad (77)$$ where $\Gamma(\lambda)$= standard gamma value for the biggest move $\left(S \gg S^0 > 0\right)$
Rule 2:	The equation for local pollination or self-pollination, following Formula (78) $$x_i^{k+1} = x_i^k + \varepsilon\left(x_m^k - x_i^k\right) \quad (78)$$ where x_m^k *and* x_i^k is a random number in the range 0–1.
Rule 3:	Set the probability switch value in the range $p\,\epsilon[0,1]$, make the transition from local to global search, and a p-value = 0.8 often gives the optimal result.

Table 17. FPA algorithm's code.

Step	Step-By-Step Explanation of FPA Algorithms
Step 1:	Set the initial parameters. The first step is setting the initial parameters consisting of population size (N), probability switch (p), the max number of iterations $(iter_{max})$, decision variable size (d), and scaling factor (λ)
Step 1:	Main FPA algorithm
	First of all, the first decision variable is chosen randomly in the lower and upper bounds, as shown in the flowchart below.
	For i = 1:n;
	$x(i) = Lb_i + (Ub_i - Lb_i).\,rand(d,1);$
	End
	Next, identify the fitness or error of the first population and do the following flowchart.
	For i = 1:n;
	$\mathrm{CF(i)} = \mathrm{PIC}\left(x_{(i)}\right)$
	End
	Where CF = current fitness and PIC is a function that combines the Matlab and Simulink models of SAPF. Normally, CF is in 50 $\times$ 1 size
	Following that, find the pollen variable/ best decision variable. Pollen has aminimum fitness value of K_p, K_I
	In the next step, pollen is updated according to rules 1 and 2, and the probability p-value is randomly selected in the range 0–1. If the random number is greater than p, then the pollen value is calculated according to Formula (79) $$\begin{bmatrix} v_\alpha \\ v_\beta \end{bmatrix} = \sqrt{\frac{2}{3}}\begin{bmatrix} 1 & \frac{-1}{2} & \frac{-1}{2} \\ 0 & \frac{\sqrt{3}}{2} & \frac{\sqrt{3}}{2} \end{bmatrix}\begin{bmatrix} v_a \\ v_b \\ v_c \end{bmatrix} \quad (79)$$

Table 17. *Cont.*

Step	Step-By-Step Explanation of FPA Algorithms
	Provide by rule 1. On the other hand, if the random number is less than p, then the pollen obeys rule 2
	Evaluate the fitness value after updating the pollen value according to the following equation.
	For I = 1:n
	CFU_i = PIC(x.u(i)); where CFU_i: updated value of fitness and x.u: updated pollen value
	End
	Updating the current global best fitness value from local best fitness is described in detail by the following equation
	If CFU < CF
	BESTP = PIC(x()i);
	CF = CFU
	End
	These steps are repeated until the value of the mathematical equation reaches convergence and the iteration becomes more than the maximum number of iterations initially set; then, the program is stopped.
	Find the K_p, K_I flower pollination value achieved with the minimum error value

The FPA algorithm applied in SAPF performs the function of stabilizing the DC link value in the SAPF filter to improve the efficiency of current compensation for noisy power sources. The issue of power quality improvement is important, and the FPA algorithm applied in SAPF has fulfilled the role of controlling the gain values in the PI controller to help SAPF select the correct compensating current to compensate for the current noise caused by the PI controller as a result of harmonics. The FPA algorithm takes care of the gain parameter adjustment to help minimize the error between the reference voltage and the actual DC link voltage. The FPA algorithm applied in SAPF optimizes the gain values to help the system reduce harmonic distortion with high efficiency and compensate current compensation time to reach the system setting in a short time with 0.01 s.

Grey Wolf Optimization (GWO) Algorithm for SAPF

GWO applied to SAPF optimizes the THD value in the power supply to meet IEEE 519-2022 standards and achieve THD = 3.815%, and the configuration applied by GWO to the SAPF is shown in detail in Figure 20.

GWO is built on action inspired by the hunting behavior of gray wolves. Gray wolves have a herd behavior of 5–12 animals and organize the herd according to four levels, including Alpha (aGWO), Beta (bGWO), Delta (dGWO), and Omega (xGWO). In it, the aGWO-level gray wolf performs hunting, arranging sleep and wake times for the whole pack and the gray wolf aGWO is the leader of the pack. The bGWO-level gray wolf is the second tier in the pack that does the job of helping the aGWO-grade gray wolf make other decisions in the pack. Gray wolves of rank xGWO are the lowest level in the pack and always perform tasks under the direction of gray wolves of other ranks, namely aGWO, bGWO and Dgwo [139–144]. The mathematical equation of GWO in the process of tracking, encircling and attacking slugs is described by Formulas (80) and (81).

$$\vec{D}_{GWO} = \left| \vec{C}_{GWO} \cdot \vec{X_p}(it) - \vec{X}(it) \right| \quad (80)$$

$$\overrightarrow{X}(it+1) = \left| \overrightarrow{X_p}(it) - \overrightarrow{A_{GWO}}.\ \overrightarrow{D_{GWO}} \right| \tag{81}$$

where it: Current iteration; $\overrightarrow{A_{GWO}} \cdot \overrightarrow{C_{GWO}}$.: Coefficient vector; $\overrightarrow{X_p}$: Position vector of sardines; $\overrightarrow{X}$: Grey wolf position vector; $\overrightarrow{D_{GWO}}$: Distance between gray wolves and sardines and $\overrightarrow{C_{GWO}} = 2 \cdot \overrightarrow{r_{1GWO}}$; $\overrightarrow{A_{GWO}} = 2 \cdot \overrightarrow{a_{GWO}} \cdot \overrightarrow{r_{2GWO}} - \overrightarrow{a_{GWO}}$ where $\overrightarrow{r_{1GWO}}$; $\overrightarrow{r_{2GWO}}$: Random parameter with a value in the range 0–1, and these two parameters are loop variables. $\overrightarrow{a_{GWO}}$: Starting from value two, this runs to zero until the end of the loop. The distance $\overrightarrow{D_\alpha}$, $\overrightarrow{D_\beta}$, $\overrightarrow{D_\delta}$ between gray wolves and sardines is determined by Formula (82).

$$\begin{cases} \overrightarrow{D_\alpha} = \left| \overrightarrow{C_1} \cdot \overrightarrow{X_\alpha} - \overrightarrow{X} \right| \\ \overrightarrow{D_\beta} = \left| \overrightarrow{C_2} \cdot \overrightarrow{X_\beta} - \overrightarrow{X} \right| \\ \overrightarrow{D_\delta} = \left| \overrightarrow{C_3} \cdot \overrightarrow{X_\delta} - \overrightarrow{X} \right| \end{cases} \tag{82}$$

where $\overrightarrow{D_\alpha}$, $\overrightarrow{D_\beta}$, $\overrightarrow{D_\delta}$: the distance between α_{GWO}, β_{GWO}, δ_{GWO} gray wolves and sardines; $\overrightarrow{C_1}$, $\overrightarrow{C_2}$, $\overrightarrow{C_3}$: the vector coefficients of the three best positions $\overrightarrow{X_1}$, $\overrightarrow{X_2}$, $\overrightarrow{X_3}$; $\overrightarrow{X_\alpha}$, $\overrightarrow{X_\beta}$, $\overrightarrow{X_\delta}$: the first-, second-, and third-best search areas. The three best positions of gray wolves are updated according to Formula (83).

$$\begin{cases} \overrightarrow{X_1} = \overrightarrow{X_\alpha} - \overrightarrow{A_1} \cdot \overrightarrow{D_\alpha} \\ \overrightarrow{X_2} = \overrightarrow{X_\beta} - \overrightarrow{A_2} \cdot \overrightarrow{D_\beta} \\ \overrightarrow{X_3} = \overrightarrow{X_\delta} - \overrightarrow{A_3} \cdot \overrightarrow{D_\delta} \end{cases} \tag{83}$$

Update gray wolf position in best location search area by Formula (84).

$$\overrightarrow{X}_{(it+1)} = \frac{\overrightarrow{X_1} + \overrightarrow{X_2} + \overrightarrow{X_3}}{3} \tag{84}$$

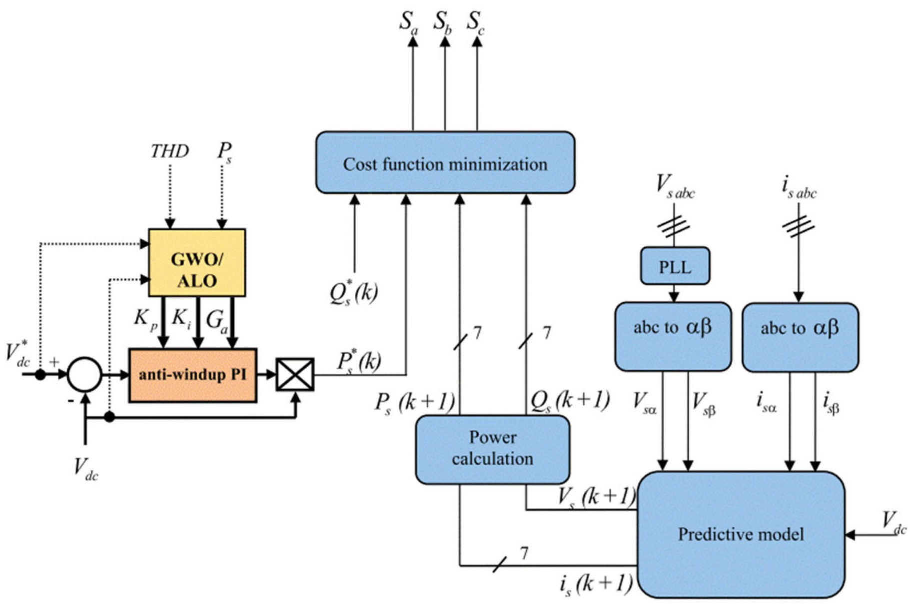

Figure 20. Configuration of GWO in SAPF.

The Pseudocode of GWO used for PI controller in SAPF by the algorithm below (Algorithm 2):

Algorithm 2: Pseudocode of GWO Algorithms

Input (Set input data of SAPF. Set initialize parameters of GWO)
K = 1
Create an initial population of search agent $(X_i \; with \; i = 1, \; 2, 3, \ldots, \; N)$ with 3 dimension $K_p, \; K_i, \; G_\alpha$
Run SAPF using $K_p, \; K_i, \; G_\alpha$ and evaluate the fitness function value in the search area
Sort the $X_\alpha, \; X_\beta, \; X_\gamma$ positions in the order of first-, second-, and third-best in the search area.
While $K \leq K_{max}$ do
    For i = 1 to the number of search agents, do
        Update the position $\overrightarrow{X_{(it+1)}}$ and update the value of $K_p, \; K_i, \; G_\alpha$ following Equation (84)
        Update α
        Update $\overrightarrow{C_{GWO}} \; and \; \overrightarrow{A_{GWO}}$
        Run SAPF using updated values of $K_p, \; K_i, \; G_\alpha$ and evaluate the fitness function value of the search area.
        Update $X_\alpha, \; X_\beta, \; X_\gamma$
        K = K + 1
    End for
End while
Return X_α (best solution)
Output: Print the optimum again $K_p, \; K_i, \; G_\alpha$ of the PI controller in SAPF in terms of X_α

The GWO algorithm applied in SAPF brings many benefits, such as simple calculation because the algorithm requires few control parameters, and the algorithm is flexible and easy to optimize globally. The gain parameters of the PI controller in SAPF are optimized by the GWO algorithm to help the SAPF unit select the correct amount of offset current to compensate for the power supply. The GWO algorithm applied in SAPF shows outstanding feedback architecture and optimization of high-performance parameters. Interference in the system is responded to quickly; the SAPF unit responds to interferences highly efficiently and provides a timely compensating current to improve power quality. The GWO-SAPF system helps the power system to measure the voltage and frequency of the power supply, helping the system to control overshoot and quickly stabilize the power system, improving the quality of electricity in operation and electrical system safety. The distribution power network currently has the participation from many renewable energy power sources, and these are also considered sources of harmonics generation and also an opportunity for researchers to apply the technique to calculate GWO in SAPF into activities to improve the quality of distribution power in the future.

3.2.4. Physics-Based Algorithms

Calculated in the period from 1966 to 2021, there are 21 methods to the advantage of Physics based Algorithms. However, the study authors have applied two methods to harmonics mitigation in shunt adaptive power filters, which is Gravitational Search Algorithm (GSA). This demonstrates that there is a large scaling problem for researchers using the remaining methods in SAPF in the future, including the direct implementation of each individual method and the possible implementation of a single method or a hybrid method in corporating individual methods.

Gravitational Search Algorithm (GSA) for SAPF

GSA applied to SAPF performs optimal compensating current selection to compensate for the loss of current on the power source and minimizes the THD value of the power supply [145,146] that meets IEEE 519-2022 standard (Figure 21), and the THD = 4.0% value meets the THD standard less than 5%.

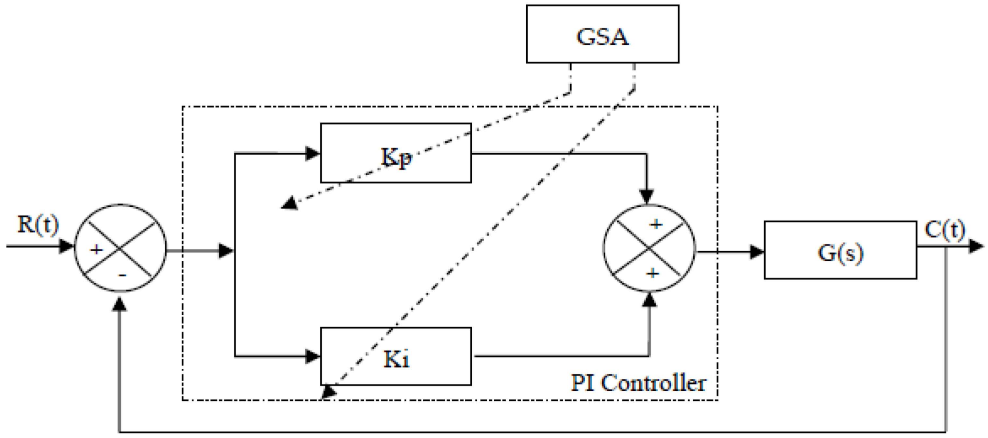

Figure 21. Block diagram applying GSA to SAPF.

The research objective function applying GSA to SAPF is performed according to Formula (85).

$$F = f(I_{THD}) \tag{85}$$

The optimal tuning parameters, including K_p and K_i, and the output function of the PI controller are calculated according to Formula (86).

$$G_c(S) = K_p + \frac{K_i}{S} \tag{86}$$

The $K_p,\ K_i$ gain value is updated in the PI controller according to Figure 4, and the output value of the PI controller is updated according to Formula (87).

$$U(t) = K_p \cdot e(t) + K_i \cdot \int_0^t e(t)dt \tag{87}$$

The system performed $K_p,\ K_i$ tuning in the PI controller.

GSA works on the basis of Newton's gravity. In the universe, cashews tend to attract each other, and particles are directly proportional to the product of their mass and inversely proportional to the square of their distance. The GSA algorithm's step-by-step explanation is shown in Algorithm 2 and Table 18, and the GSA flow chart is shown in Figure 22.

Table 18. GSA algorithm's code.

Step	Step-By-Step Explanation of the GSA Algorithms
Step 1:	The position of the third agent in the N agents is determined by Formula (88) $$X_i = \left(X_i^1,\ \ldots, X_i^d,\ \ldots,\ X_i^N\right),\ for\ i = 1,\ 2,\ \ldots .,N \tag{88}$$ where X_{id}: the ith position in the d_{in} dimension; N: the size of the search space.
Step 2:	At time t, the *i*-th force is applied from the *j*-th, and this applied force is calculated by Formula (89) $$F_{ij}^d = G(t)\frac{M_{pi}(t).M_{aj}(t)}{R_{ij}+\varepsilon}\left(X(t) - X_i^d(t)\right) \tag{89}$$ where M_{aj}: active gravity of agent *j*; M_{pi}: passive gravity of agent *I*; $G(t)$:: small constant; R_{ij}: euclidean distance between regions *i* and *j*.
Step 3:	The total force acting on *i* in the dimension *d* over time *t* is calculated by Formula (90) $$F_i^d(t) = \sum_{\substack{J \\ K_{best},\ j \neq i}}^{N} rand_j.F_{ij}^d(t) \tag{90}$$ where *r* and *i* : random numbers in the range 0–1; K_{best}: first K-zone with the best fitness value.

Table 18. *Cont.*

Step	Step-By-Step Explanation of the GSA Algorithms
Step 4:	Acceleration relative to mass i in time t in terms of size d is calculated by Formula (91) $$a_i^d = \frac{F_i d(t)}{M_{ij}(t)} \quad (91)$$ where M_{ij}: mass of inertia of agent i
Step 5:	The next velocity of space is a fraction of the current velocity plus its acceleration. The position and velocity of the agent are calculated according to Formulas (92) and (93) $$(t+1) = t + a_i.dt \quad (92)$$ $$(t+1) = t + v_i^d(t+1) \quad (93)$$
Step 6:	The weight constant (G) is first set at the start of the search, and its value is decreased over time to achieve the goal of controlling accuracy when searching in the search space and following Formula (94) $$G(t) = G_{oe} - a_T^t \quad (94)$$ where T : number of loops; G_{oe} and a: constants.
Step 7:	Gravitational mass and initial mass are updated according to Formulas (95)–(97) $$M_{ai} = M_{pi} = M_{ii} = \ldots 1, 2, \ldots N \quad (95)$$ $$M_i(t) = \frac{fit_i(t) - worst(t)}{best(t) - worst(t)} \quad (96)$$ $$M_i(t) = \frac{m_i(t)}{\sum_j^N m_j(t)} \quad (97)$$ where fit_i: fitness value of region i at time t.
Step 8:	$worst(t)$ *and* $best(t)$: the minimum and best value of the problem is calculated by Formulas (98) and (99). $$best(i) = \min j \in \{1, 2, \ldots, N\}.fit_j(t) \quad (98)$$ $$worst(t) = \max j \in \{1, 2, \ldots, N\}.fit_j(t) \quad (99)$$

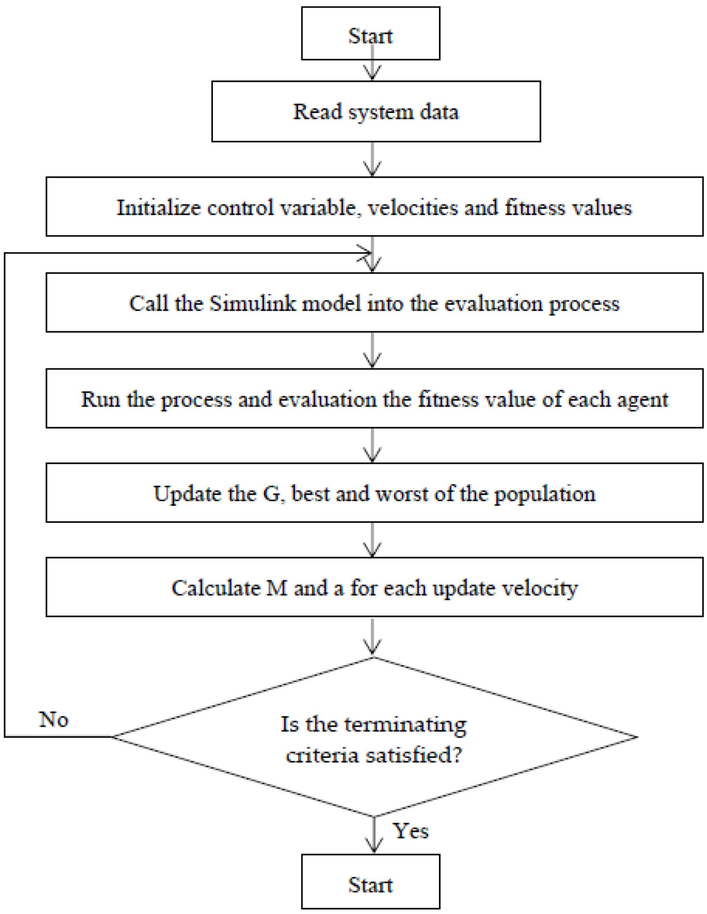

Figure 22. Flow chart of GSA for SAPF.

The GSA algorithm applied in SAPF performs optimal adjustment of parameters, including the value of SAPF filter communication impedances and the value of the DC link capacitor in SAPF and optimally adjusts the gain values in the SAPF. The PI controller helps SAPF improve efficiency, reduce power line shape distortion, improve reactive power compensation efficiency and improve the power factor value of the power supply.

3.2.5. Human Behavior Relation Algorithms

Calculated in the period from 1966 to 2021, there are 14 methods to the advantage of Human behavior relation Algorithms. However, the study authors have applied two methods to harmonics mitigation in shunt adaptive power filters, which are Teaching-Learning-Based Optimization (TLBO). Optimizing a problem requires multiple methods. Comparing the results of the methods in terms of execution time and optimal efficiency of each method as well as performing a combination of multiple optimization methods together to solve an optimization problem, is a study in the future.

Teaching-Learning-Based Optimization (TLBO)

TLBO is applied to SAPF control current to compensate for the current loss from the power supply and price THD = 1.06% to meet the IEEE 519-2022 standard with a THD value requirement less than 5% (Figure 23).

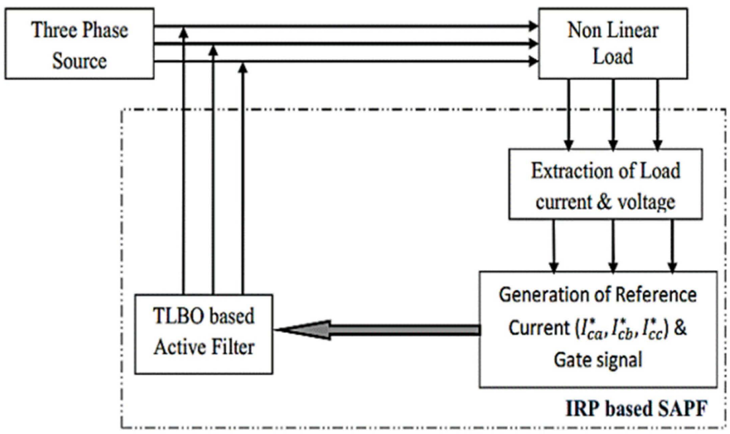

Figure 23. Block diagram of TLBO into SAPF.

TLBO performs an optimal search through learners trying to get experience as teachers and learners getting optimal results when gaining experience as teachers. Convergence speed is the most important point of all optimization algorithms. The TLBO algorithm follows the teaching and learning capacity of teachers and learners [147,148]. The TLBO algorithm adopts two operating mechanisms including through teachers and interactive activities with other learners. The flowchart of TLBO for the SAPF algorithm is shown in Figure 24.

TLBO performs optimization of the inductance and resistance values of the SAPF collector. The objective function j for optimization is the integrated time square error (ITSE) according to Formula (100):

$$j = ITSE = \int_0^t \left(e_r^2 \cdot t\right) \cdot dt \tag{100}$$

where error: the fitness function.

The TLBO algorithm applied in SAPF optimizes the reference current generated from the ideal voltage source by sensing the source voltage; the current on the load is the DC link voltage source [149,150]. The TLBO algorithm optimally controls the pulses in SAPF's bridge rectifier, helping SAPF improve its performance in providing current compensation for noisy power supplies.

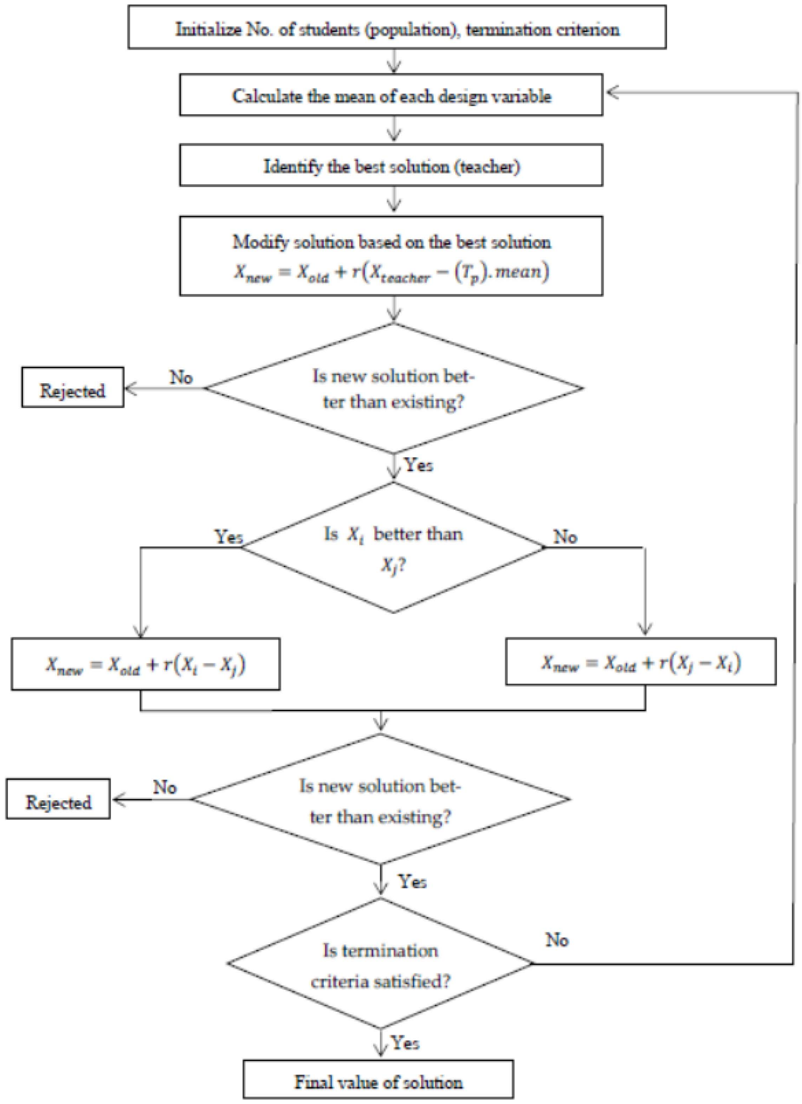

Figure 24. Flow chart of TLBO for SAPF.

4. Discussion and Future Research Problems

Modern meta-heuristic algorithms have many achievements in optimization applications for simple optimization models. However, the limitations of meta-heuristic algorithms are still too much and need some feasibility studies to improve the performance of meta-heuristic optimization algorithms. Meta-heuristic algorithms are hardly proven by specific mathematical models. In recent decades, there have been many studies proving meta-heuristic optimization algorithms by mathematical models, but not really close. Because of this, this is considered an open research direction for future researchers.

The convergence of algorithms that do not have a specific mathematical model is still too dynamic for meta-heuristic optimization algorithms. Therefore, mathematical models proving their convergence are considered an interesting research direction for future researchers. Building a new mathematical model or approaching a new mathematical model for meta-heuristic optimization algorithms is necessary, and they are considered an interesting research direction in the future. The individual variables in the meta-heuristic optimization algorithms interact with each other to produce better optimal results than using a single meta-heuristic optimization algorithm when solving optimization problems, and this is considered an optimization problem for researchers to establish hybrid methods to solve optimization problems with higher optimal performance.

In the future, the method of finding the parameters of the meta-heuristic optimization algorithms precisely so that the optimal results when solving the problem of needing to be optimized of the meta-heuristic optimization algorithms achieve the most optimal efficiency as well as a promising future study for researchers. The one-objective optimization model is not suitable for the two-objective optimization model. Therefore, it is not possible to prove a specific metric to compare the optimal performance between the optimal results of each meta-heuristic optimization algorithm. Therefore, the researchers suggest using an index of absolute objective value and numerical evaluation of the function as an alternative in comparing the efficient performance of meta-heuristic optimization algorithms, and there is no literature review to support this, and this is also an open matter for researchers and doctoral students to conduct a literature review in the future.

An optimization problem always has many options to be considered to solve, and modern meta-heuristic optimization methods are always prioritized to be carefully considered for application. In particular, the biological evolution of humans and creatures that form intelligence is increasingly high. This proves that, in the future, there will be more smart modifications to smart solutions to provide smarter solutions, more efficient in optimizing simple to complex problems.

The growing trend uses simple modern meta-heuristic optimization algorithms to solve complex optimization problems. However, sophisticated modern meta-heuristic optimization algorithms are developed to solve big data problems in the short and long term in the future, responding to the industrial 4.0 environment with the big data trend.

The variables, parameters, and components of each modern meta-heuristic optimization algorithm have been clearly understood and demonstrated. However, the connection between them in the optimal performance of problem-solving that needs to be optimized to achieve the highest efficiency is still not well understood or known as a mystery for researchers. There is a specific explanation in the future. A mathematical model that proves the convergence of the PSO algorithm has been demonstrated. However, there is no specific mathematical model that proves the convergence of meta-heuristic optimization algorithms. Research on this mathematical model is an open problem in the future.

Solving a specific problem requires determining the correct and correct meta-heuristic optimization algorithm for that problem to achieve the best optimization goal. The process of selecting a meta-heuristic optimization algorithm to solve a problem that needs to be optimized is considered the most important and urgent publicity for solving that problem. Currently, there is no review document that specifically guides the method of choosing the corresponding meta-heuristic optimal algorithm for solving the problem to be solved for nonlinear optimization for large problems. In the industrial 4.0 era, using Internet of Things (IOT) devices to connect and collect information between activities in the company's business processes together and save it as big data. Optimization problems associated with big data are often complex problems. Therefore, there is no modern meta-heuristic optimization algorithm that is sure enough to solve them with the most optimal results. Some suggested future research directions are as follows:

1. Implement improvements to some modern meta-heuristic optimization algorithms to improve functionality and improve optimal performance. In particular, PSO has a fast convergence speed but is limited in the search area, and there is a risk of virtual convergence; it is necessary to have a method to solve the search area which ensures the provision of a complete and accurate hammock number to respond to the best converged PSO optimization algorithm. For example, hybrid optimization methods include GA-PSO and DE-PSO;
2. Development of hybrid optimization algorithms between modern meta-heuristic optimization algorithms to solve each other's weaknesses and enhance each other's strengths;
3. Further changes and improvements are needed to the local and global models of some meta-heuristic optimization algorithms as the trade-off changes the complexity level between them;

4. The operation of fine-tuning the parameters of meta-heuristic optimization algorithms in solving optimization problems to be solved thoroughly in order to improve the optimal efficiency;
5. Some meta-heuristic optimization algorithms need to develop more parameters to improve the accuracy of convergence results;
6. Evaluating the performance of meta-heuristic optimization algorithms by statistical models needs to be developed;
7. Solving big data-related content problems with meta-heuristic optimization algorithms needs to use transformation learning to enhance its optimal performance;
8. A population parameter is the cause of delay in optimal processing time in optimization problem solving of modern meta-heuristic optimization algorithms;
9. The parameters of meta-heuristic optimization algorithms, including exploration, mining, searchability, convergence, and local convergence, need to be proven by specific theoretical models and mathematical models;
10. The strong growth of IOT devices used in the industrial 4.0 environment creates big data problems with their complexity and imbalance. Many numbers of decision-making variables are formed. The self-expanding meta-heuristic optimization algorithms feature self-adjusting and evolving to respond to solving big data problems;
11. There is a need for a specific way to identify subsets or classes of problems that meet the criteria for selecting the optimal meta-heuristic algorithm that meets the best convergence performance.

5. Conclusions

This study performs a literature review and provides an overview of applying modern meta-heuristic optimization algorithms to the optimization of the $K_p,\ K_i$ parameterof PI controller to perform parameter selection PWM activates the bridge rectifier of the SAPF unit, which fulfills the objective of selecting the correct and suitable compensating current to compensate for the lost current on the power supply caused by the harmonics generated by the non-linear load and improve power quality. An attempt by researchers to apply meta-heuristic optimization algorithms to SAPF was studied in this study to perform an overview including mathematical models, algorithm flowcharts and their applications to SAPF.

The process of formation and development over the years of meta-heuristic optimization algorithms is evaluated in the literature review over the corresponding time. The block diagram of SAPF overview architecture and harmonic extraction methods in the power supply are also considered to perform the review in this study. This study conducts a specific survey to apply meta-heuristic optimization algorithms to SAPF with the role of optimizing the control parameter $K_p,\ K_i$ of the PI controller in SAPF to realize the objective of selecting the optimal compensating current and compensate for the current loss on the power supply meeting the target of a THD value of less than 5% in the power supply as required by IEEE 519-2022. However, the difficult problem when applying meta-heuristic optimization algorithms to SAPF is to effectively meet the reduction of THD value on power sources that meet IEEE 519-2022 standards and some other problems of optimization algorithms. Meta-heuristic chemistry is also preferred to generalize in this study.

Provide a complete overview of the application of meta-heuristic optimization algorithms to SAPF. Suggestions suggest advanced solutions for the weaknesses of the meta-heuristic optimization algorithms that are still encountered. This proves that meta-heuristic optimization algorithms need to be developed in the future and is a promising research direction for researchers to improve the solution when applying optimization algorithms to problem-solving and optimizing the control parameter $K_p,\ K_i$ of the PI controller to improve the optimal efficiency of the model by applying the meta-heuristic optimization algorithm to SAPF. The goal of this study is to provide a springboard for researchers and graduate students to have an overview of the application of meta-heuristic optimization algorithms to SAPF and is also seen as a typical platform for future research (Table 19).

Table 19. Summary application of meta-heuristic in SAPF.

Ref.	Method	Results and Benefits of Applying Meta-Heuristic Optimization to SAPF	Limitation or Future Research
[67–70]	DE	Improve turning of the proportional-integral control loop of SAPF. The THD value reaches 3.42% to meet the IEEE 519-2022 standard.	The meta-heuristic hybrid method is different from DE; the aim is to reduce the THD value to meet the IEEE 519-2022 standard.
[71–77]	GA	Controller turning to obtain optimum gain values to switch SAPF and THD in the supply current present in the hardware is 1.4%, more than the simulation results of 1.24%.	Control technique for the SAPF system with time-varying parametric uncertainties.
[78–82]	ABC	To solve the nonlinear equation of selective harmonic elimination patterns considering unequal direct current sources, satisfying fundamental components, and eliminating low-order harmonics. The THD of the hardware is 11.78%, more than the simulation results of 10.46%.	Propose a hybrid method that combines meta-heuristics and ABC to reduce THD and meet the IEEE 519-2022 standard.
[83–87]	ACO	Optimize the gain values of the PI controller used in SAPF. The setting time (T_s) is 28 ms, and the THD of the supply current is 3.85%, 2.92%, and 3.49% for phase a, phase b, and phase c, respectively.	Consider the proposed systems to be an efficient solution to the growing demand forpower at the present and in the future.
[88–91]	ALO	To properly tune the circuit in order to reduce the harmonics in the source current and load voltages, the THD of the supply current with RL load is 3.73%, and the RLC load is 4.03%. The THD of the supply voltage with RL load is 4.2%, and the RLC load is 4.44%.	The technique works for different load variations in the system.
[92–94]	BA	Proportional resonant controller-based pulse width modulation. Current control for three-phase, three-leg SAPF with the optimized DC-link controller. The THD value reaches 0.7% to meet the IEEE 519-2022 standard.	BA is very promising for solving other multi-objective optimization problems.
[95–97]	BFO	To optimize the parameters of the PI controller through an online self-adaptive self-turning algorithm. The THD value reaches 1.9% to meet the IEEE 519-2022 standard.	BFO-based SAPF proves to be a significant approach to reducing the ripple current harmonics.
[98–106]	FA	Optimization problems with the objective of minimizing the THD and solving it using predator-prey-based firefly optimization. The THD is 1.9092%.	The proposed method can be extended to designing hybrid active power filters in future works.
[107,108]	ASNS	The optimization of conventional control scheme used in SAPF. THD of supply current is 1.21%, 1.14%, and 1.11% for balanced, unbalanced, and distorted loads, respectively. Compensation time (Ts) is 0.055 (s), 0.003 (s), and 0.001 (s) for balanced, unbalanced, and distorted loads, respectively.	Design for all different types of HAPF.
[109–112]	TS	The instantaneous power theory with Fourier and the optimal design of the current predictive controller. The THD of the supply current is 0.96%.	The proposed novel active filter can be applied to higher-frequency systems.
[113–119]	WOA	To control the DC − link voltage to a constant value, a PI controller is used by the gains of the controller $(K_p,\ K_i)$. The THD of the supply current is 3.07%	A tuned PI controller can be used in hardware for real-time implementation. The proposed modern industrial optimization should be tested under various range constraints by using new techniques to handle the constraints.

Table 19. *Cont.*

Ref.	Method	Results and Benefits of Applying Meta-Heuristic Optimization to SAPF	Limitation or Future Research
[120–133]	PSO	The selection of a proper reference compensation current extraction scheme plays the most crucial role in the performance of SAPF and includes conventional instantaneous active and reactive power (p-q),modified p-q, and instantaneous active and reactive current component (i_d-i_q) schemes.THD of supply current is 3.45%, 2.97%, and 3.07%, based on phase a, phase b, and phase c, respectively.	A hybrid method that combines other meta-heuristic methods into the search area of PSO to help limit the fast convergence error of PSO, such as DE-PSO, GA-PSO, and Levy-flight-PSO.
[133–138]	FPA	To maintain the DC link voltage constant, the proportional-integral (PI) controller being employed on the DC side of SAPF is used to minimize the error between voltage and actual value. The THD of the supply current is 3.13%, and T_s is 0.001 s.	Application of some hybrid optimization algorithm for the determination of optimal controller parameters.
[139–144]	GWO	To reduce the maximum overshoot and undershoot of the DC-link voltage variation and minimize power ripples with current distortion in IEEE 519-2022. Improve the predictive direct power control of three-phase SAPF. The THD of the supply current is 3.8% and 57%, based on simulation and experimental data, respectively.	Propose a hybrid method that combines meta-heuristics and GWO to enhance work efficiency.
[145,146]	GSA	The harmonic content reduction in the source current is carried out with optimal turning of the PI controller. The THD of the supply current is 1.76%.	Propose a hybrid method that combines meta-heuristics and GSA with the aim of maximizing work efficiency.
[147–150]	TLBD	The reference current signals are generated by sensing the source voltage load current and DC bus voltage; with these signals, the gate driving pulses are generated by a band current controller. THD of the supply current is 1.06%.	Propose a hybrid method that combines meta-heuristics and TLBO to maximize productivity.

Author Contributions: Conceptualization, M.L.D. and P.B.; methodology, M.L.D.; software, M.L.D.; validation, M.L.D. and P.B.; formal analysis, M.L.D. and L.H.; investigation, M.L.D.; resources, M.L.D.; data curation, M.L.D. and L.H.; writing—original draft preparation, M.L.D.; writing—review and editing, M.L.D. and L.H.; visualization, M.L.D. and L.H.; supervision, P.B. and R.M.; project administration, P.B. and R.M.; funding acquisition, P.B. and R.M. All authors have read and agreed to the published version of the manuscript.

Funding: This work was supported in part by the Ministry of Education of the Czech Republic (Project No. SP2023/090).

Data Availability Statement: Not applicable.

Acknowledgments: The authors are extremely grateful to VSB Technical University of Ostrava, Czechia, for financial support. They would also like to express their gratitude to Van Lang University, Vietnam, for supporting this research.

Conflicts of Interest: The authors declare no conflict of interest.

References

1. Li, D.; Wang, T.; Pan, W.; Ding, X.; Gong, J. A comprehensive review of improving power quality using active power filters. *Electr. Power Syst. Res.* **2021**, *199*, 107389. [CrossRef]
2. Soliman, H.M.; Saleem, A.; Bayoumi, E.H.E.; De Santis, M. Harmonic Distortion Reduction of Transformer-Less Grid-Connected Converters by Ellipsoidal-Based Robust Control. *Energies* **2023**, *16*, 1362. [CrossRef]

3. Adineh, B.; Keypour, R.; Davari, P.; Blaabjerg, F. Review of Harmonic Mitigation Methods in Microgrid: From a Hierarchical Control Perspective. *IEEE J. Emerg. Sel. Top. Power Electron.* **2020**, *9*, 3044–3060. [CrossRef]
4. Aziz, M.H.A.; Azizan, M.M.; Sauli, Z.; Yahya, M.W. A review on harmonic mitigation method for non-linear load in electrical power system. *Proceeding Green Des. Manuf.* **2020**, *2239*, 020022. [CrossRef]
5. Keypour, R.; Adineh, B.; Khooban, M.H.; Blaabjerg, F. A New Population-Based Optimization Method for online Minimization of Voltage Harmonics in Islanded Microgrids. *IEEE Trans. Circuits Syst. II Express Briefs* **2019**, *67*, 1084–1088. [CrossRef]
6. Langlang, G.; Arif, N.A.; Denis, E.C.; Eli, H.S.; Ahmad, A.B.A. Application of line reactors and harmonic filter in electric power system are integrated renewable energy in Mesh topology. In Proceedings of the 2022 4th International Conference on Cybernetics and Intelligent System (ICORIS) IEEE, Prapat, Indonesia, 8–9 October 2022; pp. 1–5. [CrossRef]
7. Manish, V.; Neeraj, B.; Scott, D.; Todd, O. Isolation Techniques for Medium-Voltage Adjustable Speed Drives. *IEEE Ind. Appl. Mag.* **2019**, *1*, 1077–2018. [CrossRef]
8. Zailan, F.H.; Soomro, D.M. Mitigating Harmonics by using K-transformer. *Evol. Electr. Electron. Eng.* **2022**, *3*, 510–515.
9. Abbas, A.S.; El-Sehiemy, R.A.; Abou El-Ela, A.; Ali, E.S.; Mahmoud, K.; Lehtonen, M.; Darwish, M.M.F. Optimal Harmonic Mitigation in Distribution Systems with Inverter Based Distributed Generation. *Appl. Sci.* **2021**, *11*, 774. [CrossRef]
10. Iturra, R.G.; Cruse, M.; Figge, K.; Thiemann, P.; Dresel, C. Ultra-Low Losses SiC-Based Active Damper for Industrial Power Systems: Mitigating Harmonic Distortion and Maximizing Harmonic Power Recovery. *IEEE Trans. Energy Convers.* **2022**, *37*, 2926–2940. [CrossRef]
11. Park, B.; Lee, J.; Yoo, H.; Jang, G. Harmonic Mitigation Using Passive Harmonic Filters: Case Study in a Steel Mill Power System. *Energies* **2021**, *14*, 2278. [CrossRef]
12. Chuen, L.T.; Chee, W.T. DC traction power substation using an eighteen-pulse rectifier transformer system. *Int. J. Power Electron. Drive Syst.* **2021**, *12*, 2284–2394. [CrossRef]
13. Du, Q.; Fang, Z.; Gao, L.; Li, Q.; Li, F.; Meng, F. Open-Phase Fault Research on the Parallel-Connected 40-Pulse Rectifier with Multi-Output Auto-Connected Phase-Shifting Transformer. *IEEE J. Emerg. Sel. Top. Power Electron.* **2023**, *1*, 1–8. [CrossRef]
14. Ghayal, S.P.; Gour, S. Analysis of harmonics and neutral to ground (N to G) voltage diminution nusing isolation transformer. In Proceedings of the 2017 Third International Conference on Science Technology Engineering & Management (ICONSTEM), Chennai, India, 23–24 March 2017; Volume 17, pp. 1–4. [CrossRef]
15. Ragonese, E.; Spina, N.; Parisi, A.; Palmisano, G. An Experimental Comparison of Galvanically Isolated DC-DC Converters: Isolation Technology and Integration Approach. *Electronics* **2021**, *10*, 1186. [CrossRef]
16. Yu, Q.; Chu, S.; Li, W.; Tian, L.; Wang, X.; Cheng, Y. Electromagnetic Shielding Analysis of a Canned Permanent Magnet Motor. *IEEE Trans. Ind. Electron.* **2019**, *67*, 8123–8130. [CrossRef]
17. Lu, G.; Zheng, D.; Zhang, Q.; Zhang, P. Effects of Converter Harmonic Voltages on Transformer Insulation Ageing and an Online Monitoring Method for Interlayer Insulation. *IEEE Trans. Power Electron.* **2022**, *37*, 3504–3514. [CrossRef]
18. Hoon, Y.; Mohd Radzi, M.A.; Mohd Zainuri, M.A.A.; Zawawi, M.A.M. Shunt Active Power Filter: A Review on Phase Synchronization Control Techniques. *Electronics* **2019**, *8*, 791. [CrossRef]
19. Sanjan, P.S.; Gowtham, N.; Bhaskar, M.S.; Subramaniam, U.; Almakhles, D.J.; Padmanaban, S.; Yamini, N.G. Enhancement of Power Quality in Domestic Loads Using Harmonic Filters. *IEEE Access* **2020**, *8*, 197730–197744. [CrossRef]
20. Thulaseedharan, K.R.; Parambil, A.; Puthenveetil, M.J.; Arunodayam, R.A. Compact microstrip plowpass filter with high harmonics suppression using defected structures. *AEU Int. J. Electron. Commun.* **2020**, *115*, 153032. [CrossRef]
21. Du, Q.; Gao, L.; Li, Q.; Liu, W.; Yin, X.; Meng, F. Harmonic Reduction Methods at DC Link of Series-Connected Multi-Pulse Rectifiers: A Review. *IEEE Trans. Power Electron.* **2022**, *37*, 3143–3160. [CrossRef]
22. Kim, J.; Lai, J.-S. Analysis of a Shunt Wye-Delta Transformer for Multi-Generator Harmonic Elimination Under Non-Ideal Phase-Shift Conditions. *IEEE Trans. Ind. Appl.* **2019**, *55*, 2412–2420. [CrossRef]
23. Cheng, Q.; Wang, C.; Wang, J. Analysis on Displacement Angle of Phase-Shifted Carrier PWM for Modular Multilevel Converter. *Energies* **2020**, *13*, 6743. [CrossRef]
24. Stephen, B.J.; Emmanuel, G.D.; Afeez, A.; David, O.O.; Ban, M.K. Metaheuristic algorithms for PID controller parameters tuning: Review, approaches and open problems. *Helyon* **2022**, *8*, e09399. [CrossRef]
25. Yang, B.; Wang, J.; Zhang, X.; Yu, T.; Yao, W.; Shu, H.; Sun, L. Comprehensive overview of meta-heuristic algorithm applications on PV cell parameter identification. *Energy Convers. Manag.* **2020**, *208*, 112595. [CrossRef]
26. *IEEE Std 519™-2022*; IEEE Standard for Harmonic Control in Electric Power Systems. Transmission and Distribution Committee of the IEEE Power and Energy Society. The Institute of Electrical and Electronics Engineers, Inc. 3 Park Avenue: New York, NY, USA, 2022; STDPD25432; pp. 10016–15997. [CrossRef]
27. Jaros, R.; Byrtus, R.; Dohnal, J.; Danys, L.; Baros, J.; Koziorek, J.; Zmij, P.; Martinek, R. Advanced Signal Processing Methods for Condition Monitoring. *Arch. Computat. Methods Eng.* **2022**, *1163*, 1553–1577. [CrossRef]
28. Hanna, N.A.F.; Fadel, M.; Kanaan, H.Y. Design of a direct control strategy for a static shunt compensator to improve power quality in polluted and unbalanced grids. *Math. Comput. Simul.* **2018**, *158*, 199–215. [CrossRef]
29. Ouchen, S.; Gaubert, J.-P.; Steinhart, H.; Betka, A. Energy quality improvement of three-phase shunt active power filter under different voltage conditions based on predictive direct power control with disturbance rejection principle. *Math. Comput. Simul.* **2018**, *158*, 506–519. [CrossRef]

30. Gao, T.; Lin, Y.; Chen, D.; Xiao, L. A novel active damping control based on grid-side current feedback for LCL-filter active power filter. *Energy Rep.* **2020**, *6*, 1318–1324. [CrossRef]
31. Xiao, G.; Hongyi, L.; Guozhu, C. SiC-MOSFET shunt active power filter based on half-cycle SDFT and repetitive control. *Energy Rep.* **2021**, *7*, 246–252. [CrossRef]
32. Karthikeyan, M.; Sharmilee, K.; Balasubramaniam, P.M.; Prakash, N.B.; Rajesh Babu, M.; Subramaniyaswamy, V.; Sudhakar, S. Design and Implementation of ANN-based SAPF Approach for Current Harmonics Mitigation in Industrial Power Systems. *Microprocess. Microsyst.* **2020**, *77*, 103194. [CrossRef]
33. Agrawal, S.; Palwalia, D.K.; Kumar, M. Performance Analysis of ANN Based three-phase four-wire Shunt Active Power Filter for Harmonic Mitigation under Distorted Supply Voltage Conditions. *IETE J. Res.* **2019**, *68*, 566–574. [CrossRef]
34. Chen, D.; Xiao, L.; Lian, H.; Xu, Z. A fault tolerance method based on switch redundancy for shunt active power filter. *Energy Rep.* **2021**, *7*, 449–457. [CrossRef]
35. Chen, D.; Xiao, L.; Yan, W.; Li, Y.; Guo, Y. A harmonics detection method based on triangle orthogonal principle for shunt active power filter. *Energy Rep.* **2021**, *7*, 98–104. [CrossRef]
36. Dongdong, C.; Long, X.; Wenduan, Y.; Yan, L.; Yinbiao, G. A heat dissipation design strategy based on computational fluid dynamics analysis method for shunt active power filter. *Energy Rep.* **2022**, *8*, 229–238. [CrossRef]
37. Amit, V. Shunt active power filtering with reference current generation based on dual second order generalized integrator and LMS algorithm. *Energy Rep.* **2022**, *8*, 886–893. [CrossRef]
38. Hiral, H.; Vaidehi, D.; Amit, V. Modified symmetrical sinusoidal integrator and instantaneous reactive power theory-based control of shunt active filter. *Energy Rep.* **2022**, *8*, 515–523. [CrossRef]
39. Fang, Y.; Fei, J.; Wang, T. Adaptive Backstepping Fuzzy Neural Controller Based on Fuzzy Sliding Mode of Active Power Filter. *IEEE Access* **2020**, *8*, 96027–96035. [CrossRef]
40. Liu, L.; Fei, J.; An, C. Adaptive Sliding Mode Long Short-Term Memory Fuzzy Neural Control for Harmonic Suppression. *IEEE Access* **2021**, *9*, 69724–69734. [CrossRef]
41. Radhamani, R.; Balamurugan, R. An Enhanced Modified Multiport Interleaved Flyback Converter for Photovoltaic-Shunt Active Power Filter (PV-SHAPF) Applications. *Int. Trans. Electr. Energy Syst.* **2022**, *2022*, 1537319. [CrossRef]
42. Martinek, R.; Rzidky, J.; Jaros, R.; Bilik, P.; Ladrova, M. Least Mean Squares and Recursive Least Squares Algorithms for Total Harmonic Distortion Reduction Using Shunt Active Power Filter Control. *Energies* **2019**, *12*, 1545. [CrossRef]
43. Baros, J.; Sotola, V.; Bilik, P.; Martinek, R.; Jaros, R.; Danys, L.; Simonik, P. Review of Fundamental Active Current Extraction Techniques for SAPF. *Sensors* **2022**, *22*, 7985. [CrossRef]
44. Martinek, R.; Bilik, P.; Baros, J.; Brablik, J.; Kahankova, R.; Jaros, R.; Danys, L.; Rzidky, J.; Wen, H. Design of a Measuring System for Electricity Quality Monitoring within the SMART Street Lighting Test Polygon: Pilot Study on Adaptive Current Control Strategy for Three-Phase Shunt Active Power Filters. *Sensors* **2020**, *20*, 1718. [CrossRef] [PubMed]
45. Bilal, P.M.; Zaheer, H.; Garcia-Hernandez, L.; Abraham, A. Differential Evolution: A review of more than two decades of research. *Eng. Appl. Artif. Intell.* **2020**, *90*, 103479. [CrossRef]
46. Jesús, G.F.; Carlos, A. Indicator-based Multi-objective Evolutionary Algorithms: A Comprehensive Survey. *ACM Comput. Surv.* **2020**, *53*, 1–35. [CrossRef]
47. Rostami, M.; Berahmand, K.; Nasiri, E.; Forouzandeh, S. Review of swarm intelligence-based feature selection methods. *Eng. Appl. Artif. Intell.* **2021**, *100*, 104210. [CrossRef]
48. Tang, J.; Liu, G.; Pan, Q. A Review on Representative Swarm Intelligence Algorithms for Solving Optimization Problems: Applications and Trends. *IEEE/CAA J. Autom.* **2021**, *8*, 1627–1643. [CrossRef]
49. Shashank, R.V.; Sai, N.B.; John, C.M.; Elizabeth, M. A review of physics-based machine learning in civil engineering. *Results Eng.* **2022**, *13*, 100316. [CrossRef]
50. Burton, J.W.; Stein, M.; Jensen, T.B. A systematic review of algorithm aversion in augmented decision making. *J. Behav. Decis. Mak.* **2019**, *33*, 220–239. [CrossRef]
51. Lorenz-Spreen, P.; Lewandowsky, S.; Sunstein, C.R.; Hertwig, R. How behavioural sciences can promote truth, autonomy, and democratic discourse online. *Nat. Hum. Behav.* **2020**, *4*, 1102–1109. [CrossRef]
52. Micallef, A. A Review of the Current Challenges and Methods to Mitigate Power Quality Issues in Single-Phase Microgrids. *IET Gener. Transm. Distrib.* **2018**, *13*, 2044–2054. [CrossRef]
53. Khan, I.; Vijay, J.; Doolla, S. Nonlinear Load Harmonic Mitigation Strategies in Microgrids: State of the Art. *IEEE Syst. J.* **2022**, *16*, 4243–4255. [CrossRef]
54. Schweizer, D.; Ried, V.; Rau, G.C.; Tuck, J.E.; Stoica, P. Comparing Methods and Defining Practical Requirements for Extracting Harmonic Tidal Components from Groundwater Level Measurements. *Math. Geosci.* **2021**, *53*, 1147–1169. [CrossRef]
55. Kashif, M.; Hossain, M.J.; Fernandez, E.; Taghizadeh, S.; Sharma, V.; Ali, S.M.N.; Irshad, U.B. A Fast Time-Domain Current Harmonic Extraction Algorithm for Power Quality Improvement Using Three-Phase Active Power Filter. *IEEE Access* **2020**, *8*, 103539–103549. [CrossRef]
56. Chen, D.; Lin, Y.; Xiao, L.; Xu, Z.; Lian, H. A harmonics detection method based on an improved comb filter of sliding discrete Fourier for the grid-tied inverter. *Energy Rep.* **2020**, *6*, 1303–1311. [CrossRef]
57. Imam, A.A.; Sreerama Kumar, R.; Al-Turki, Y.A. Modeling and Simulation of a PI Controlled Shunt Active Power Filter for Power Quality Enhancement Based on P-Q Theory. *Electronics* **2020**, *9*, 637. [CrossRef]

58. Zhen, Y.T.; Yap, H.; Mohd, A.M. Synchronous Reference Frame with Finite Impulse Response Filter for Operation of Single-phase Shunt Active Power Filter. In Proceedings of the MATEC Web Conference 14th EURECA 2020—International Engineering and Computing Research Conference "Shaping the Future through Multidisciplinary Research", Subang Jaya, Malaysia, 25 November 2020; Volume 335, pp. 1–8. [CrossRef]
59. Xu, M.; Sang, Z.; Li, X.; You, Y.; Dai, D. An Observer-Based Harmonic Extraction Method with Front SOGI. *Machines* **2022**, *10*, 95. [CrossRef]
60. Chi, Y.; Yang, S.; Jiao, W.; He, J.; Gu, X.; Papatheou, E. Spectral DCS-based feature extraction method for rolling element bearing pseudo-fault in the rotor-bearing system. *Measurement* **2018**, *132*, 22–34. [CrossRef]
61. Kashif, M.; Hossain, M.J.; Nawazish Ali, S.M.; Sharma, V.; Nizami, M.S.H. Harmonic Identification based on DSC and MAF for Three-phase Shunt Active Power Filter. In Proceedings of the 2019 29th Australasian Universities Power Engineering Conference (AUPEC), Nadi, Fiji, 26–29 November 2019; Volume 1, pp. 1–6. [CrossRef]
62. Mohamadian, S.; Pairo, H.; Ghasemian, A. A Straightforward Quadrature Signal Generator for Single-Phase SOGI-PLL with Low Susceptibility to Grid Harmonics. *IEEE Trans. Ind. Electron.* **2021**, *69*, 6997–7007. [CrossRef]
63. Dubey, A.K.; Mishra, J.P.; Kumar, A.; Dongre, A.A. MSOGI-FLL based Robust Harmonics Compensation under Distorted Grid Voltage Condition. In Proceedings of the 2020 3rd International Conference on Energy, Power and Environment: Towards Clean Energy Technologies, Shillong, India, 5–7 March 2021; Volume 1, pp. 1–5. [CrossRef]
64. Mukherjee, S.; Mazumder, S.; Adhikary, S. Harmonic Compensation for Nonlinear Loads Fed by Grid Connected Solar Inverters Using Active Power Filters. In Proceedings of the 2020 IEEE VLSI Device Circuit and System (VLSI DCS), Kolkata, India, 18–19 July 2020; Volume 1, pp. 1–6. [CrossRef]
65. Zhang, J.; Wang, Z.; Han, X. Fast Transient Harmonic Selective Extraction Based on Modulation-CDSC-SDFT. In Proceedings of the 2021 IEEE International Instrumentation and Measurement Technology Conference (I2MTC), Glasgow, UK, 17–20 May 2021; pp. 1–6. [CrossRef]
66. Golestan, S.; Guerrero, J.M.; Musavi, F.; Vasquez, J.C. Single-Phase Frequency-Locked Loops: A Comprehensive Review. *IEEE Trans. Power Electron.* **2019**, *34*, 11791–11812. [CrossRef]
67. Geng, J.; Li, X.; Liu, Q.; Chen, J.; Xin, Z.; Loh, P.C. Frequency-Locked Loop Based on a Repetitive Controller for Grid Synchronization Systems. *IEEE Access* **2020**, *8*, 154861–154870. [CrossRef]
68. Vishwakarma, A.P.; Milan Singh, K. Comparative Analysis of Adaptive PI Controller for Current Harmonic Mitigation. In Proceedings of the 2020 International Conference on Computational Performance Evaluation (ComPE), Shillong, India, 2–4 July 2020; Volume 1, pp. 643–648. [CrossRef]
69. Marquez Alcaide, A.; Leon, J.I.; Laguna, M.; Gonzalez-Rodriguez, F.; Portillo, R.; Zafra-Ratia, E.; Vazquez, S.; Franquelo, L.G.; Bayhan, S.; Abu-Rub, H. Real-Time Selective Harmonic Mitigation Technique for Power Converters Based on the Exchange Market Algorithm. *Energies* **2020**, *13*, 1659. [CrossRef]
70. Costa, B.L.G.; Bacon, V.D.; da Silva, S.A.O.; Angelico, B.A. Tuning of a PI-MR Controller Based on Differential Evolution Metaheuristic Applied to the Current Control Loop of a Shunt-APF. *IEEE Trans. Ind. Electron.* **2017**, *64*, 4751–4761. [CrossRef]
71. Biswas, P.P.; Suganthan, P.N.; Amaratunga, G.A.J. Minimizing harmonic distortion in power system with optimal design of hybrid active power filter using differential evolution. *Appl. Soft Comput.* **2017**, *61*, 486–496. [CrossRef]
72. Sao, J.K.; Naayagi, R.T.; Panda, G.; Patidar, R.D.; Swain, S.D. SAPF Parameter Optimization with the Application of Taguchi SNR Method. *Electronics* **2022**, *11*, 348. [CrossRef]
73. Sundaram, E.; Gunasekaran, M.; Krishnan, R.; Padmanaban, S.; Chenniappan, S.; Ertas, A.H. Genetic algorithm based reference current control extraction based shunt active power filter. *Int. Trans. Electr. Energy Syst.* **2020**, *31*, e12623. [CrossRef]
74. Mohamed, A.A.S.; Berzoy, A.; Mohammed, O.A. Adaptive Transversal digital Filter for reference current detection in shunt active power filter. In Proceedings of the 2015 IEEE Power & Energy Society General Meeting, Denver, CO, USA, 26–30 July 2015; Volume 2, pp. 1–5. [CrossRef]
75. Song, W.; Yang, Y.; Qin, W.; Wheeler, P. Switching State Selection for Model Predictive Control Based on Genetic Algorithm Solution in an Indirect Matrix Converter. *IEEE Trans. Transp. Electrif.* **2022**, *8*, 4496–4508. [CrossRef]
76. Khalid, S. Power Quality Improvement of Constant Frequency Aircraft Electric Power System Using Genetic Algorithm and Neural Network Control Based Control Scheme. *J. Electr. Electron. Syst.* **2016**, *5*, 1000206. [CrossRef]
77. Devaraj, S.V.; Gunasekaran, M.; Sundaram, E.; Venugopal, M.; Chenniappan, S.; Almakhles, D.J.; Subramaniam, U.; Bhaskar, M.S. Robust Queen Bee Assisted Genetic Algorithm (QBGA) Optimized Fractional Order PID (FOPID) Controller for Not Necessarily Minimum Phase Power Converters. *IEEE Access* **2021**, *9*, 93331–93337. [CrossRef]
78. Sakthivel, A.; Vijayakumar, P.; Senthilkumar, A.; Lakshminarasimman, L.; Paramasivam, S. Experimental investigations on Ant Colony Optimized PI control algorithm for Shunt Active Power Filter to improve Power Quality. *Control. Eng. Pract.* **2015**, *42*, 153–169. [CrossRef]
79. Mousazadeh Mousavi, S.Y.; Zabihi Laharami, M.; Niknam Kumle, A.; Fathi, S.H. Application of ABC algorithm for selective harmonic elimination switching pattern of cascade multilevel inverter with unequal DC sources. *Int. Trans. Electr. Energy Syst.* **2018**, *28*, e2522. [CrossRef]
80. Rajalakshmi, R.; Rajasekaran, V. Improved PLL Tuning of Shunt Active Power Filter for Grid Connected Photo Voltaic Energy System. *Circuits Syst.* **2016**, *7*, 3063–3080. [CrossRef]

81. Yamarthi, R.B.; Rao, R.S.; Reddy, P.L. Optimal load compensation by shunt active power filter employing artificial bee colony optimization. In Proceedings of the 2016 International Conference on Electrical, Electronics, and Optimization Techniques (ICEEOT), Chennai, India, 3–5 March 2016; Volume 1, pp. 1–5. [CrossRef]
82. Sinha, R. Design of Shunt Active Power Filter with Optimal PI Controller—A Comparative Analysis. In Proceedings of the 2019 International Conference on Applied Machine Learning (ICAML), Bhubaneswar, India, 25–26 May 2019; Volume 1, pp. 1–8. [CrossRef]
83. Rameshkumar, K.; Indragandhi, V. Real Time Implementation and Analysis of Enhanced Artificial Bee Colony Algorithm Optimized PI Control algorithm for Single Phase Shunt Active Power Filter. *J. Electr. Eng. Technol.* **2020**, *15*, 1541–1554. [CrossRef]
84. Berbaoui, B.; Saba, D.; Dehini, R.; Dahbi, A.; Maouedj, R. Optimal control of shunt active filter based on Permanent Magnet Synchronous Generator (PMSG) using ant colony optimization algorithm. In Proceedings of the 7th International Conference on Software Engineering and New Technologies—ICSENT, New York, NY, USA, 26 December 2018; Volume 1, pp. 1–8. [CrossRef]
85. Khosravi, N.; Abdolmohammadi, H.R.; Bagheri, S.; Miveh, M.R. Improvement of harmonic conditions in the AC/DC microgrids with the presence of filter compensation modules. *Renew. Sustain. Energy Rev.* **2021**, *143*, 110898. [CrossRef]
86. Balasubramaniam, P.M.; Sudhakar, S.; Krishnamoorthy, S.; Sriram, V.P.; Dhanaraj, S.; Subramaniyaswamy, V. Investigation and strategy of intelligent controller (ACBIC) for DC link control in SAPF system for industrial power systems. *J. Discret. Math. Sci. Cryptogr.* **2020**, *24*, 1–17. [CrossRef]
87. Tiwari, A.K.; Dubey, S.P. Ant colony optimization based hybrid active power filter for harmonic compensation. In Proceedings of the 2016 International Conference on Electrical, Electronics, and Optimization Techniques (ICEEOT), Chennai, India, 3–5 March 2016; Volume 1, pp. 1–6. [CrossRef]
88. Kumar, R.; Bansal, H.O.; Kumar, D. Improving power quality and load profile using PV-Battery-SAPF system with metaheuristic tuning and its HIL validation. *Int. Trans. Electr. Energy Syst.* **2020**, *30*, e12335. [CrossRef]
89. Baliyan, A.; Shrivastava, N.; Alam, J. An Antlion Optimization technique based Hybrid Series APF for Harmonic Mitigation. In Proceedings of the IECON 2021—47th Annual Conference of the IEEE Industrial Electronics Society, Toronto, ON, Canada, 13–16 October 2021; pp. 1–5. [CrossRef]
90. Bekakra, Y.; Zellouma, L.; Malik, O. Improved predictive direct power control of shunt active power filter using GWO and ALO—Simulation and experimental study. *Ain Shams Eng. J.* **2021**, *12*, 3859–3877. [CrossRef]
91. Amritha, K.; Rajagopal, V.; Raju, K.N.; Arya, S.R. Ant lion algorithm for optimized controller gains for power quality enrichment of off-grid wind power harnessing units. *Chin. J. Electr. Eng.* **2020**, *6*, 85–97. [CrossRef]
92. Deenadayalan, V.; Vaishnavi, P. Improvised deep learning techniques for the reliability analysis and future power generation forecast by fault identification and remediation. *J. Ambient. Intell. Humaniz. Comput.* **2021**, *13*, 57. [CrossRef]
93. Parandhaman, B.; Nataraj, S.K.; Baladhandautham, C.B. Optimization of DC-link voltage regulator using Bat algorithm for proportional resonant controller-based current control of shunt active power filter in distribution network. *Int. Trans. Electr. Energy Syst.* **2020**, *30*, e12369. [CrossRef]
94. Ürgün, S.; Yiğit, H.; Mirjalili, S. Investigation of Recent Metaheuristics Based Selective Harmonic Elimination Problem for Different Levels of Multilevel Inverters. *Electronics* **2023**, *12*, 1058. [CrossRef]
95. Rajesh, P.; Shajin, F.H.; Umasankar, L. A Novel Control Scheme for PV/WT/FC/Battery to Power Quality Enhancement in Micro Grid System: A Hybrid Technique. *Energy Sources Part A Recovery Util. Environ. Eff.* **2021**, *1*, 1–18. [CrossRef]
96. Patnaik, S.S.; Panda, A.K. Optimal load compensation by 3-phase 4-wire shunt active power filter under distorted mains supply employing bacterial foraging optimization. In Proceedings of the 2011 Annual IEEE India Conference, Hyderabad, India, 16–18 December 2011; pp. 1–6. [CrossRef]
97. Patnaik, S.S.; Panda, A.K. Optimizing current harmonics compensation in three-phase power systems with an Enhanced Bacterial foraging approach. *Int. J. Electr. Power Energy Syst.* **2014**, *61*, 386–398. [CrossRef]
98. Patnaik, S.S.; Panda, A.K. Particle Swarm Optimization and Bacterial Foraging Optimization Techniques for Optimal Current Harmonic Mitigation by Employing Active Power Filter. *Appl. Comput. Intell. Soft Comput.* **2012**, *1*, 1. [CrossRef]
99. Abdul-Hameed, T.A.; Akorede, M.F.; Abdulrahman, Y.; Tijani, O.M. An investigation of the harmonic effects of nonlinear loads on power distributon network. *Niger. J. Technol.* **2019**, *38*, 401–405. [CrossRef]
100. Mahaboob, S.; Ajithan, S.K.; Jayaraman, S. Optimal design of shunt active power filter for power quality enhancement using predator-prey based firefly optimization. *Swarm Evol. Comput.* **2019**, *44*, 522–533. [CrossRef]
101. Soumya, R.D.; Prakash, K.R.; Sahoo, A.; Gaurav, D. Application of optimisation technique in PV integrated multilevel inverter for power quality improvement. *Comput. Electr. Eng.* **2022**, *97*, 107606. [CrossRef]
102. Farhoodnea, M.; Mohamed, A.; Shareef, H.; Zayandehroodi, H. Optimum D-STATCOM placement using firefly algorithm for power quality enhancement. In Proceedings of the 2013 IEEE 7th International Power Engineering and Optimization Conference (PEOCO), Langkawi, Malaysia, 3–4 June 2013; pp. 1–5. [CrossRef]
103. Apon, H.J.; Abid, M.S.; Morshed, K.A.; Nishat, M.M.; Faisal, F.; Ibrahim, N.N. Power System Harmonics Estimation using Hybrid Archimedes Optimization Algorithm-based Least Square Method. In Proceedings of the 2021 13th International Conference on Information & Communication Technology and System (ICTS), Surabaya, Indonesia, 20–21 October 2021; pp. 312–317. [CrossRef]
104. Buła, D.; Grabowski, D.; Maciążek, M. A Review on Optimization of Active Power Filter Placement and Sizing Methods. *Energies* **2022**, *15*, 1175. [CrossRef]

105. Nagarajan, A.; Sivachandran, P.; Suganyadevi, M.V.; Muthukumar, P. A study of UPQC: Emerging mitigation techniques for the impact of recent power quality issues. *Circuit World* **2020**, *47*, 11–21. [CrossRef]
106. Saifullah, K. THD and Compensation Time Analysis of Three-Phase Shunt Active Power Filter Using Adaptive Spider Net Search Algorithm (ASNS) for Aircraft System. *Int. J. Com. Dig. Sys.* **2016**, *5*, 1–18. [CrossRef]
107. Chau, M.T. A new design algorithm for hybrid active power filter. *Int. J. Electr. Comput. Eng. (IJECE)* **2019**, *9*, 4507–4515. [CrossRef]
108. Ravi, T.; Sathish, K. Analysis, monitoring, and mitigation of power quality disturbances in a distributed generation system, Front. *Energy Res.* **2022**, *10*, 989474. [CrossRef]
109. Saifullah, K. Application of Adaptive Tabu Search Algorithm in Hybrid Power Filter and Shunt Active Power Filters: Application of ATS Algorithm in HPF and APF. *Sustain. Power Resour. Through Energy Optim. Eng.* **2016**, *1*, 1–4. [CrossRef]
110. Khalid, S. Performance evaluation of Adaptive Tabu search and Genetic Algorithm optimized shunt active power filter using neural network control for aircraft power utility of 400 Hz. *J. Electr. Syst. Inf. Technol.* **2017**, *5*, 723–734. [CrossRef]
111. Tiyarachakun, S.; Areerak, K.; Areerak, K. Instantaneous Power Theory with Fourier and Optimal Predictive Controller Design for Shunt Active Power Filter. *Model. Simul. Eng.* **2014**, *2014*, 381760 . [CrossRef]
112. Saifullah, K. A novel Algorithm Adaptive Autarchoglossans Lizard Foraging (AALF) in a shunt active power filter connected to MPPT-based photovoltaic array. *E Prime-Adv. Electr. Eng. Electron. Energy* **2023**, *3*, 100100. [CrossRef]
113. Yusuf, S.D.; Loko, A.Z.; Abdullahi, J.; Abdulhamid, A.A. Performance Analysis of Three-Phase Shunt Active Power Filter for Harmonic Mitigation. *Asian J. Res. Rev. Phys.* **2022**, *6*, 7–24. [CrossRef]
114. Darvish Falehi, A. Optimal harmonic mitigation strategy based on multiobjective whale optimization algorithm for asymmetrical half-cascaded multilevel inverter. *Electr. Eng.* **2020**, *102*, 1639–1650. [CrossRef]
115. Abhishek, S.; Dushmanta, K.D. A Whale Optimization Algorithm Based Shunt Active Power Filter for Power Quality Improvement. *Int. J. Electr. Energy* **2018**, *6*, 7–12. [CrossRef]
116. Son, T.J.; Yun, L.K.; Haur, Y.K. Shunt Active Power Filter Design with Whale Optimization Algorithm for Three Phase Power System. In Proceedings of the 2020 2nd International Conference on Electrical, Control and Instrumentation Engineering (ICECIE), Kuala Lumpur, Malaysia, 28 November 2020; Volume 1, pp. 1–10. [CrossRef]
117. Alasali, F.; Nusair, K.; Foudeh, H.; Holderbaum, W.; Vinayagam, A.; Aziz, A. Modern Optimal Controllers for Hybrid Active Power Filter to Minimize Harmonic Distortion. *Electronics* **2022**, *11*, 1453. [CrossRef]
118. Shrivastava, N.; Baliyan, A.; Alam, S.J. Hybrid Series Active Power Filter for Harmonic Compensation Using PI Controller Tuned with WOA Technique. *Russ. Electr. Eng.* **2022**, *93*, 129–140. [CrossRef]
119. Thakur, N.; Awasthi, Y.K.; Hooda, M.; Siddiqui, A.S. Parametric Analysis of Adaptive Whale Optimization Technique for Power Quality Enhancement in Restructured Electricity Market. In Proceedings of the 2019 2nd International Conference on Power Energy, Environment and Intelligent Control (PEEIC), Greater Noida, India, 18–19 October 2019; pp. 1–7. [CrossRef]
120. Aguilar-Mejía, O.; Minor-Popocatl, H.; Tapia-Olvera, R. Comparison and Ranking of Metaheuristic Techniques for Optimization of PI Controllers in a Machine Drive System. *Appl. Sci.* **2020**, *10*, 6592. [CrossRef]
121. Gali, V.; Gupta, N.; Gupta, R.A. Improved dynamic performance of shunt active power filter using particle swarm optimization. In Proceedings of the 2017 IEEE International Conference on Intelligent Techniques in Control, Optimization and Signal Processing (INCOS), Srivilliputtur, India, 23–25 March 2017; pp. 1–7. [CrossRef]
122. Nasyrov, R.R.; Aljendy, R.I.; Diab, A.A.Z. Adaptive PI controller of active power filter for compensation of harmonics and voltage fluctuation based on particle swarm optimization (PSO). In Proceedings of the 2018 IEEE Conference of Russian Young Researchers in Electrical and Electronic Engineering (EIConRus), Moscow/St. Petersburg, Russia, 29 January–1 February 2018; pp. 1–6. [CrossRef]
123. Cao, W.; Liu, K.; Wu, M.; Xu, S.; Zhao, J. An Improved Current Control Strategy Based on Particle Swarm Optimization (PSO) and Steady State Error Correction for SAPF. *IEEE Trans. Ind. Appl.* **2019**, *55*, 4268–4274. [CrossRef]
124. Awasthi, A.; Chandra, D.; Rajasekar, S.; Singh, A.K.; Karuppanan, P.; Raj, A.-D.-V. An Improved PSO approach for optimal tuning of PI controller for shunt active power filter using FPGA with hardware co-simulation. In Proceedings of the 2016 IEEE International Conference on Power Electronics, Drives and Energy Systems (PEDES), Trivandrum, India, 14–17 December 2016; pp. 1–6. [CrossRef]
125. Gowtham, N.; Shankar, S. PI tuning of Shunt Active Filter using GA and PSO algorithm. In Proceedings of the 2016 2nd International Conference on Advances in Electrical, Electronics, Information, Communication and Bio-Informatics (AEEICB), Chennai, India, 27–28 February 2016; pp. 1–7. [CrossRef]
126. Diab, M.; El-Habrouk, M.; Abdelhamid, T.H.; Deghedie, S. Switched Capacitor Active Power Filter Optimization Using Nature-Inspired Techniques. In Proceedings of the 2019 21st International Middle East Power Systems Conference (MEPCON), Cairo, Egypt, 17–19 December 2019; pp. 1–6. [CrossRef]
127. He, N.; Xu, D.; Huang, L. The Application of Particle Swarm Optimization to Passive and Hybrid Active Power Filter Design. *IEEE Trans. Ind. Electron.* **2009**, *56*, 2841–2851. [CrossRef]
128. Patnaik, S.S.; Panda, A.K. Real-time performance analysis and comparison of various control schemes for particle swarm optimization-based shunt active power filters. *Int. J. Electr. Power Energy Syst.* **2013**, *52*, 185–197. [CrossRef]
129. Ravinder, K. Fuzzy particle swarm optimization control algorithm implementation in photovoltaic integrated shunt active power filter for power quality improvement using hardware-in-the-loop. *Sustain. Energy Technol. Assess.* **2022**, *50*, 101820. [CrossRef]

130. Torabian, E.; Hosseinian, B.; Vahidi, B. A new optimal approach for improvement of active power filter using FPSO for enhancing power quality. *Electr. Power Energy Syst.* **2015**, *69*, 188–199. [CrossRef]
131. Sujith, M.; Padma, S. Implementation of PSOANN Optimized PI Control Algorithm for Shunt Active Filter. *Comput. Model. Eng. Sci. CMES* **2020**, *122*, 863–888. [CrossRef]
132. Djerboub, K.; Allaoui, T.; Champenois, G.; Denai, M.; Habib, C. Particle Swarm Optimization Trained Artificial Neural Network to Control Shunt Active Power Filter Based on Multilevel Flying Capacitor Inverter. *Eur. J. Electr. Eng.* **2020**, *22*, 199–207. [CrossRef]
133. Abdedjebbar, T.; Zellouma Mohamed, T.; Benchouia Abdelbasset, K. Adaptive linear neuron control of three-phase shunt active powerfilter with an anti-windup PI controller optimized by particleswarm optimization. *Comput. Electr. Eng.* **2020**, *96*, 107471. [CrossRef]
134. Ismael, K.S.; Kamal, S. Power quality improvement of distribution systems asymmetry caused by power disturbances based on particle swarm optimization-artificial neural network. *Indones. J. Electr. Eng. Comput. Sci.* **2022**, *25*, 666–679. [CrossRef]
135. Patel, R.; Samal, P.; Panda, A.K.; Guerrero, J.M. Implementation of Bio-Inspired Flower Pollination Algorithm in Distribution System Harmonic Mitigation Scheme. In Proceedings of the 2021 1st International Conference on Power Electronics and Energy (ICPEE), Bhubaneswar, India, 2–3 January 2021; pp. 1–7. [CrossRef]
136. Patel, R.; Samal, P. Performance analysis of bio inspired flower pollination algorithm based 3-phase shunt active power filter for dynamic condition in distribution system. *Int. J. Syst. Assur. Eng. Manag.* **2023**, *2*, 1–15. [CrossRef]
137. Prince, S.K.; Panda, K.P.; Patowary, M.; Panda, G. FPA tuned Extended Kalman Filter for Power Quality Enhancement in PV integrated Shunt Active Power Filter. In Proceedings of the 2019 International Conference on Computing, Power and Communication Technologies (GUCON), New Delhi, India, 27–28 September 2019; pp. 257–262.
138. Riad, N.; Anis, W.; Elkassas, A.; Hassan, A.E.-W. Three-Phase Multilevel Inverter Using Selective Harmonic Elimination with Marine Predator Algorithm. *Electronics* **2021**, *10*, 374. [CrossRef]
139. Ranjan, S.; Jaiswal, S.; Latif, A.; Das, D.C.; Sinha, N.; Hussain, S.M.S.; Ustun, T.S. Isolated and Interconnected Multi-Area Hybrid Power Systems: A Review on Control Strategies. *Energies* **2021**, *14*, 8276. [CrossRef]
140. Reddy, A.K.V.K.; Narayana, K.V.L. Optimal total harmonic distortion minimization in multilevel inverter using improved whale optimization algorithm. *Int. J. Emerg. Electr. Power Syst.* **2020**, *21*, 1–25. [CrossRef]
141. Golla, M.; Chandrasekaran, K.; Simon, S.P. PV integrated universal active power filter for power quality enhancement and effective power management. *Energy Sustain. Dev.* **2021**, *61*, 104–117. [CrossRef]
142. Lakshmi Kanthan Bharathi, S.; Selvaperumal, S. MGWO-PI controller for enhanced power flow compensation using unified power quality conditioner in wind turbine squirrel cage induction generator. *Microprocess. Microsyst.* **2020**, *76*, 103080. [CrossRef]
143. Rao, B.C.; Sahu, P.; Jhapte, R. Comparative analysis of SRF based Shunt Active Filter using Grey Wolf and Eagle Perching Optimization. In Proceedings of the 2022 Second International Conference on Advances in Electrical, Computing, Communication and Sustainable Technologies (ICAECT), Bhilai, India, 21–22 April 2022; pp. 1–7. [CrossRef]
144. Mishra, A.K.; Das, S.R.; Ray, P.K.; Mallick, R.K.; Mohanty, A.; Mishra, D.K. PSO-GWO Optimized Fractional Order PID based Hybrid Shunt Active Power Filter for Power Quality Improvements. *IEEE Access* **2020**, *8*, 74497–74512. [CrossRef]
145. Almani, A.A.; Han, X.; Umer, F.; ul Hassan, R.; Nawaz, A.; Shah, A.A.; Mustafa, E. Optimal Solution for Frequency and Voltage Control of an Islanded Microgrid Using Square Root Gray Wolf Optimization. *Electronics* **2022**, *11*, 3644. [CrossRef]
146. Alam, S.J.; Arya, S.R. Observer-based control for UPQC-S with optimized gains of PI controller. *Int. Trans. Electr. Energy Syst.* **2020**, *30*, e47233. [CrossRef]
147. Manimegalai, M.; Sebasthirani, K. An Optimal Model for Power Quality Improvement in Smart Grid using Gravitational Search-based Proportional Integral Controller and Node Microcontroller Unit. *Electr. Power Compon. Syst.* **2022**, *50*, 989–1005. [CrossRef]
148. Pattnayak, S.K.; Choudhury, S.; Nayak, N.; Bagarty, D.P.; Biswabandhya, M. Maximum Power Tracking & Harmonic Reduction on grid PV System Using Chaotic Gravitational Search Algorithm Based MPPT Controller. In Proceedings of the 2020 International Conference on Computational Intelligence for Smart Power System and Sustainable Energy (CISPSSE), Keonjhar, India, 29–31 July 2020; pp. 1–6. [CrossRef]
149. Mishra, S.; Ray, P.K. Power quality improvement with shunt active filter under various mains voltage using Teaching Learning Based optimization. In Proceedings of the 2015 2nd International Conference on Recent Advances in Engineering & Computational Sciences (RAECS), Chandigarh, India, 21–22 December 2015; pp. 1–6. [CrossRef]
150. Ali, S.; Bhargava, A.; Saxena, A.; Kumar, P. A Hybrid Marine Predator Sine Cosine Algorithm for Parameter Selection of Hybrid Active Power Filter. *Mathematics* **2023**, *11*, 598. [CrossRef]